Eye Velocity Gain Fields for Visuo-Motor Coordinate Transformations: A Multi-Level Analysis of Neuronal Activity in Cortical Area MSTd

Lukas A. Brostek

Graduate School of
Systemic Neurosciences

LMU Munich

München 2012

Eye Velocity Gain Fields for Visuo-Motor Coordinate Transformations: A Multi-Level Analysis of Neuronal Activity in Cortical Area MSTd

Lukas A. Brostek

Dissertation
an der Graduate School of Systemic Neurosciences
der Ludwig–Maximilians–Universität
München

vorgelegt von
Lukas A. Brostek
aus Danzig

München, den 15.10.2012

Erstgutachter: Prof. Dr.-Ing. Stefan Glasauer
Zweitgutachter: Prof. Dr. Ulrich Büttner
Tag der mündlichen Prüfung: 19.12.2012

Summary

'Gain-field-like' tuning behavior is characterized by a modulation of the neuronal response depending on a certain variable, without changing the actual receptive field characteristics in relation to another variable. Eye position gain fields were first observed in area 7a of the posterior parietal cortex (PPC), where visually responsive neurons are modulated by ocular position. Analysis of artificial neural networks has shown that this type of tuning function might comprise the neuronal substrate for coordinate transformations.

In this work, neuronal activity in the dorsal medial superior temporal area (MSTd) has been analyzed with an focus on it's involvement in oculomotor control. MSTd is part of the extrastriate visual cortex and located in the PPC. Lesion studies suggested a participation of this cortical area in the control of eye movements. Inactivation of MSTd severely impairs the optokinetic response (OKR), which is an reflex-like kind of eye movement that compensates for motion of the whole visual scene.

Using a novel, information-theory based approach for neuronal data analysis, we were able to identify those visual and eye movement related signals which were most correlated to the mean rate of spiking activity in MSTd neurons during optokinetic stimulation. In a majority of neurons firing rate was non-linearly related to a combination of retinal image velocity and eye velocity. The observed neuronal latency relative to these signals is in line with a system-level model of OKR, where an efference copy of the motor command signal is used to generate an internal estimate of the head-centered stimulus velocity signal.

Tuning functions were obtained by using a probabilistic approach. In most MSTd neurons these functions exhibited gain-field-like shapes, with eye velocity modulating the visual response in a multiplicative manner. Population analysis revealed a large diversity of tuning forms including asymmetric and non-separable functions. The distribution of gain fields was almost identical to the predictions from a neural network model trained to perform the summation of image and eye velocity. These findings therefore strongly support the hypothesis of MSTd's participation in the OKR control system by implementing the transformation from retinal image velocity to an estimate of stimulus velocity. In this sense, eye velocity gain fields constitute an intermediate step in transforming the eye-centered to a head-centered visual motion signal.

Another aspect that was addressed in this work was the comparison of the irregularity of MSTd spiking activity during optokinetic response with the behavior during pure visual stimulation. The goal of this study was an evaluation of potential neuronal mechanisms underlying the observed gain field behavior. We found that both inter- and intra-trial variability were decreased with increasing retinal image velocity, but increased with eye velocity. This observation argues against a symmetrical integration of driving and modulating inputs. Instead, we propose an architecture where multiplicative gain modulation is achieved by simultaneous increase of excitatory and inhibitory background synaptic input. A conductance-based single-compartment model neuron was able to reproduce realistic gain modulation and the observed stimulus-dependence of neural variability, at the same time.

In summary, this work leads to improved knowledge about MSTd's role in visuomotor transformation by analyzing various functional and mechanistic aspects of eye velocity gain fields on a systems-, network-, and neuronal level.

Contents

1 Introduction

Vision is the sense humans most rely on. Seeing enables us to sense and perceive the world around us. By identifying the color, shape and movement of countless objects, our visual sense allows us to distinguish important from irrelevant things, as well as their position and velocity relative to us.

In humans, like in all primates and a number of other mammals and birds, eyes have developed in such a way that a relatively small part of the retina is populated by a comparatively high density of photoreceptor cells. This area is called fovea. Due to that, only a small part of our visual field is perceived in full sharpness and color. For compensation we perform frequent eye movements, capturing all interesting details of the visual scene. The composition of the full picture of the perceived environment from all these 'snappshots' happens subconsciously.

While enabling us to see the world in high detail, foveal vision also poses a number of challenges for the visual system. To prevent loss of small moving objects from our sight they need to be tracked by our eyes. On the other hand, we often see objects in motion not because they move in front of us, but because we move our eyes. Therefore, compensation of eye-movement induced visual motion is crucial for proper perception. Furthermore, to avoid blurred vision during self-motion through space, the visual image needs to be stabilized on the fovea. This task is accomplished by compensating optokinetic eye movements into the opposite direction of self-movement.

These examples demonstrate that both physiological systems for vision and the generation of eye movements need to be coupled. Today, there is strong evidence for the existence of specialized brain regions where this coupling might occur. This doctoral thesis focuses on the Medial Superior Temporal Cortex, a region assumed to perform such function.

In the following sections an introduction to the current state of scientific knowledge about the visual system, processing of visual motion, smooth pursuit, and optokinetic eye movements is given. Hereafter, the aim of this thesis is presented.

1.1 The Visual System

The visual system begins with the eyes, where photoreceptor cells in the retina transform light into electric signals. The density of photoreceptor cells is not uniform, but concentrated around the fovea, wich is an area of about one square millimeter diameter. Being much more than just a simple organ for sensing light, the eye already extracts an enormous amount of information about different facets of the visual image by it's retinal neural networks. Important parts of signal processing for visual motion detection, for instance, are realized by the network of retinal ganglion cells already (Gollisch and Meister, 2010).

The neuronal pathway that leaves the eye is called retinofugal projection (Fig. 1.1). Most of the optic nerve neurons innervate the lateral geniculate nucleus (LGN) of the dorsal thalamus. Neurons in the LGN give rise to axons that project to the primary visual cortex (V1) in the occipital lobe, which is also called striate cortex. V1 is organized retinotopically, meaning that neighboring cells in the retina feed information to neighboring places in the primary visual cortex (Hubel and Wiesel, 1962). Many neurons in V1 respond best to an elongated bar of light moving across their receptive fields. The greatest response is given to a bar with a particular orientation.

Signals from the striate cortex are projected to more than two dozens of different extrastriate cortical areas in the temporal and parietal lobes (Felleman and Van Essen, 1991). The extrastriate areas are functionally and anatomically subdivided into two major pathways. The ventral pathway is assumed to be involved in the perception of the visual world and the recognition of objects (Mishkin et al., 1983). It runs from the primary visual cortex into the infratemporal cortex. Neurons in area V4 have larger receptive fields than cells in the striate cortex and are selective for orientation and color. The inferior temporal lobe (IT) lies behind V4 and has complex spatial receptive fields. Neurons in this area respond to a variaty of colors and abstract shapes. A percentage of neurons responds even strongly to stimuli as complex as pictures of faces (Desimone, 1991). Therefore, this area is presumed to be important for visual perception and visual memory.

The dorsal pathway, on the other hand, projects from the primary visual cortex into the posterior parietal cortex. This pathway is assumed to carry information regarding the movement of visual objects and self-motion and will be reviewed in the following section.

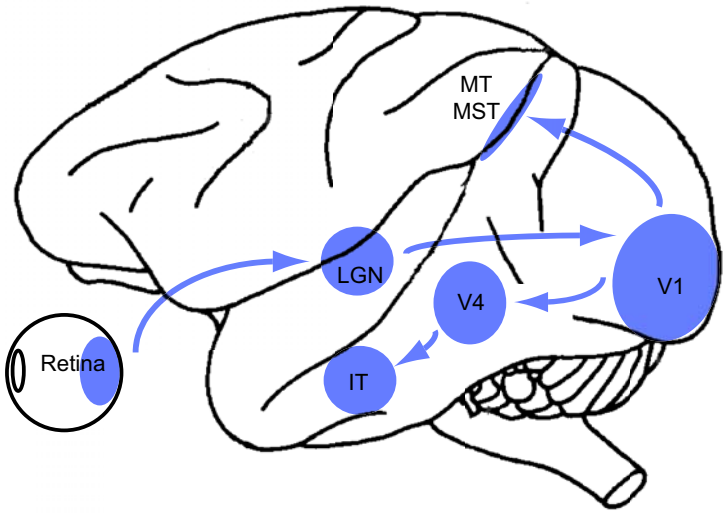

Figure 1.1: The visual system. The retinofugal projection innervates the lateral geniculate nucleus (LGN) and then projects to primary visual cortex (V1). From there the ventral pathway goes to V4 and the inferior temporal lobe (IT). The dorsal pathway projects to the middle temporal (MT) and medial superior temporal (MST) areas. (According to Mishkin et al. (1983))

1.2 Processing of Visual Motion

Two areas in the dorsal pathway are assumed to be crucial for visual motion processing: the middle temporal (MT) and medial superior temporal (MST) areas in the parietal cortex.

1.2.1 The Middle Temporal Cortex

MT is located in the posterior bank of the superior temporal sulcus and is one of the most studied areas in macaque cortex. MT is also known as visual area 5 (V5) and receives retinotopically organized input from a number of other cortical areas such as V2 and V3, and is also directly innervated by cells in the striate cortex. Cells in this area have larger receptive fields than V1.

Visual responses of MT neurons are determined principally by several properties of the stimulus: retinal position, direction and speed of motion (Maunsell and Van Essen, 1983a), stimulus size (Born and Tootell, 1992), and binocular disparity (Maunsell and Van Essen, 1983b). Whether or not MT receives other than retinal input, is still disputed (Newsome et al., 1988). A recent work suggests that MT neurons use eye movement signals to code depth-sign from motion parallax (Nadler et al., 2009).

Lesions in macaque cortical area MT produce motion-perceptual (Newsome and Pare, 1988) and oculomotor (Dürsteler and Wurtz, 1988) deficits. Electrical microstimulation of MT neurons influences perceptuel judgements of motion direction (Salzman et al., 1990). Further support for the idea of MT's involvement in the processing of visual motion comes from the finding that in a motion direction discrimination task the trial-to-trial variability in MT neuronal signals is correlated with the choices the monkey makes (Britten et al., 1996).

MT's key output target stuctures are implicated in the analysis of optic flow and the generation of eye movements (Mishkin et al., 1983). Further along the dorsal pathway lies a region with more specialized types of movement selectivity: area MST, which is reviewed in the following paragraph.

1.2.2 The Medial Superior Temporal Cortex

The medial superior temporal cortex (MST) is part of the posterior parietal lobe and receives direct projections from adjacent area MT. MST is usually divided into two subregions with different functional properties: the dorsal (MSTd), and the ventrolateral region (MSTl).

Many MST neurons respond to visual stimuli and have large, often bilateral, receptive fields exceeding 15 degree of the visual field (Komatsu and Wurtz, 1988). The neuronal latency to visual stimulation is about 50 ms (Kawano et al., 1994). MSTd neurons respond to rotating, expanding and planar large field motion. The neuronal response is invariant of the position, form and size of these optic patterns (Duffy and Wurtz, 1991). MST neurons modulate their visual response when the field of expansion is shifted (Duffy and Wurtz, 1995) or when the rate of expansion changes (Duffy and Wurtz, 1997). As in area MT, neurons in MST are selective for binocular disparity (Roy et al., 1992).

There is strong evidence that, aside from retinal input, MST receives extraretinal input as well. Many MSTd and some MSTl cells show strong modulation during smooth pursuit eye movements and continue firing during blinking of the target. In MSTl neuronal response starts before the onset of eye movements (Ilg et al., 2004). On the contrary, in most of the MSTd neurons the pursuit response begins after the onset of eye movements (Newsome et al., 1988). Many neurons also respond to an imaginary target (Ilg and Thier, 2003). During fixation as well as smooth pursuit eye movements, the response of most MST neurons to a visual stimulus is modulated by eye position (Bremmer et al.,

1997). Another extraretinal input is provided by the vestibular system. Two thirds of MSTd neurons that are sensitive to optic flow also show spatial tuning for inertial motion without optic flow, pointing out to vestibular input (Gu et al., 2007).

Due to these characteristics, three functional roles have been proposed for this area. First, MST is probably involved in the perception of motion. Lesions in MST produce similar motion-perceptual deficits as in area MT (Rudolph and Pasternak, 1999). Second, MST might be involved in the generation of smooth pursuit and optokinetic eye movements. This assumption is also supported by lesion studies (Dürsteler and Wurtz, 1988). Third, MST is probably involved in the integration of visual and vestibular motion cues for the perception of heading direction during self-motion. This was shown by studies, where the behavioral estimates of direction of self-motion were affected after electrical stimulation of MST neurons (Britten and van Wezel, 1998). In regard of this view, it is supposed that MSTd might compensate for self generated eye movements in heading perception (Bradley et al., 1996).

1.3 Tracking Eye Movements

A distinction is made between the voluntary tracking or pursuit of small moving objects and the involuntary tracking of a moving large-field visual scene.

1.3.1 Smooth Pursuit Eye Movements

Developed in mammals with frontal eyes only, the smooth pursuit eye movement (SPEM) system is an evolutionary young feature. SPEMs are used for tracking small moving objects within the high-acuity region near the fovea. Pursuit usually only occurs in response to a moving visual stimulus. Pursuit eye movements are most effective when the target speed is relatively slow. Like saccades, SPEMs are voluntary eye movements. The movement initiation latency is usually about 100–150 ms, which is generally shorter than for saccades. Both humans and monkeys can reach maximum pursuit velocities of about $80 - 100\,^{\circ}/_{\mathrm{s}}$ (Lisberger et al., 1981).

SPEMs are already present in 4-week-old infants and are fully developed at about 3 months of age (Phillips et al., 1997). Even at higher ages, the SPEM system stays adaptive. When patients with ocular muscle weakness are forced to view monocularly with their weak eye for several days, the pursuit system shows changes in the movements of the normal eye consistent with an increased central innervation designed to decrease the time

it takes to bring the target's image onto the fovea of the weak eye and to keep it there (Optican et al., 1985). Another form of adaptation in the pursuit system is the so called smooth pursuit gain modulation. When a stimulus is presented with brief perturbations superimposed on the target movement, pursuit of these perturbations gets better with increasing eye velocity (Churchland and Lisberger, 2001, 2002). Furthermore, the SPEM system is highly predictive. When subjects follow a target moving on a periodically repeating trajectory, they are able to anticipate changes in target motion after one period only and follow them without further delay (Barnes and Asselman, 1991).

In the view of control system theory, the tracking eye movement system can be seen as a negative feedback servo control (Fig. 1.2) whose function is to pursue the image of a small moving object on the fovea. The difference between stimulus and eye velocity is called retinal slip or image velocity. It is sensed by the retina and then further processed by the dorsal pathway of the visual system. In a simple negative feedback system, this image velocity signal could serve already as control command to the eye plant. However, to replicate the actual temporal characteristics observed in humans and monkeys, the implemantation of an additional internal feedback has been proposed (Robinson et al., 1986). The addition of an efference copy of the oculomotor command allows the estimation of the stimulus velocity signal, which then serves as the central control command. The efferent pathways project this signal to motoneurons, and the eyeball, including the retina, is moved in an effort to match eye and stimulus motion.

The neuronal basis of the pursuit control circuit is shown in Fig. 1.3. It is assumed that two parallel pathways are involved in the generation of SPEMs (Büttner and Büttner-Ennever, 2006; Nuding et al., 2008). One path includes the dorsal visual stream, pons and cerebellum. As described in the previous sections, areas MT and MST are the sources of visual motion information. Lesion studies (Dürsteler and Wurtz, 1988) and microstimulation (Komatsu and Wurtz, 1989) give strong evidence for the involvement of areas MT and MSTl in the generation of SPEMs. It is assumed that the dorsal subpart MSTd plays a minor role in pursuit (Newsome et al., 1988). Area MST projects to the dorsolateral pontine nuclei (DLPN) (Distler et al., 2002). Lesions in this area produce mainly ipsilateral SPEM deficits (May et al., 1988). DLPN projects to the flocculus (FL) in the cerebellum, where lesions also impair the pursuit system (Zee et al., 1981). From the FL originate projections to the vestibular nuclei (VN) in the brainstem, from where SPEM signals can reach the oculomotor nuclei (OMN).

The second pathway in the SPEM system includes the frontal cortex, brainstem and

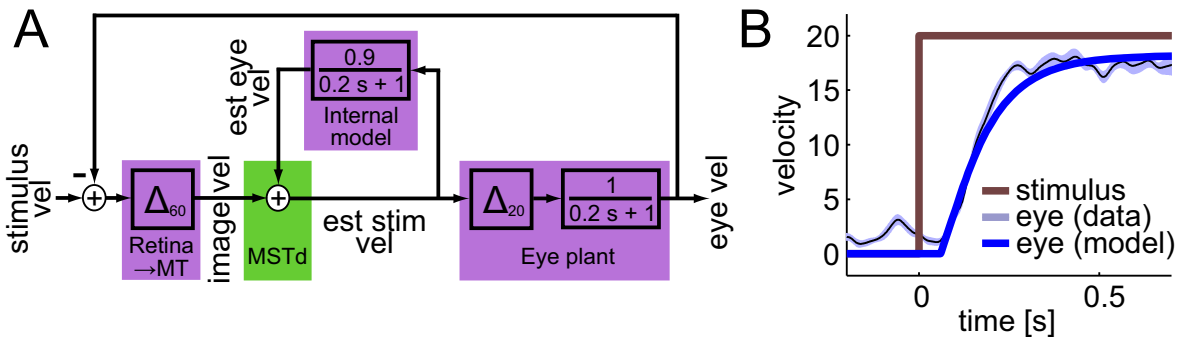

Figure 1.2: (A) Computational model of the tracking eye movement control system. Image velocity is the difference between stimulus and eye velocity. The internal eye plant model provides an efference copy, which is used to estimate stimulus velocity. This signal serves as control signal for the eye plant. This simple model does not account for any latencies, nor adaptive and predictive mechanisms. Latencies were chosen to fit OKR charakteristics. (B) The step function response of the model (blue) for a sudden increase in stimulus velocity (brown). The light blue trace shows example eye velocity data. (see section 2.5)

cerebellum. Areas MT and MST have reciprocal connections with the frontal eye fields (FEF). Lesions in the FEF in monkeys (Shi et al., 1998) and humans (Morrow and Sharpe, 1995) cause severe ipsidirectional deficits particularly in predictive aspects of SPEM. FEF projects mainly to the nucleus reticularis tegmenti pontis (NRTP) (Ono et al., 2005). NRTP has neuronal connections to the ocular vermis (OV) and the paraflocculus (Glickstein et al., 1994) in the cerebellum. Lesions in OV lead to SPEM deficits (Takagi et al., 2000). OV projects to the caudal part of the fastigial nucleus in the vermis, where lesions also impair SPEM (Robinson et al., 1997). In addition to the two pathways mentioned, it is known that the basal ganglia (Basso et al., 2005) and thalamus (Tanaka, 2005) are involved in the SPEM system.

1.3.2 Optokinetic Response

The optokinetic response (OKR) describes reflex driven eye movements that compensate for motion of the entire visual scene as occurs with self-motion through space. OKR eye movements move in the direction of visual motion, thus improving image stabilization on the retina. The combination of OKR and fast resetting saccades during unidirectional stimulation is called optokinetic nystagmus (OKN), which plays an important role in maintaining maximal periods of clear vision during continuous uni-directional movement of the visual scene (Leigh and Zee, 2006).

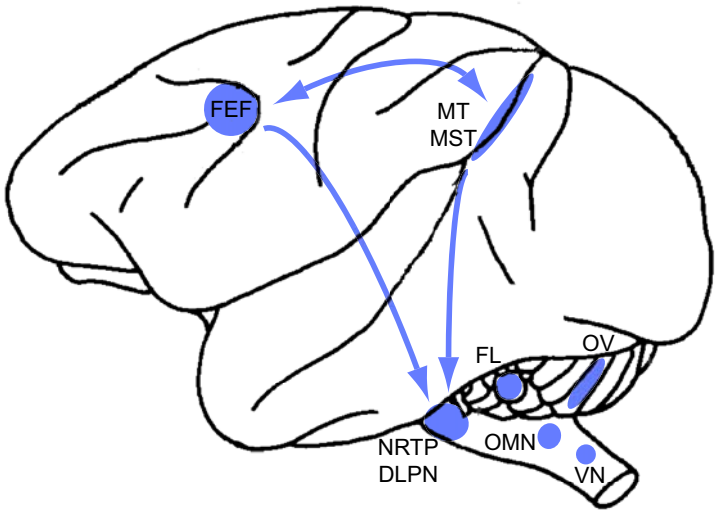

Figure 1.3: The two cortical pathways of the tracking eye movement system. The first pathway is shared by both SPEM and OKR. It originates from areas MT/MST and projects to the dorsolateral pontine nuclei (DLPN). From there go connections to the flocculus (FL), which projects to the vestibular nuclei (VN) and oculomotor nuclei (OMN). The second pathway is assumed to be part of the SPEM system only. It originates in the frontal eye fields (FEF) and goes to the nucleus reticularis tegmenti pontis (NRTP). From there go connections to the ocular vermis (OV), which projects to the fastigial nucleus in the vermis. Areas MT/MST and the FEF are connected reciprocally. (According to Büttner and Büttner-Ennever (2006))

In the generation of OKR two components can be distinguished. The direct component occurs shortly after the onset of the optokinetic stimulus and is also known as ocular following response (OFR). The term OFR generally refers to the immediate OKR response after the motion onset of a large visual stimulus (Miles, 1998). The indirect component leads to a more gradual increase in slow-phase eye velocity during continuous stimulation. OFR has a short latency of about 50 ms in monkeys (Miles et al., 1986) and 70 ms in humans (Gellman et al., 1990), which is shorter than the 100-150 ms for SP eye movements. This in addition to the size of the visual stimulus and the involuntary character of the eye movements are major features to differentiate between OKR and SPEM. For extended stimulation, OKN can reach velocities of about 180 deg/s in monkeys, and about 120 deg/s in humans (Cohen et al., 1977). These velocities are the sum of the direct and indirect components of OKN.

The major neuronal pathways for generation of the indirect component of OKR seem to lie in the brainstem. Fibers from the retina terminate in the nuclei of the accessory optic tract and the nucleus of the optic tract (Büttner and Büttner-Ennever, 2006). During

OKN also the vestibular nuclei are activated (Waespe and Henn, 1987). The cerebellum is not thought to be involved in the indirect component of OKR (Büttner and Waespe, 1984). Although the indirect component is basically transmitted via brainstem pathways, these pathways are under cerebral cortical control, particularly in humans and monkeys. Accordingly, bilateral occipital lesions impair the indirect OKR component (Zee et al., 1981).

For the direct component of OKR, there is strong evidence for involvement of similar neuronal areas as used for the generation of SPEM (Fig. 1.3). Both, pursuit and optokinetic eye movements are severely impaired following lesions of areas MT/MST (Dürsteler and Wurtz, 1988; Takemura et al., 2007), DLPN (May et al., 1988), flocculus (Zee et al., 1981) or Vermis (Takagi et al., 2000). The involvement of MST in the direct component of OKR has also been shown in a number of other studies. The response latencies of MST neurons change in parallel with the response latencies of the simultaneously observed eye movements when different visual stimuli are used to elicit OKR (Kawano et al., 1994). Moreover, many MSTd neurons reflect the post-saccadic enhancement of the OKR/OFR in their neuronal response (Takemura and Kawano, 2006). The fronto-cortical SPEM pathway, however, seems to be less involved in the generation of OKR. Bilateral lesions of the FEF slowed SPEM but did not affect the OKR (Keating et al., 1996).

1.4 Neuronal Data Analysis

This section provides a brief introduction to selected techniques in neuronal data analysis. The objective of all these methods is a characterization and identification of the underlying neural information processing system.

1.4.1 Regression Analysis

Regression analysis is the estimation of the dependency of a *dependent* variable on some other *independent* variables. In the most commonly used form of linear regression analysis, the maximum likelihood estimate of parameters $\underline{\beta}$ from observations $\underline{x}$ is determined using a linear model $\mathbf{C}$ according to

$$\underline{x} = \mathbf{C} \cdot \underline{\beta} + \underline{r}, \tag{1.1}$$

with $\underline{r}$ denoting normally distributed residual error. The solution is given by the 'pseudo inverse' of $\mathbf{C}$

$$\underline{\beta} = (\mathbf{C}^T \cdot \mathbf{C})^{-1} \cdot \mathbf{C}^T. \tag{1.2}$$

In neural data analysis, the observations $\underline{x}$ are typically given by the neuronal firing rate (FR), whereas the linear model is composed of n stimulus- and/or behavior-related variables ($\underline{var}$):

$$FR = \beta_0 + var_1 \cdot \beta_1 + \ldots + var_n \cdot \beta_n. \tag{1.3}$$

The dependency of the firing rate on the different independent variables is then expressed by parameters $\underline{\beta}$.

1.4.2 Information-theoretic Approaches

Information-theory based methods offer an alternative to model-based approaches of system identification. This technique allows the estimation of dependency of neuronal activity on certain independent variables without further assumptions on the exact form of this dependency.

Entropy $H(X)$ is a measure for the uncertainty of a single random variable X. The reduction in uncertainty due to another random variable is called 'mutual information' (Shannon and Weaver, 1949; Cover and Thomas, 1991). For two random variables X and Y with probability distributions $p(x)$ and $p(y)$ the mutual information is

$$I(X;Y) = H(Y) - H(Y|X). \tag{1.4}$$

The entropy of Y and the conditional entropy of Y given X are defined as

$$H(Y) = -\sum_{Y} p(y) \log p(y) \tag{1.5}$$

$$H(Y|X) = -\sum_{X} p(x) \sum_{Y} p(y|x) \log p(y|x), \tag{1.6}$$

with $p(y|x)$ being the conditional probability distribution of Y given X. The mutual information is a measure for the dependence between the two random variables. It is symmetric in X and Y, always non-negative, and equal to zero only if X and Y are mutually independent.

In analysis of neuronal data, mutual information is usually used to determine how much information spiking activity carries about some stimulus- or behavior-related variable. One means of estimating the information contained in the neuronal response is comparing the occurence of specific spiking patterns over a large number of trials where the same stimulus was presented and the same behavior was consistently observed (Rieke et al., 1997; Borst and Theunissen, 1999). Alternatively, the information of the spiking rate can

be determined, ignoring certain patterns of spiking activity. The latter approach will be further elaborated in sections 2.2 and 2.3.

1.4.3 Neuronal Variability

The term 'neuronal variability' usually refers to the regularity of spiking activity. Investigating the temporal structure of the neuronal response allows a characterization of the spiking process and puts certain constraints on the amount of transmitted information and the underlying neuronal structure. Analysis of neuronal variability is therefore one of the elementary system identification techniques in neuroscience.

Neuronal variability can be measured in various ways. The two most commonly used measures are the Fano factor (FF) and the coefficient of variation (CV). The FF (Fano, 1947) measures the variability of the spike count *across* trials which were recorded during identical conditions according to

$$FF = \frac{Var[SC]}{E[SC]}, \tag{1.7}$$

with E and Var symbolizing mean and variance, respectively, and SC denoting the spike counts of the trials. The FF is usually determined for time intervals of 50 or 100 ms length and analyzed over time.

The CV (Cox and Lewis, 1966), on the other hand, determines the variability of the inter-spike intervals *within* a single trial:

$$CV = \frac{\sqrt{Var[ISI]}}{E[ISI]}, \tag{1.8}$$

with $ISI = [isi_1, isi_2, \ldots, isi_n]$ denoting the inter-spike intervals of each analyzed spike train.

For a stationary renewal process, in which inter-spike intervals are assumed to be independent and identically distributed, it holds that

$$FF = CV^2 \tag{1.9}$$

for the limit of long observations (Cox and Lewis, 1966).

The special case where the number of spikes in non-overlapping intervals is independent for all intervals, and the probability to obtain an event in the interval $[t, t + \Delta t]$ equals $\lambda \cdot \Delta t$, is called 'Poisson process'. The inter-spike interval distribution of this homogeneous point process has the exponential form

$$P(ISI) = \lambda \cdot e^{-\lambda \cdot ISI}. \tag{1.10}$$

For the Poisson process, it holds that

$$FF = CV = 1 \tag{1.11}$$

for the limit of long observations (Cox and Lewis, 1966).

1.5 Aim of this Thesis

During the recent decades a lot of knowledge about eye movements has been gained. The psychophysical properties of smooth pursuit and optokinetic eye movements have been thoroughly investigated. Based on these findings and control system theory, computational models were developed to simulate the different oculomotor systems. From these models we can learn which signals need to be provided to the oculomotor system to produce the observed behaviour. Furthermore, computational models propose architectures for the processing of signals and give an idea which mathematical operations could be performed by the neuronal structures.

From the anatomical and physiological point of view, a variety of brain regions is assumed to be involved in visual processing and control of eye movements. Focal lesion and electrical microstimulation studies not only determine whether some area is involved in a specific task or not. Often the observed deficits allow conclusions about the function of the analyzed area. Recording the neuronal activity in a specific brain area allows further analysis. Electrophysiological studies enable us to determine constraints on the kind and amount of information coded by a neuronal population. The onset latency of neuronal activity allows conclusions about the signal flow.

Today much is known about the early parts of the visual system and the first steps in processing of visual inputs. There is strong evidence that areas MT and MST are involved in the perception of visual motion. Yet, their exact function in participation and control of tracking eye movements is still not known.

The aim of this doctoral thesis is analyzing monkey neuronal recordings from area MSTd during optokinetic eye movements. Using system identification techniques and information theory, the goal is to better understand the information coded by MSTd neurons in the context of eye movements. MSTd's functional role will be evaluated and a link between MSTd and the optokinetic system established. A substantial part of this work focuses on the question of how information might be encoded in general by MSTd neurons, as the analysis of electrophysiological data requires understanding of neuronal coding mechanisms. Trying to understand neuronal processes in a deeper level, we will not only be focusing on the analysis of neuronal firing rates, but further will investigate aspects like the intra- and inter-trial variability of the spiking activity. The following section presents all studies that were performed within the scope of this doctoral thesis.

2 Cumulative Thesis

This cumulative thesis consists of four studies that were peer-reviewed and accepted for publication in scientific journals. Furthermore, one submitted manuscript, and an additional results section were included. In the following, the abstracts of the papers are presented. The contribution of the author of this doctoral thesis to the respective publications is indicated. The full published papers and the submitted manuscript are enclosed in the appendix of this thesis.

2.1 The Response of MSTd Neurons to Perturbations in Target Motion During Ongoing Smooth-Pursuit Eye Movements

Ono S, Brostek L, Nuding U, Glasauer S, Büttner U, Mustari MJ (2010). The Response of MSTd Neurons to Perturbations in Target Motion During Ongoing Smooth-Pursuit Eye Movements. *J Neurophysiol* 103: 519-530.

Several regions of the brain are involved in smooth-pursuit eye movement (SPEM) control, including the cortical areas MST (medial superior temporal) and FEF (frontal eye field). It has been shown that the eye-movement responses to a brief perturbation of the visual target during ongoing pursuit increases with higher pursuit velocities. To further investigate the underlying neuronal mechanism of this nonlinear dynamic gain control and the contributions of different cortical areas to it, we recorded from MSTd (dorsal division of the MST area) neurons in behaving monkeys (Macaca mulatta) during step-ramp SPEM ($5 - 20\,^{\circ}/_{s}$) with and without superimposed target perturbation (one cycle, 5 Hz, $10\,^{\circ}/_{s}$). Smoothpursuit related MSTd neurons started to increase their activity on average 127 ms after eye-movement onset. Target perturbation consistently led to larger eye-movement responses and decreasing latencies with increasing ramp velocities, as predicted by dynamic gain control. For 36% of the smooth-pursuitrelated MSTd neurons the eye-movement perturbation was accompanied by detectable changes in neuronal activity with a latency of 102 ms, with respect to the eye-movement response. The remaining smooth-pursuitrelated MSTd neurons (64%) did not reflect the eye-movement perturbation. For the large majority of cases this finding could be predicted by the dynamic properties of the step-ramp responses. Almost all these MSTd neurons had large visual receptive fields responding to motion in preferred directions opposite to the optimal SPEM stimulus. Based on these findings it is unlikely that MSTd plays a major role for dynamic gain control and initiation of the perturbation response. However, neurons in MSTd could still participate in SPEM maintenance. Due to their visual field properties they could also play a role in other functions such as self-motion perception.

The author of this doctoral thesis contributed to this work by performing the data analysis, writing parts of the manuscript and designing the figures.

2.2 An Information-theoretic Approach for Evaluating Probabilistic Tuning Functions of Single Neurons

Brostek L, Eggert T, Ono S, Mustari MJ, Büttner U, Glasauer S (2011). An Information-Theoretic Approach for Evaluating Probabilistic Tuning Functions of Single Neurons. *Front Comput Neurosci* 5: 15.

Neuronal tuning functions can be expressed by the conditional probability of observing a spike given any combination of explanatory variables. However, accurately determining such probabilistic tuning functions from experimental data poses several challenges such as finding the right combination of explanatory variables and determining their proper neuronal latencies. Here we present a novel approach of estimating and evaluating such probabilistic tuning functions, which offers a solution for these problems. By maximizing the mutual information between the probability distributions of spike occurrence and the variables, their neuronal latency can be estimated and the dependence of neuronal activity on different combinations of variables can be measured. This method was used to analyze neuronal activity in cortical area MSTd in terms of dependence on signals related to eye and retinal image movement. Comparison with conventional feature detection and regression analysis techniques shows that our method offers distinct advantages, if the dependence does not match the regression model.

The author of this doctoral thesis contributed to this work by developing the novel data analysis approach, performing the data analysis, writing the manuscript and designing the figures.

2.3 A Method for Evaluating Tuning Functions of Single Neurons based on Mutual Information Maximization

Brostek L, Eggert T, Ono S, Mustari MJ, Büttner U, Glasauer S (2011). A Method for Evaluating Tuning Functions of Single Neurons based on Mutual Information Maximization. *AIP Conf Proc* 1305: 423–429.

We introduce a novel approach for evaluation of neuronal tuning functions, which can be expressed by the conditional probability of observing a spike given any combination of independent variables. This probability can be estimated out of experimentally available data. By maximizing the mutual information between the probability distribution of the spike occurrence and that of the variables, the dependence of the spike on the input variables is maximized as well. We used this method to analyze the dependence of neuronal activity in cortical area MSTd on signals related to movement of the eye and retinal image movement.

The author of this doctoral thesis contributed to this work by developing the data analysis approach, performing the data analysis, writing the manuscript and designing the figures.

2.4 Neuronal Variability of MSTd Neurons Changes Differentially With Eye Movement and Visually Related Variables

Brostek L, Büttner U, Mustari MJ, Glasauer S (2012). Neuronal Variability of MSTd Neurons Changes Differentially With Eye Movement and Visually Related Variables. *Cereb Cortex* in press.

Neurons in macaque cortical area MSTd are driven by visual motion and eye movement related signals. This multimodal characteristic makes MSTd an ideal system for studying the dependence of neuronal activity on different variables. Here we analyzed the temporal structure of spiking patterns during visual motion stimulation using two distinct behavioural paradigms: fixation and optokinetic response. For the fixation condition inter- and intra-trial variability of spiking activity decreased with increasing stimulus strength, complying with a recent neurophysiological study reporting stimulus-related decline of neuronal variability. In contrast, for the optokinetic condition variability increased together with increasing eye velocity while retinal image velocity remained low. Analysis of stimulus signal variability revealed a correlation between the normalized variance of image velocity and neuronal variability, but no correlation with normalized eye velocity variance. We further show that the observed difference in neuronal variability allows classifying spike trains according to the paradigm used, even when mean firing rates were similar. The stimulus-dependence of neuronal variability may result from the local network structure and/or the variability characteristics of the input signals, but may also reflect additional timing-based mechanisms independent of the neuron's mean firing rate and related to the modality driving the neuron.

The author of this doctoral thesis contributed to this work by designing the experiment, performing the data analysis, writing the manuscript and creating the figures.

2.5 Eye Velocity Gain Fields in MSTd for Visuomotor Coordinate Transformations

Brostek L, Büttner U, Mustari MJ, Glasauer S. Eye Velocity Gain Fields in MSTd for Visuomotor Coordinate Transformations. *Submitted.*

Lesion studies argue for an involvement of cortical area MSTd in the control of optokinetic response (OKR) eye movements. Neurons in this area respond to visual motion and eye movement related signals. However, MSTd's function in visuomotor transformation is still unclear. Using a novel approach for characterizing neural tuning with high resolution, we show that during optokinetic stimulation the majority of MSTd neurons exhibits gain field-like tuning functions. Rather than coding one variable, neural responses showed a large diversity of tuning to combinations of retinal and extra-retinal input. Eye velocity related activity was observed prior to the actual eye movements, reflecting an efference copy. The observed tuning functions resembled those emerging in a network model trained to perform summation of two population-coded signals. Together, our findings support the hypothesis that MSTd implements the transformation from retinal to head-centered stimulus velocity signals for the control of OKR.

The author of this doctoral thesis contributed to this work by designing the experiment, performing the data analysis, developing the computational models, writing the manuscript and creating the figures.

2.6 Gain Modulation from Balanced Excitatory-Inhibitory Synaptic Input

In this section additional results are presented which have not been published or submitted for publication yet.

Cortical neurons *in vivo* continuously receive input from thousands of excitatory and inhibitory synapses (Kandel et al., 2000). Given a 'spontaneous' average firing rate of 5-20 Hz in neocortical neurons, the resulting synaptic currents present a significant influence on the integrative properties of the target neuron. Here, we investigated whether this synaptic background activity may explain the gain-field-like tuning behavior we observed in MSTd neurons. First, we present a point-conductance neural model proposed by Destexhe et al. (2001) to analyze the influence of balanced excitatory and inhibitory input on neuronal gain. After this, we compare the predictions from this model with our MSTd data shown in Brostek et al. (2012).

To represent the currents generated by thousands of stochastically releasing synapses a point-conductance model was used. Synaptic activity was represented by two independent fast glutamatergic and GABA-ergic conductances described by stochastic random-walk processes (Destexhe et al., 2001).
The total synaptic current I_{syn} was decomposed into a sum of two independent conductances:

$$I_{syn} = g_e(t)(V - E_e) + g_i(t)(V - E_i) \tag{2.1}$$

where $g_e(t)$ and $g_i(t)$ are time-dependent excitatory and inhibitory conductances, and E_e and E_i their reversal potentials, respectively. The conductances $g_e(t)$ and $g_i(t)$ were described by a one-variable stochastic process similar to the Ornstein-Uhlenbeck process (Uhlenbeck and Ornstein, 1930):

$$\frac{dg_e(t)}{dt} = -\frac{1}{\tau_e}[g_e(t) - g_{e0}] + \frac{\sqrt{2}\sigma_e}{\sqrt{\tau_e}}\chi_1(t) \tag{2.2}$$

$$\frac{dg_i(t)}{dt} = -\frac{1}{\tau_i}[g_i(t) - g_{i0}] + \frac{\sqrt{2}\sigma_i}{\sqrt{\tau_i}}\chi_2(t) \tag{2.3}$$

where g_{e0} and g_{i0} are average conductances, τ_e and τ_i are time constants, σ_e and σ_i are 'diffusion' standard deviations, and $\chi_1(t)$ and $\chi_2(t)$ are Gaussian white noise of zero mean and unit standard deviation. The parameters for this random-walk process were adapted from Destexhe et al. (2001) and are shown in table 2.1.

The stochastic point-conductance model of background synaptic input activity was inserted into a single compartment Hodgkin-Huxley-type model (Hodgkin and Huxley, 1952), shown in Fig. 2.1A:

$$C_m \frac{dV}{dt} = -g_L(V - E_L) - I_{Na} - I_K - I_M - \frac{1}{a} I_{syn} - I_{inj} \quad (2.4)$$

$$I_{Na} = g_{Na} m^3 h (V - E_{Na}) \quad (2.5)$$

$$I_K = g_K n^4 (V - E_K) \quad (2.6)$$

$$I_M = g_M p (V - E_K) \quad (2.7)$$

where C_m is the specific membrane capacitance, g_L is the leak conductance density, and E_L ist the leak reversal potential. I_{Na} is the voltage-dependent Na^+ current and I_K is the 'delayed-rectifier' K^+ current responsible for action potentials. I_M is a non-inactivating K^+ current responsible for slow afterhyperpolarization and spike frequency adaptation. The parameters of the gating variables m, h, n, and p were the same as in Destexhe et al. (2001). All other parameters were also adapted for the originally modeled layer VI pyramidal cell from cat parietal cortex and are shown in table 2.2. $a = 34636\ \mu m^2$ is the total membrane area of the modeled neuron, and I_{inj} is an additionally injected input current.

To analyze in what way the level of background synaptic input is modulating the gain of a neuronal response to an excitatory 'driving' signal, we determined firing rate and trial-to-trial variability of the model neuron for different values of I_{inj} and I_{syn} (Fig. 2.1B). In the latter case, excitatory and inhibitory currents were scaled with the same factor, denoted at the ordinate of the figure. The scaling of I_{syn} affects both mean and standard deviation of synaptic input currents, which corresponds to increases of overall synaptic activity and higher correlation of synaptic inputs, respectively (Fellous et al., 2003). For each condition 100 trials of 1000 ms length were simulated. The Fano factor was determined for a window length of 100 ms and averaged over the whole trial. As the figure shows, the firing rate increased with an increase of I_{inj}, which was enhanced for higher values of I_{syn}. This tuning strongly resembles the gain-field-like behavior we have observed in MSTd neurons. In this sense, I_{inj} would correspond to the 'driving' image velocity input,

Table 2.1: Parameters of the two random-walk processes

E_e	$0\ mV$	E_i	$-75\ mV$
g_{e0}	$0.0121\ \mu S$	g_{i0}	$0.0573\ \mu S$
σ_e	$0.003\ \mu S$	σ_i	$0.0066\ \mu S$
τ_e	$2.728\ ms$	τ_i	$10.49\ ms$

Table 2.2: Parameters of the Hodgkin-Huxley-type model

E_{Na}	$45\ mV$	g_{Na}	$120\ \frac{mS}{cm^2}$
E_K	$-82\ mV$	g_K	$100\ \frac{mS}{cm^2}$
E_L	$-80\ mV$	g_L	$0.045\ \frac{mS}{cm^2}$
		g_M	$1\ \frac{mS}{cm^2}$

whereas different levels of I_{syn} could be interpreted as changes of the 'modulatory' eye velocity signal.

In contrast to the firing rate, trial-to-trial variability of spiking activity showed differential behavior for increasing values of I_{inj} and I_{syn} (Fig. 2.1B2). An increase of synaptic background activity caused a strong increase of the Fano factor, whereas neural variability exhibited little dependency or even a small decline for increasing values of I_{inj}. This finding is in good accordance with our data. In Brostek et al. (2012) we analyzed neuronal variability of MSTd neurons during two different conditions: fixation with visual stimulation (FIX) and optokinetic response (OKR). For FIX, the monkey's task was to fixate a a small target spot located at the center of the screen. After some random time the LF stimulus started to move with constant velocity in the neurons preferred direction for a period between 1000 and 1800 ms. During OKR, the spot was turned off and the monkey's eye movements followed the visual motion. As shown in Fig. 2.2, the Hodgking-Huxley-type neural model exhibits very similar behavior in firing rate and trial-to-trial variability of spiking activity like MSTd neurons when either the 'driving' signal, or 'modulatory' signal is increased, while the other signal is held close to zero. In the following section we will discuss the implications of this finding on a potentially underlying neuronal structure that exhibits gain-field-like tuning behavior.

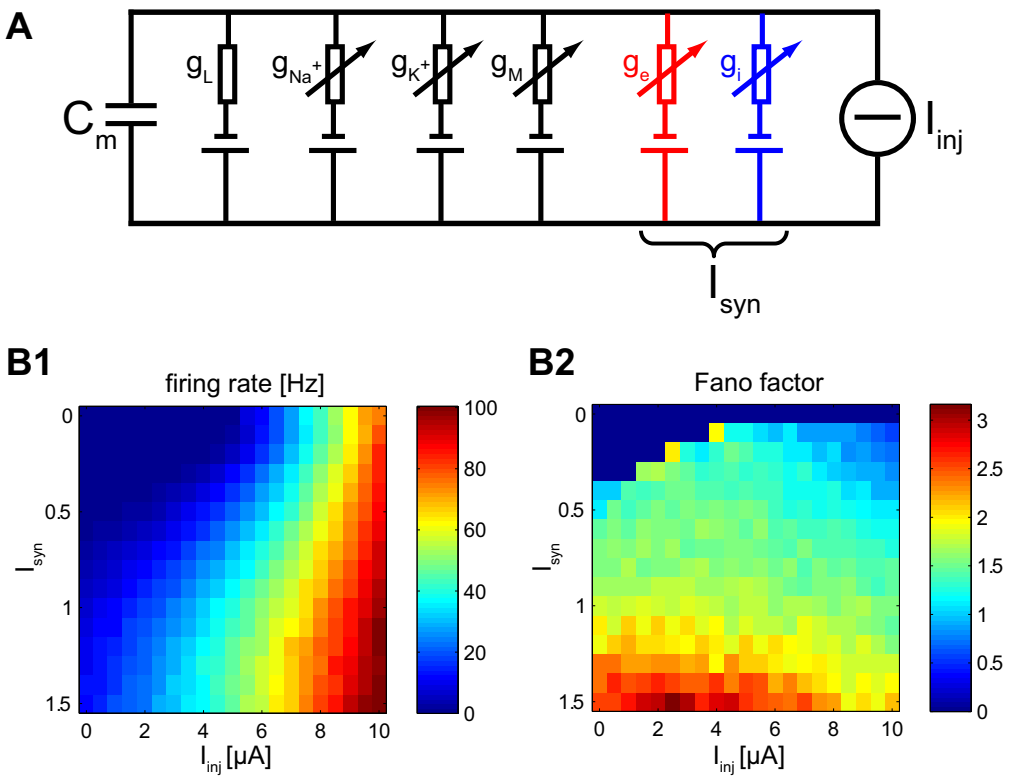

Figure 2.1: *(A)* Hodgking-Huxley-type neural model. I_{syn} describes the background synaptic input consisting of excitatory and inhibitory stochastic currents. I_{inj} is an additionally injected input current. *(B)* Firing rate and Fano factor of the Hodgking-Huxley-type neural model depending on I_{inj} and I_{syn}. Dark blue areas mark conditions in which no spiking activity occured.

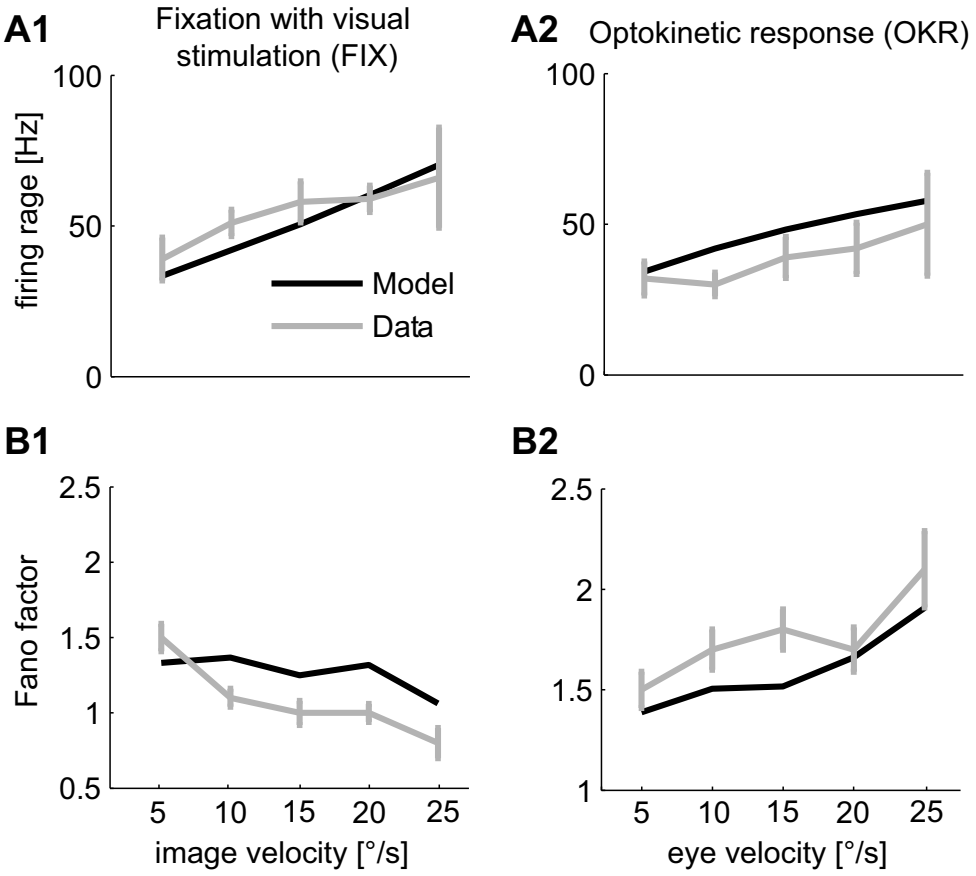

Figure 2.2: Firing rate *(A)* and Fano factor *(B)* of the Hodgking-Huxley-type neural model (black) and MSTd neurons (grey) during fixation with visual stimulation (FIX) and optokinetic response (OKR). For the model data, I_{inj} was increased from 6.3 to 9 μA during FIX. During OKR, the scaling factor of I_{syn} was increased from 0.5 to 1.2. The MSTd data is from Brostek et al. (2012). Vertical lines mark standard errors.

3 Discussion

Within the framework of this doctoral thesis several aspects of neuronal activity in cortical area MSTd have been investigated. Focusing on the neuronal responses during optokinetic response (OKR) and smooth pursuit (SP), we were able to improve scientific knowledge regarding the involvement of MSTd in these kinds of tracking eye movements. We analyzed the function of eye velocity gain fields in the context of tracking eye movements on both systems and network level. Furthermore, we explored potential underlying mechanisms of gain modulation on the neuronal level.

To allow a model-free analysis of neuronal tuning behavior, we developed a novel mutual-information-based approach for the evaluation of multi-dimensional probabilistic tuning functions (Brostek et al., 2011a,b). Traditional model-based approaches like regression analysis critically depend on the validity of their assumptions. Simple linear models often are not sufficient for analyzing neuronal data. Our information-theoretic approach overcomes these difficulties by maximizing the mutual information between stimulus variables and neuronal response. It allows us to estimate the neuronal latency and to compare the correlations between spiking activity and certain explanatory variables. This technique can be applied in unbalanced designs and allows quantification of any possible dependence of neuronal activity on selected explanatory variables. However, the length of the neuronal recording sets limiting constraints on the dimension of the analyzed tuning function.

We applied this novel approach to analyze MSTd neuronal activity during visual stimulation using a so called 'white noise motion' paradigm. In this experimental setting a large-field random-dot pattern moves continuously and randomly in the axis of each neuron's preferred direction. The monkey's task is to follow the stimulus as well as possible, performing OKR eye movements. However, using stimulus velocities above maximal eye velocity allowed us to cover wide ranges of both eye velocity and retinal image velocity values at the same time. We found that neuronal responses showed a large diversity of tuning to combinations of retinal and extra-retinal input instead of coding one of these variables *explicitely*. The majority of MSTd neurons exhibited rather gain-field-like tuning functions. Analysis of neuronal latency revealed a leading of eye velocity related activity relative to the actual eye movements. This signal can therefore not be of sensory origin and reflects an efference copy.

The distribution of eye velocity gain fields we found closely resembled the predictions from a neural network model trained to perform the summation of image and eye velocity. The diversity of MSTd gain field shapes including asymmetric and non-separable tuning functions was almost identical to the model results after completion of the learning process. Some neurons exhibited sharp, vertical tuning functions, whereas other units showed rather horizontal, image velocity related tuning. Together with the measured neuronal latencies, these results provide strong evidence for MSTd participating in the OKR control system by implementing the transformation from retinal image velocity to a head-centered stimulus velocity signal.

Beside the mean rate, there are more features of neuronal responses that may depend systematically on certain stimuli. One of these is the regularity or variabitity of spiking activity. In Brostek et al. (2012) we analyzed the variability of neuronal activity in MSTd neurons during fixation with large-field visual stimulation and optokinetic eye movements. Our analysis revealed two major features: first, in MSTd neurons the trial-to-trial variability of neuronal activity, expressed by the Fano factor, is quenched by the onset of visual stimulation. This change in variability is not necessarily directly related to stimulation, as proposed earlier (Churchland et al., 2010). During visual stimulation and fixating eye movements we found a sustained low level of variability. For optokinetic response, however, only a transient decline of the Fano factor was observable. Second, and more remarkable, the relationship between spiking irregularity and the two stimulation variables, image and eye velocity, was opposite. Both variables, which were uncoupled by using two orthogonal paradigms, affected the intra- and inter-trial variability of neuronal activity, meaning that the change in variability did not dependent on the task. All three measures of neuronal variability we analyzed, Fano factor, squared coefficient of variation, and 'Varience of the Conditional Expectation' (Churchland et al., 2011), were negatively correlated with retinal image velocity and positively correlated with eye velocity.

Our finding of decreasing spiking variability with an increasing 'driving' signal image velocity and increasing variability with an increase of the 'modulatory' signal eye velocity puts certain constraints on the underlying neuronal structure. A conductance-based single-compartment model neuron where multiplicative gain modulation is achieved by a simultaneous increase of excitatory and inhibitory background synaptic input yields realistic increases of firing rate and can reproduce the observed stimulus-dependence of neural variability.

Figure 3.2 provides a summary of our main results, illustrating the three different levels that were analyzed within the scope of this doctoral thesis. In the following sections certain aspects of our results will be discussed in more detail and compared with previous findings. This chapter ends with an outlook on potential further investigations.

3.1 Comparison with previous MSTd studies

Most MSTd neurons show different behavior during smooth pursuit and OKR (Kawano et al., 1994), as well as for radial and planar visual stimulation (Duffy and Wurtz, 1991), respectively. Prior studies in area MSTd, which were focusing on its role in perception of self-motion and heading direction, generally used *radial* visual stimulation in combination with small target pursuit eye movements. Our OKR results, which were recorded during *planar* visual stimulation, may therefore not be directly comparable to these previous studies. Nevertheless, those studies that were using smooth pursuit and radial stimulation also found that visual responses of MSTd neurons are modulated during eye movements (Bradley et al., 1996; Ben Hamed et al., 2003; Bremmer et al., 2010). In this sense, our results are in compliance with these earlier studies.

A number of other prior studies investigated neuronal tuning in MSTd during *planar* visual stimulation with combined small target pursuit and yielded diverging conclusions. Kawano and colleagues, for instance, suggested that MSTd neurons might directly encode the velocity of a large-field visual stimulus in head or world-centered coordinates (Inaba et al., 2007). A similar study by Chukoskie and Movshon 2009 could only partially confirm this hypothesis. They found some neurons in MSTd that encoded stimulus velocity. Most of the neurons, however, exhibited a variety of different other tuning behaviors ranging from pure retinal to head-centered stimulus velocity coding. This finding has remarkable similarity to our results, considering the difference of paradigms. We found only few neurons with a transformation index close to zero, which could also be interpreted as coding stimulus velocity in a restricted range of stimulus space. Nevertheless, instead of smooth pursuit, we were using an OKR paradigm and could therefore assume an involvement of the analyzed neurons in oculomotor control (Dürsteler and Wurtz, 1988). This allowed us to shift the focus from the question 'which signals are coded?' to 'what functions are implemented?'. Our coordinate transformation hypothesis offers a straightforward explanation for the diversity in tuning behaviors found in MSTd.

3.2 Gain Fields for Sensorimotor Coordinate Transformations

Numerous other studies in the posterior parietal cortex (PPC) have found gain-fields-like tuning behavior before. For instance, visual responses of neurons in the lateral intraparietal area (LIP) and cortical area 7A are gain-modulated by eye and head position signals (Snyder et al., 1998). The activity of neurons in the parietal reach region (PRR) is modulated by eye and limb position (Chang et al., 2009). Zipser and Andersen 1988 were the first to show that eye position gain fields might be used to transform the reference frame of eye-centered visual responses into head-centered responses. Beyond sensorimotor transformations, the computational function of gain fields might be a general method for neural computation when transformations between different brain representations are required (Salinas and Thier, 2000).

Yet, all previous studies were limited in a certain sense: the characterization of neuronal responses was incomplete as only very few and specific combinations of visual input and motor output could be tested. Our novel approach overcomes these limitations and allows us to characterize neural tuning with high resolution and over a large input-output range by dissociating visual motion and eye movements without additional task requirements. This enabled us to analyze novel aspects as for instance the distribution of gain field types, which could not have been investigated using any of the traditional approaches.

It is common practice to correlate neuronal activity with certain variables, assuming a *direct* encoding of sensory or motor signals by different neuronal populations. This approach may be appropriate for the early input or output stages of neuronal processing. It poses, however, serious difficulties when intermediate processing steps of sensorimotor transformation are analyzed. Theoretical studies have shown that a neural coding scheme where each object in each reference frame is represented by a different set of neurons quickly will reach limitations due to the combinatorial explosion in the number of required cells (Poggio, 1990). It was therefore suggested that a much more efficient scheme for neuronal representation might be used: instead of representing each variable by a certain pool of neurons, one set of basis functions can represent a number of different variables simultaneously. Arbitrary variables are then represented by a simple linear combination of these basis functions (Girosi et al., 1995; Pouget and Sejnowski, 1997).

Gain fields, as demonstrated by Pouget and Sejnowksi 1997, exhibit all characteristics necessary to form a set of basis functions. The diversity of tuning functions we observed in our data is consistent with this theory. Hence, eye velocity gain fields in MSTd could be used to generate a number of other visual motion related variables, as for instance an es-

timate of heading direction (Ben Hamed et al., 2003) or perceived self-motion velocity. In our case of planar visual stimulation, perceived self-motion velocity is simply the stimulus velocity signal directed towards the opposite side. Such inversion can be easily obtained by changing the weights of the connections to the output layer in our neural network model. The self-motion signal might be generalized for head- and body-motion by the inclusion of vestibular information (Gu et al., 2007). Our results are therefore compatible with the idea of area MSTd serving various functions in self-motion perception, as well as in oculomotor control.

3.3 Underlying Neuronal Structure

It is generally assumed that neuronal activity arises from an interaction between ongoing spiking generated spontaneously by neuronal circuits and responses driven by external stimuli (Dayan and Abbott, 2001). In this view the observed variability in neuronal activity is generally interpreted as noise, interfering with the actual signal coded by the neurons (Shadlen and Newsome, 1998). Recurrent networks are a kind of topological structure that is presumed to be found in many cortical areas. A general feature of this type of networks is the stimulus-driven suppression of chaotic, spontaneous activity. The decline in variability depends on stimulus frequency and amplitude (Rajan et al., 2010).

The decline of spiking irregularity with visual stimulation we observed in MSTd (Brostek et al., 2012) may be explained by the presence of recurrent circuitry. However, the increase in neuronal variability with higher eye velocity remains unexplained by the recurrent network hypothesis. The change in neuronal variability in our data is not just related to the presence of stimulation. A network topology that could explain the observed behavior is therefore probably asymmetrical and processes both input signals, image velocity and eye velocity, differently.

Anatomical observations led Sherman and Guillery (1998) propose that neurons might have two classes of inputs, one responsible for driving neural responses and the other for modulating those responses. Based on this idea, Chance et al. (2002) suggested a gain field mechansism where the gain of a neuronal response to excitatory drive can be modulated by varying the level of balanced excitatory and inhibitory synaptic input. Using both, an in vitro neuron model, and an analytic firing rate model, they could show that simultaneously increasing the background firing rates in a balanced manner results in a gain modulation of the neuronal response. In contrast to our work, however, they were

analyzing *divisive* gain modulation, where the gain decreases with an increase of the modulatory signal. Interestingly, the authors did not observe changes of neuronal variability with gain modulation in their in vitro model.

Using a far more detailed Hodgking-Huxley-type model with inserted stochastic conductances mimicking balanced excitatory and inhibitory synaptic input, we could show that an increase of backgound activity can actually result in *multiplicative* gain modulation, as well. Furthermore, our model is able to reproduce the differential behavior in neural variability we have observed in MSTd neurons. A comparatively simple feedforward mechanism allowed us to explain both, a decrease of spiking irregularity with increase of image velocity, and an increase with eye velocity, without the inclusion of recurrent or feedback circuitry.

3.4 Temporal Coding in MSTd?

A great amount of knowledge about neuronal information processing has been gained by relating the mean neuronal firing rate to any variables supposed to be coded in the analyzed area. Beside the mean rate, however, there are more features of neural responses that may depend systematically on certain stimuli. Theoretical and experimental studies in numerous cortical and sub-cortical regions indicated that the temporal pattern of spiking activity carries important information as well (Buracas and Albright, 1999; Rieke et al., 1997). For instance in auditory neurons the mean firing rate represents some combination of amplitude and frequency of a tone. At the same time there is the tendency for inter-spike intervals (ISIs) to cluster around integer multiples of the stimulus period, allowing the separation of frequency and amplitude information. Also in cortical areas spiking irregularity has been used as an evidence to support the temporal coding hypotheses (Softky and Koch, 1993).

As we have shown, in MSTd neurons the mean firing rate, which is the reciprocal of the mean inter-spike interval, codes some non-linear combination of visual and eye movement related signals (Brostek et al., 2011a). At the same time the variance of the ISI decreases with visual and increases with oculomotor stimulation (Brostek et al., 2012). This independent temporal code may allow the separation of the two signals, similar to phase-locking in auditory neurons.

In a renewal process ISIs are assumed to be independent and identically distributed (Cox,

1962). The approximate one-to-one relation between FF and CV^2 observed in our data argues for the renewal assumption. Both across-trial and within-trial variability are determined by the distribution of ISIs of the corresponding renewal process. The gamma distribution is an appropriate approximation for the distribution of ISIs in most neuronal systems (Stein, 1965). A change in spiking irregularity is associated with a modification of the ISI distribution. This again may result from changing membrane properties in single neurons, circuit properties of networks of neurons, or a combination of both. Miura et al. 2007 for instance proposed a network architecture, where the firing rate could be decoupled from the ISI distribution by proper balance of excitatory and inhibitory inputs. However, the questions whether the change of the ISI distribution in dependence of visual and oculomotor input has a functional meaning, and whether the additional information, embodied in changing spiking irregularity, is actually used by MSTd and subsequent areas, or reflects just an epiphenomenon, remain to be solved by future investigations.

3.5 Is MSTd Involved in Smooth Pursuit Control?

There is strong evidence from lesion studies that the dorsal visual pathway, which is responsible for motion processing, is involved in the generation of SPEMs (Dürsteler and Wurtz, 1988). Microlesions in areas MT and MSTl lead to two kinds of pursuit deficits: the retinotopic deficit, which describes problems of matching eye speed to target speed when the target is moving in any direction in the visual field contralateral to the side of the brain with the lesion, and the directional deficit, which is the inability to match eye speed to target speed when the target is moving towards the side of the lesion. Lesions in MSTd, however, only lead to retinotopic deficits, indicating a minor role of this area in pursuit control. This view is supported by electrical microstimulation studies, as in MSTd only few neurons were found, where stimulation produced an acceleration of pursuit (Komatsu and Wurtz, 1989).

Nevertheless, many neurons in MSTd show significantly increased activity during SPEMs in the abscence of other visual stimulation (Komatsu and Wurtz, 1988). In Ono et al. (2010) we found that about one third of MSTd neurons belong to the subpopulation of the so called 'smooth pursuit neurons'. These neurons continue to respond during pursuit despite a blink (Newsome et al., 1988) or even complete disappearance (Ilg and Thier, 2003) of the pursuit target. Furthermore, the pursuit related activity in MSTd has been reported to be higher than the visually induced activity in many neurons (Churchland and Lisberger, 2005).

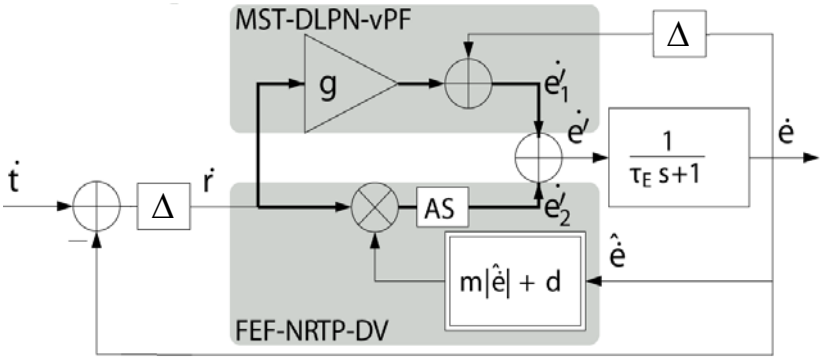

Figure 3.1: A dual pathway model for smooth pursuit, extend with temporal delays (Δ) to match the onset latency measured in psycho-physical experiments. The upper branch represents the signal pathway from cortical structure MST via pontine structures (DLPN) to the cerebellum (vPF), while the lower branch stands for signal processing in FEF via pontine NRTP and cerebellar vermis (DV). The MST-branch receives an efference copy of the eye velocity signal, which is delayed by about the same amount as the eye lags behind target motion. (Adapted from (Nuding et al., 2008))

Previous studies reported that the onset of the SPEM component in MSTd neurons usually starts about 100 ms after onset of eye movement (Newsome et al., 1988). We found in our data an average neuronal delay of 127 ms for pursuit neurons. Similarly, the perturbation response occurred on average 102 ms after the eye movement (Ono et al., 2010).

When tested with the white noise motion paradigm, most of the neurons with late eye-velocity-related latency exhibited also significant differences in tuning behavior. In about one third of neurons spiking activity correlated rather with eye position or eye acceleration than with image and eye velocity. Another third of units had visual and eye movement related activity components with opposite preferred directions, which had been described for MSTd pursuit neurons previously (Newsome et al., 1988; Shenoy et al., 2002; Ono et al., 2010).

The late onset of the eye-velocity-related component of neuronal response seems to argue against a participation of MSTd neurons in the generation of SPEMs. Nevertheless, given the highly direction specific nature and responsiveness to smooth pursuit, the delay in neuronal response does not exclude a role of MSTd in the SPEM control circuit. Rather, pursuit neurons in MSTd could provide an efference copy of the eye movement signal (Holst and Mittelstaedt, 1950) which could be used to reconstruct a target velocity signal in space, in the same way as we could demonstrate for OKR. For stability reasons, the

Table 3.1: List of potential further investigations

	OKR	SP
MSTd	done	Eye velocity gain fields for coordinate transformations?
MSTl	?	Eye velocity gain fields for coordinate transformations?
MT	Modulation of visual response by eye movements?	
FEF	Visual response in FEF?	Gain fields for gain modulation of smooth pursuit?

efference copy should have a similar delay as the image velocity signal. Given a typical eye movement onset latency of about 100 ms for SPEM, the observed neuronal delay fits very well with the efference copy hypothesis, as demonstrated by the computational model in Fig. 3.1. Nevertheless, further experiments need to be performed to investigate whether MSTd also contains eye velocity gain fields for transforming the image velocity signal during SPEM as we have found for OKR eye movements.

3.6 Further Investigations

The studies performed within the framework of this doctoral thesis mainly focused on the analysis of neuronal activity in MSTd during optokinetic response (OKR) eye movements. Nevertheless, the information-theoretic data analysis approach we have developed can be adapted easily to investigate the tuning behavior of other cortical and subcortical regions. Table 3.1 summarizes some potential further investigations.

As discussed in the previous section, it is still unknown whether MSTd plays a similar role in sensorimotor coordinate transformations during smooth pursuit (SP), as we propose for OKR. Preliminary results have shown that the 'white noise motion' paradigm we have used for visual large-field stimulation can be adapted to the tracking of small-field targets, as well. The finding of eye velocity gain fields in MSTd, or adjacent MSTl, during SP would further strengthen the importance of these areas for the control of tracking eye movements.

Visual information is projected to areas MSTd and MSTl through connections with extra-striate area MT (Tusa and Ungerleider, 1988). Whereas for long time it was assumed that MT does not receive extra-retinal input (Newsome et al., 1988), a recent work suggested that MT neurons might use eye movement signals to code depth-sign from motion parallax (Nadler et al., 2009). Our method could be used to solve this controversy by analyzing whether visual responses in MT are indeed modulated by eye movements, or not.

Another cortical area which is involved in tracking eye movements is the frontal eye field (FEF). It is assumed that this area participates in the control of SP (Lisberger, 2010). A recent TMS study suggested that the FEF might be involved in smooth pursuit gain control (Nuding et al., 2009). The finding of gain-field-like tuning functions in this area might provide further evidence for this hypothesis.

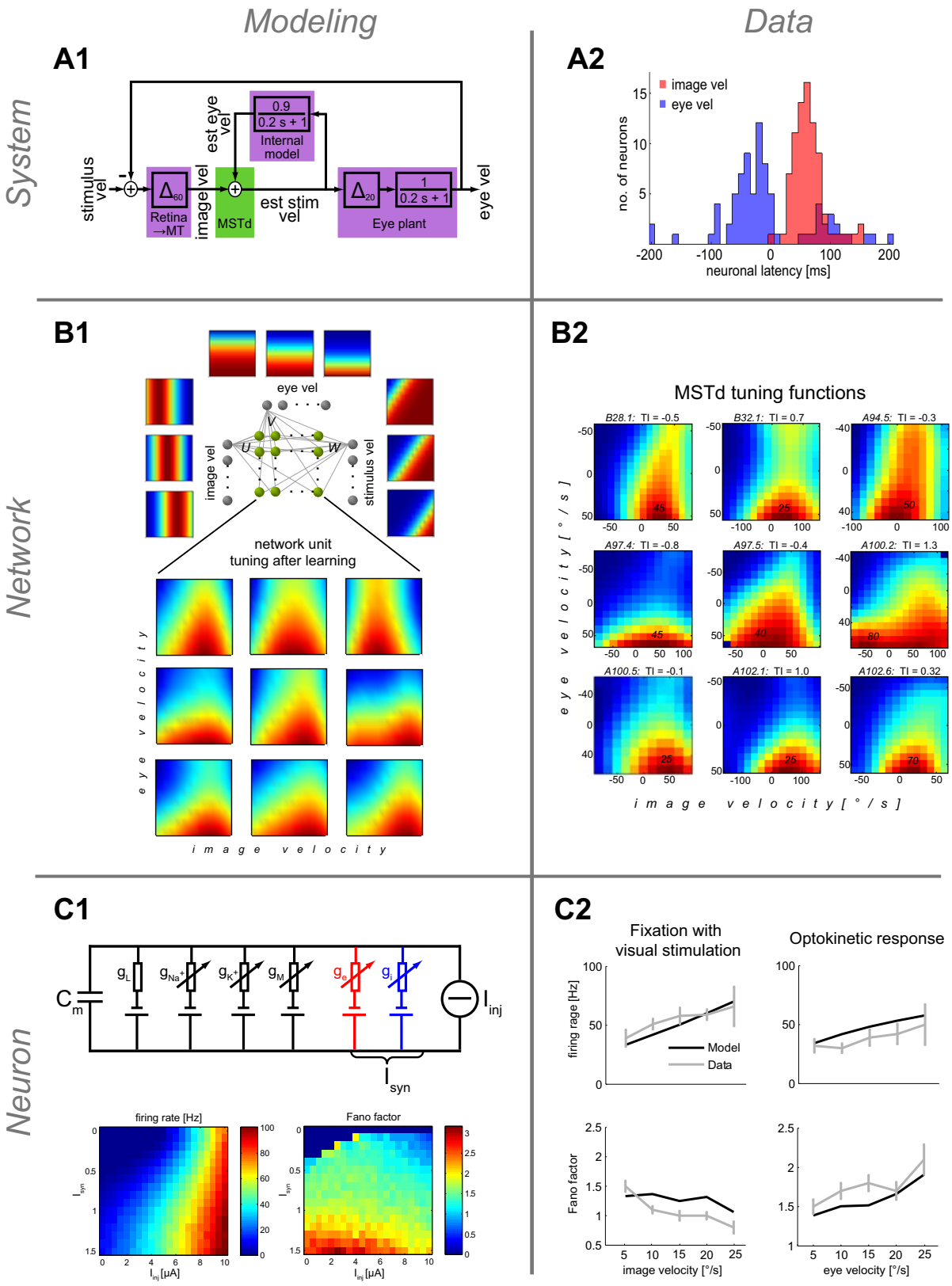
Modeling
Data
System
Network
Neuron
A1
A2
B1
B2
C1
C2
stimulus vel
image vel
est eye vel
0.9
0.2 s + 1
Internal model
Retina →MT
MSTd
est stim vel
Eye plant
eye vel
image vel
eye vel
no. of neurons
neuronal latency [ms]
eye vel
image vel
stimulus vel
network unit
tuning after learning
eye velocity
image velocity
MSTd tuning functions
B28.1: TI = -0.5
B32.1: TI = 0.7
A94.5: TI = -0.3
A97.4: TI = -0.8
A97.5: TI = -0.4
A100.2: TI = 1.3
A100.5: TI = -0.1
A102.1: TI = 1.0
A102.6: TI = 0.32
eye velocity [°/s]
image velocity [°/s]
firing rate [Hz]
Fano factor
Fixation with visual stimulation
Optokinetic response
firing rage [Hz]
Model
Data
Fano factor
image velocity [°/s]
eye velocity [°/s]

Figure 3.2 *(facing page)*: A multi-level analysis of neuronal activity in MSTd.
(A1) Basic system-level model of the optokinetic response (OKR) control system. Image velocity is the difference between stimulus and eye velocity. A delay of 60 ms accounts for the latency of the image velocity signal due to retinal and neural processing along the visual system. The eye plant is modeled by a low-pass filter with a time constant of 200 ms and an additional delay of 20 ms. Image velocity is transformed to an estimated stimulus velocity signal by adding the estimated eye velocity signal, provided by an internal model of the eye plant. We assume that this coordinate transformation involves area MSTd.
(A2) Neural latency of MSTd neurons relative to image and eye velocity. For each neuron two latency values were estimated: (1) relative to image velocity (red), and (2) relative to eye velocity (blue). Neural activity lagged about 60 ms behind the image velocity signal. In contrast, most neurons fired before the eye velocity signal, as indicated by negative latency values. This finding corresponds to the latencies assumed in the OKR model.
(B1) Neural network model of the coordinate transformation. The network consists of two input layers, one intermediate network unit layer, and an output layer. The image velocity units are Gaussian tuned with differing preferred image velocity. The eye velocity units have sigmoid tuning with differing inflection velocity. The stimulus velocity output layer also consists sigmoidally tuned units. Each of the intermediate units is connected with each input and output unit. During the back-propagation learning process the weights of these connections are modified. Below the model, the tuning functions for image and eye velocity of 9 example network units after learning are shown.
(B2) Two-dimensional tuning curves of 9 example MSTd neurons exhibiting gain-field-like behavior. Colors from blue to red indicate the mean firing rate [Hz] dependent on image velocity (horizontal axis) and eye velocity (vertical axis). Peak values and corresponding transformation indices (TI) are denoted in each colormap. The form and distribution of gain fields is almost identical to the predictions from the neural network model.
(C1) Top: Hodgking-Huxley-type neural model with inserted stochastic conductances mimicking excitatory and inhibitory synaptic input activity (see Additional Results section). Bottom: Firing rate and Fano factor of the Hodgking-Huxley-type neural model depending on the injected current I_{inj} and the level of background synaptic input I_{syn}.
(C2) Firing rate and Fano factor of the Hodgking-Huxley-type neural model (black) correspond to our observation in MSTd neurons (grey) during fixation with visual stimulation (FIX) and optokinetic response (OKR).

Bibliography

Barnes GR, Asselman PT (1991) The mechanism of prediction in human smooth pursuit eye movements. *J Physiol* 439:439–461.

Basso MA, Pokorny JJ, Liu P (2005) Activity of substantia nigra pars reticulata neurons during smooth pursuit eye movements in monkeys. *Eur J Neurosci* 22:448–464.

Ben Hamed S, Page W, Duffy C, Pouget A (2003) MSTd neuronal basis functions for the population encoding of heading direction. *J Neurophysiol* 90:549–558.

Born RT, Tootell RB (1992) Segregation of global and local motion processing in primate middle temporal visual area. *Nature* 357:497–499.

Borst A, Theunissen FE (1999) Information theory and neural coding. *Nature Neurosci* 2:947–9571.

Bradley DC, Maxwell M, Andersen RA, Banks MS, Shenoy KV (1996) Mechanisms of heading perception in primate visual cortex. *Science* 273:1544–1547.

Bremmer F, Ilg UJ, Thiele A, Distler C, Hoffmann KP (1997) Eye position effects in monkey cortex. I. visual and pursuit-related activity in extrastriate areas MT and MST. *J Neurophysiol* 77:944–961.

Bremmer F, Kubischik M, Pekel M, Hoffmann KP, Lappe M (2010) Visual selectivity for heading in monkey area MST. *Exp Brain Res* 200:51–60.

Britten KH, Newsome WT, Shadlen MN, Celebrini S, Movshon JA (1996) A relationship between behavioral choice and the visual responses of neurons in macaque MT. *Visual Neurosci* 13:87–100.

Britten KH, van Wezel RJA (1998) Electrical microstimulation of cortical area MST biases heading perception in monkeys. *Nature Neurosci* 1:59–63.

Brostek L, Büttner U, Mustari MJ, Glasauer S (2012) Neuronal variability of MSTd neurons changes differentially with eye movement and visually related variables. *Cereb Cortex* in press.

Brostek L, Eggert T, Ono S, Mustari MJ, Büttner U, Glasauer S (2011a) An information-theoretic approach for evaluating probabilistic tuning functions of single neurons. *Front Comput Neurosci* 5.

Brostek L, Eggert T, Ono S, Mustari MJ, Büttner U, Glasauer S (2011b) A method for evaluating tuning functions of single neurons based on mutual information maximization. *AIP Conf Proc* 1305:423–429.

Buracas GT, Albright TD (1999) Gauging sensory representations in the brain. *Trends Neurosci* 22:303–309.

Büttner U, Büttner-Ennever J (2006) Present concepts of oculomotor organization. *Prog Brain Res* 151:1–43.

Büttner U, Waespe W (1984) Purkinje cell activity in the primate flocculus during optokinetic stimulation, smooth pursuit eye movements and VOR-suppression. *Exp Brain Res* 55:97–104.

Chance FS, Abbott LF, Reyes AD (2002) Gain modulation from background synaptic input. *Neuron* 35:773–782.

Chang SWC, Papadimitriou C, Snyder LH (2009) Using a compound gain field to compute a reach plan. *Neuron* 64:744–755.

Chukoskie L, Movshon JA (2009) Modulation of visual signals in macaque MT and MST neurons during pursuit eye movement. *J Neurophysiol* 102:3225–3233.

Churchland AK, Kiani R, Chaudhuri R, Wang XJ, Pouget A, Shadlen MN (2011) Variance as a signature of neural computations during decision making. *Neuron* 69:818–831.

Churchland AK, Lisberger SG (2002) Gain control in human smooth-pursuit eye movements. *J Neurophysiol* 87:2936–2945.

Churchland AK, Lisberger SG (2005) Relationship between extraretinal component of firing rate and eye speed in area MST of macaque monkeys. *J Neurophysiol* 94:2416–2426.

Churchland MM, Lisberger SG (2001) Experimental and computational analysis of monkey smooth pursuit eye movements. *J Neurophysiol* 86:741–759.

Churchland MM, Yu BM, Cunningham JP, Sugrue LP, Cohen MR, Corrado GS, Newsome WT, Clark AM, Hosseini P, Scott BB, Bradley DC, Smith MA, Kohn A, Movshon JA, Armstrong KM, Moore T, Chang SW, Snyder LH, Lisberger SG, Priebe NJ, Finn IM, Ferster D, Ryu SI, Santhanam G, Sahani M, Shenoy KV (2010) Stimulus onset quenches neural variability: a widespread cortical phenomenon. *Nature Neurosci* 13:369378.

Cohen B, Matsuo V, Raphan T (1977) Quantitative analysis of the velocity characteristics of optokinetic nystagmus and optokinetic after-nystagmus. *J Physiol* 270:321–344.

Cover TM, Thomas JA (1991) *Elements of Information Theory* Wiley-Interscience.

Cox D, Lewis P (1966) *The Statistical Analysis of Series of Events* Methuen.

Cox DR (1962) *Renewal theory* Methuen.

Dayan P, Abbott LF (2001) *Theoretical Neuroscience* MIT Press.

Desimone R (1991) Face-selective cells in the temporal cortex of monkeys. *J Cognitive Neurosci* 3:1 – 8.

Destexhe A, Rudolph M, Fellous JM, Sejnowski TJ (2001) Fluctuating synaptic conductances recreate in vivo-like activity in neocortical neurons. *Neuroscience* 107:13 – 24.

Distler C, Mustari MJ, Hoffmann KP (2002) Cortical projections to the nucleus of the optic tract and dorsal terminal nucleus and to the dorsolateral pontine nucleus in macaques: a dual retrograde tracing study. *J Comp. Neurol* 444:144–158.

Duffy CJ, Wurtz RH (1991) Sensitivity of MST neurons to optic flow stimuli. I. a continuum of response selectivity to large-field stimuli. *J Neurophysiol* 65:1329–1345.

Duffy CJ, Wurtz RH (1995) Response of monkey MST neurons to optic flow stimuli with shifted centers of motion. *J Neurosci* 15:5192–5208.

Duffy CJ, Wurtz RH (1997) Medial superior temporal area neurons respond to speed patterns in optic flow. *J Neurosci* 17:2839–2851.

Dürsteler MR, Wurtz RH (1988) Pursuit and optokinetic deficits following chemical lesions of cortical areas MT and MST. *J Neurophysiol* 60:940–965.

Fano U (1947) Ionization yield of radiations. II. the fluctuations of the number of ions. *Phys Rev* 72:26.

Felleman DJ, Van Essen DC (1991) Distributed hierarchical processing in the primate cerebral cortex. *Cereb Cortex* 1:1–47.

Fellous JM, Rudolph M, Destexhe A, Sejnowski TJ (2003) Synaptic background noise controls the input/output characteristics of single cells in an in vitro model of in vivo activity. *Neuroscience* 122:811–829.

Gellman RS, Carl JR, Miles FA (1990) Short latency ocular following responses in man. *Visual Neurosci* 5:107–122.

Girosi F, Jones M, Poggio T (1995) Regularization theory and neural networks architectures. *Neural Comput* 7:219–269.

Glickstein M, Gerrits N, Kralj-Hans I, Mercier B, Stein J, Voogd J (1994) Visual pontocerebellar projections in the macaque. *J Comp Neurol* 349:51–72.

Gollisch T, Meister M (2010) Eye smarter than scientists believed: Neural computations in circuits of the retina. *Neuron* 65:150 – 164.

Gu Y, DeAngelis GC, Angelaki DE (2007) A functional link between area MSTd and heading perception based on vestibular signals. *Nature Neurosci* 10:1038–1047.

Hodgkin AL, Huxley AF (1952) A quantitative description of membrane current and its application to conduction and excitation in nerve. *J Physiol* 117:500–544.

Holst E, Mittelstaedt H (1950) Das Reafferenzprinzip. *Naturwissenschaften* 37:464–476.

Hubel DH, Wiesel TN (1962) Receptive fields, binocular interactions and functional architecture in the cat's visual cortex. *J Physiol* 160:106–154.

Ilg UJ, Schumann S, Thier P (2004) Posterior parietal cortex neurons encode target motion in world-centered coordinates. *Neuron* 43:145 – 151.

Ilg UJ, Thier P (2003) Visual tracking neurons in primate area MST are activated by smooth-pursuit eye movements of an imaginary target. *J Neurophysiol* 90:1489–1502.

Inaba N, Shinomoto S, Yamane S, Takemura A, Kawano K (2007) MST neurons code for visual motion in space independent of pursuit eye movements. *J Neurophysiol* 97:3473–3483.

Kandel ER, Schwartz JH, Jessell TM (2000) *Principles of Neural Science* McGraw-Hill.

Kawano K, Shidara M, Watanabe Y, Yamane S (1994) Neural activity in cortical area MST of alert monkey during ocular following responses. *J Neurophysiol* 71:2305–2324.

Keating EG, Pierre A, Chopra S (1996) Ablation of the pursuit area in the frontal cortex of the primate degrades foveal but not optokinetic smooth eye movements. *J Neurophysiol* 76:637–641.

Komatsu H, Wurtz RH (1989) Modulation of pursuit eye movements by stimulation of cortical areas MT and MST. *J Neurophysiol* 62:31–47.

Komatsu H, Wurtz RH (1988) Relation of cortical areas MT and MST to pursuit eye movements. I. localization and visual properties of neurons. *J Neurophysiol* 60:580–603.

Leigh RJ, Zee DS (2006) *The Neurology of Eye Movements* Oxford University Press.

Lisberger SG (2010) Visual guidance of smooth pursuit eye movements: sensation, action, and what happens in between. *Neuron* 66:477–491.

Lisberger SG, Evinger C, Johanson GW, Fuchs AF (1981) Relationship between eye acceleration and retinal image velocity during foveal smooth pursuit in man and monkey. *J Neurophysiol* 46:229–249.

Maunsell JH, Van Essen DC (1983a) Functional properties of neurons in middle temporal visual area of the macaque monkey. I. selectivity for stimulus direction, speed, and orientation. *J Neurophysiol* 49:1127–1147.

Maunsell JH, Van Essen DC (1983b) Functional properties of neurons in middle temporal visual area of the macaque monkey. II. binocular interactions and sensitivity to binocular disparity. *J Neurophysiol* 49:1148–1167.

May JG, Keller EL, Suzuki DA (1988) Smooth-pursuit eye movement deficits with chemical lesions in the dorsolateral pontine nucleus of the monkey. *J Neurophysiol* 59:952–977.

Miles FA (1998) The neural processing of 3-D visual information: evidence from eye movements. *Eur J Neurosci* 10:811–822.

Miles FA, Kawano K, Optican LM (1986) Short-latency ocular following responses of monkey. I. dependence on temporospatial properties of visual input. *J Neurophysiol* 56:1321–1354.

Mishkin M, Ungerleider LG, Macko KA (1983) Object vision and spatial vision: two cortical pathways. *Trends Neurosci* 6:414 – 417.

Miura K, Tsubo Y, Okada M, Fukai T (2007) Balanced excitatory and inhibitory inputs to cortical neurons decouple firing irregularity from rate modulations. *J Neurosci* 27:13802 –13812.

Morrow MJ, Sharpe JA (1995) Deficits in smooth pursuit eye movements after unilateral frontal lobe lesions. *Ann Neurol* 37:443–451.

Nadler JW, Nawrot M, Angelaki DE, DeAngelis GC (2009) MT neurons combine visual motion with a smooth eye movement signal to code depth-sign from motion parallax. *Neuron* 63:523–532.

Newsome WT, Pare EB (1988) A selective impairment of motion perception following lesions of the middle temporal visual area (MT). *J Neurosci* 8:2201–2211.

Newsome WT, Wurtz RH, Komatsu H (1988) Relation of cortical areas MT and MST to pursuit eye movements. II. differentiation of retinal from extraretinal inputs. *J Neurophysiol* 60:604–620.

Nuding U, Kalla R, Muggleton NG, Büttner U, Walsh V, Glasauer S (2009) TMS evidence for smooth pursuit gain control by the frontal eye fields. *Cereb Cortex* 19:1144–1150.

Nuding U, Ono S, Mustari MJ, Büttner U, Glasauer S (2008) A theory of the dual pathways for smooth pursuit based on dynamic gain control. *J Neurophysiol* 99:2798–2808.

Ono S, Das VE, Economides JR, Mustari MJ (2005) Modeling of smooth pursuit-related neuronal responses in the DLPN and NRTP of the rhesus macaque. *J Neurophysiol* 93:108–116.

Ono S, Brostek L, Nuding U, Glasauer S, Büttner U, Mustari MJ (2010) The response of MSTd neurons to perturbations in target motion during ongoing smooth-pursuit eye movements. *J Neurophysiol* 103.

Optican LM, Zee DS, Chu FC (1985) Adaptive response to ocular muscle weakness in human pursuit and saccadic eye movements. *J Neurophysiol* 54:110–122.

Phillips JO, Finocchio DV, Ong L, Fuchs AF (1997) Smooth pursuit in 1- to 4-month-old infants. *Vision Res* 37:3009–3020.

Poggio T (1990) A theory of how the brain might work. *Cold Spring Harb Symp Quant Biol* 55:899–910.

Pouget A, Sejnowski TJ (1997) Spatial transformations in the parietal cortex using basis functions. *J Cognitive Neurosci* 9:222–237.

Rajan K, Abbott LF, Sompolinsky H (2010) Stimulus-dependent suppression of chaos in recurrent neural networks. *Phys Rev E* 82:011903.

Rieke F, Warland D, de Ruyter van Steveninck R, Bialek W (1997) *Spikes: Exploring the Neural Code* MIT Press.

Robinson DA, Gordon JL, Gordon SE (1986) A model of the smooth pursuit eye movement system. *Biol Cybern* 55:43–57.

Robinson DR, Straube A, Fuchs AF (1997) Participation of caudal fastigial nucleus in smooth pursuit eye movements. II. effects of muscimol inactivation. *J Neurophysiol* 78:848–859.

Roy JP, Komatsu H, Wurtz RH (1992) Disparity sensitivity of neurons in monkey extrastriate area MST. *J Neurosci* 12:2478–2492.

Rudolph K, Pasternak T (1999) Transient and permanent deficits in motion perception after lesions of cortical areas MT and MST in the macaque monkey. *Cereb Cortex* 9:90–100.

Salinas E, Thier P (2000) Gain modulation: A major computational principle of the central nervous system. *Neuron* 27:15–21.

Salzman CD, Britten KD, Newsome WT (1990) Cortical microstimulation influences perceptual judgements of motion direction. *Nature* 346:174–177.

Shadlen MN, Newsome WT (1998) The variable discharge of cortical neurons: implications for connectivity, computation, and information coding. *J Neurosci* 18:3870–96.

Shannon CE, Weaver W (1949) *The mathematical theory of communication* University of Illinois Press.

Shenoy KV, Crowell JA, Andersen RA (2002) Pursuit speed compensation in cortical area MSTd. *J Neurophysiol* 88:2630–2647.

Sherman SM, Guillery RW (1998) On the actions that one nerve cell can have on another: distinguishing drivers from modulators. *PNAS* 95:71217126.

Shi D, Friedman HR, Bruce CJ (1998) Deficits in smooth pursuit eye movements after muscimol inactivation within the primate's frontal eye field. *J Neurophysiol* 80:458–464.

Snyder LH, Grieve KL, Brotchie P, Andersen RA (1998) Separate body- and world-referenced representations of visual space in parietal cortex. *Nature* 394:887–891.

Softky WR, Koch C (1993) The highly irregular firing of cortical cells is inconsistent with temporal integration of random EPSPs. *J Neurosci* 13:334–350.

Stein RB (1965) A theoretical analysis of neuronal variability. *Biophys J* 5:173–194.

Takagi M, Zee DS, Tamargo RJ (2000) Effects of lesions of the oculomotor cerebellar vermis on eye movements in primate: smooth pursuit. *J Neurophysiol* 83:2047–2062.

Takemura A, Kawano K (2006) Neuronal responses in MST reflect the post-saccadic enhancement of short-latency ocular following responses. *Exp Brain Res* 173:174–179.

Takemura A, Murata Y, Kawano K, Miles FA (2007) Deficits in short-latency tracking eye movements after chemical lesions in monkey cortical areas MT and MST. *J Neurosci* 27:529–541.

Tanaka M (2005) Involvement of the central thalamus in the control of smooth pursuit eye movements. *J Neurosci* 25:5866 –5876.

Tusa RJ, Ungerleider LG (1988) Fiber pathways of cortical areas mediating smooth pursuit eye movements in monkeys. *Ann Neurol* 23:174–183.

Uhlenbeck GE, Ornstein LS (1930) On the theory of the brownian motion. *Phys Rev* 36:823–841.

Waespe W, Henn V (1987) Gaze stabilization in the primate. the interaction of the vestibulo-ocular reflex, optokinetic nystagmus and smooth pursuit. *Rev Physiol Biochem Pharmacol* 106:37–125.

Zee DS, Yamazaki A, Butler PH, Gücer G (1981) Effects of ablation of flocculus and paraflocculus on eye movements in primates. *J Neurophysiol* 46:878–899.

Zipser D, Andersen RA (1988) A back-propagation programmed network that simulates response properties of a subset of posterior parietal neurons. *Nature* 331:679–684.

Acknowledgements

I would like to express my sincere gratitude to the people that helped me during the time of my thesis.

First of all, I want to thank Prof. Dr. Ulrich Büttner and Prof. Dr.-Ing. Stefan Glasauer for giving me the opportunity to conduct my doctoral study in their group. I am grateful that both supervisors provided me continuous support while guaranteeing freedom to develop my own ideas and concepts at the same time. I thank our partners in Seattle, Prof. Michael J. Mustari and Dr. Seiji Ono, for providing the experimental data and for the great collaboration. Further, I thank Dr.-Ing. Thomas Eggert for his very helpful support.

I would like to thank Prof. Dr.-Ing. Werner Hemmert for being part of my thesis advisory committee and for giving valuable suggestions during our meetings. I thank the Bernstein Center for Computational Neuroscience for funding. I am also very glad for having the opportunity to be part of the Graduate School for Systemic Neuroscience.

Last but not least, I am grateful for the lifelong support from my family and the countless scientific discussions with Dr. Stefanova!

List of Publications

- Ono S, Brostek L, Nuding U, Glasauer S, Büttner U, Mustari MJ (2010). The Response of MSTd Neurons to Perturbations in Target Motion During Ongoing Smooth-Pursuit Eye Movements. *Journal of Neurophysiology* 103: 519-530.

- Brostek L, Eggert T, Ono S, Mustari MJ, Büttner U, Glasauer S (2011). An Information-Theoretic Approach for Evaluating Probabilistic Tuning Functions of Single Neurons. *Frontiers in Computational Neuroscience* 5: 15.

- Brostek L, Eggert T, Ono S, Mustari MJ, Büttner U, Glasauer S (2011). A Method for Evaluating Tuning Functions of Single Neurons based on Mutual Information Maximization. *AIP Conference Proceedings* 1305: 423–429.

- Brostek L, Büttner U, Mustari MJ, Glasauer S (2012). Neuronal Variability of MSTd Neurons Changes Differentially With Eye Movement and Visually Related Variables. *Cerebral Cortex* in press.

J Neurophysiol 103: 519–530, 2010.
First published November 18, 2009; doi:10.1152/jn.00563.2009.

The Response of MSTd Neurons to Perturbations in Target Motion During Ongoing Smooth-Pursuit Eye Movements

Seiji Ono,[2] Lukas Brostek,[3] Ulrich Nuding,[3] Stefan Glasauer,[3] Ulrich Büttner,[3] and Michael J. Mustari[1]
[1]*Washington National Primate Research Center, University of Washington, Seattle, Washington;* [2]*Yerkes National Primate Research Center, Emory University, Atlanta, Georgia; and* [3]*Bernstein Center for Computational Neuroscience, University of Munich, Munich, Germany*

Submitted 1 July 2009; accepted in final form 10 November 2009

Ono S, Brostek L, Nuding U, Glasauer S, Büttner U, Mustari MJ. The response of MSTd neurons to perturbations in target motion during ongoing smooth-pursuit eye movements. *J Neurophysiol* 103: 519–530, 2010. First published November 18, 2009; doi:10.1152/jn.00563.2009. Several regions of the brain are involved in smooth-pursuit eye movement (SPEM) control, including the cortical areas MST (medial superior temporal) and FEF (frontal eye field). It has been shown that the eye-movement responses to a brief perturbation of the visual target during ongoing pursuit increases with higher pursuit velocities. To further investigate the underlying neuronal mechanism of this nonlinear dynamic gain control and the contributions of different cortical areas to it, we recorded from MSTd (dorsal division of the MST area) neurons in behaving monkeys (*Macaca mulatta*) during step-ramp SPEM (5–20°/s) with and without superimposed target perturbation (one cycle, 5 Hz, ±10°/s). Smooth-pursuit–related MSTd neurons started to increase their activity on average 127 ms after eye-movement onset. Target perturbation consistently led to larger eye-movement responses and decreasing latencies with increasing ramp velocities, as predicted by dynamic gain control. For 36% of the smooth-pursuit–related MSTd neurons the eye-movement perturbation was accompanied by detectable changes in neuronal activity with a latency of 102 ms, with respect to the eye-movement response. The remaining smooth-pursuit–related MSTd neurons (64%) did not reflect the eye-movement perturbation. For the large majority of cases this finding could be predicted by the dynamic properties of the step-ramp responses. Almost all these MSTd neurons had large visual receptive fields responding to motion in preferred directions opposite to the optimal SPEM stimulus. Based on these findings it is unlikely that MSTd plays a major role for dynamic gain control and initiation of the perturbation response. However, neurons in MSTd could still participate in SPEM maintenance. Due to their visual field properties they could also play a role in other functions such as self-motion perception.

INTRODUCTION

Moving visual stimuli can induce slow tracking eye movements. For small objects these are called smooth-pursuit eye movements (SPEMs). They are used to keep the image of the moving object on or near the fovea where visual acuity is best. SPEMs are produced by volitional effort and depend on motivation, attention, and target motion.

SPEMs can reach velocities up to ≥60°/s (for review see Krauzlis 2004; Leigh and Zee 2006). In the laboratory, SPEMs are often investigated with a step-ramp paradigm (Rashbass 1961). In this paradigm, the monkey fixates a stationary target, which after a delay is replaced by a target located slightly eccentrically that moves toward the fovea at a constant speed. It allows SPEMs to be elicited at short latency (100–140 ms) without contamination by initial saccades.

In recent years it was shown that during ongoing constant-velocity SPEMs, brief perturbations of target motion exhibit a velocity-dependent effect on eye velocity. Typically a short-duration (<200 ms) single cycle (5–10 Hz) of sinusoidal motion is added to the ongoing target motion, resulting in a corresponding perturbation of eye motion. The eye motion response depends on current SPEM speed in both humans (Churchland and Lisberger 2002) and monkeys (Churchland and Lisberger 2005b), even when the same perturbing stimulus motion is applied. While fixating a stationary target, perturbation responses are still produced but at a lower gain (Schwartz and Lisberger 1994). This nonlinear response is thought to reveal an underlying dynamic gain control mechanism in SPEM (Churchland and Lisberger 2005b; Nuding et al. 2008). Even though the neural mechanisms and regions involved in dynamic gain control are not completely understood, recent studies point toward cortical areas as being the main site of smooth-pursuit gain control (Nuding et al. 2008; Tanaka and Lisberger 2001).

From single-unit and lesion studies it is known that frontal lobe and parietal–occipital lobe structures play complementary roles in SPEM (Krauzlis 2004). These areas include the middle temporal (MT) and medial superior temporal (MST) areas in the parietooccipital region and the frontal eye field (FEF) cortex. These cortical areas are reciprocally connected (Tusa and Ungerleider 1988) and also send projections to the brain stem (Distler et al. 2002). Area MT, which has extensive connections with MST, is well known to play a role in visual motion processing, including foveal and parafoveal visual motion appropriate for SPEMs (Maunsell and Van Essen 1983). MST is divided into several subregions, including dorsal (MSTd), lateral (MSTl), and ventral (MSTv), with different functional properties. Lesions of MST cause deficits in SPEM when the subject tracks a target moving toward the lesioned side (Newsome et al. 1988).

Early single-unit recording studies demonstrated that during SPEM neurons in MSTd and MSTl show strong modulation that was often due to an extraretinal signal (Newsome et al. 1988). The extraretinal origin was revealed by briefly (100–400 ms) extinguishing the target spot during maintained SPEM. In this target blink condition, well-trained monkeys maintain most of their smooth-pursuit eye velocity (e.g., Ono

Address for reprint requests and other correspondence: M. J. Mustari, Washington National Primate Research Center, University of Washington, Seattle, WA 98195 (E-mail: mmustar@wanprc.org).

and Mustari 2006), MSTd and some MSTl neurons continue to discharge (Newsome et al. 1988), but MT neurons do not.

Neurons in MSTd have large visual receptive fields (>14°) that can include both contralateral, foveal, and ipsilateral visual field components (Churchland and Lisberger 2005b). The large-field visual and smooth-pursuit response components of MSTd neurons generally have opposing direction preferences (Komatsu and Wurtz 1988). Based on the interaction of the visual and extraretinal components it has been argued that MSTd might be a critical structure for self-motion perception (Shenoy et al. 2002).

During step-ramp testing a large proportion of MSTd neurons begin firing only 50–100 ms after pursuit onset (Newsome et al. 1988). Only a small subset of MSTd neurons has short-latency responses starting as much as 100 ms before smooth-pursuit initiation (Newsome et al. 1988). This early response component might be due to retinal image motion of the target (Ilg and Thier 2003).

We have demonstrated in earlier studies that MST projects to the dorsolateral pontine nuclei (DLPN) (Distler et al. 2002). Similarly, the FEF projects to the nucleus reticularis tegmenti pontis (NRTP) (Ono and Mustari 2009). Both DLPN (Mustari et al. 1988; Thier et al. 1988) and NRTP (Ono et al. 2004; Suzuki et al. 2003) are known to play a role in SPEM. The DLPN and NRTP have been shown in anatomical studies to project to mostly different regions of the cerebellum including the floccular complex and vermis. In turn, the floccular complex and vermis deliver signals important for SPEM through the vestibular nuclei and caudal fastigial nuclei, respectively (Büttner and Büttner-Ennever 2006). Moreover, there is now strong evidence for a feedback loop via the thalamus back to the cortex (Tanaka 2005), which might carry an efference copy of SPEM commands (Nuding et al. 2008).

The goal of our studies was to determine the potential role of MSTd neurons in the control of visually induced perturbation responses during SPEM. To accomplish this, we recorded single-unit activity in MSTd of the alert behaving monkey during a step-ramp paradigm, which included a target perturbation task. We found that a minority of MSTd neurons was modulated during the perturbation task, with neuronal response onsets about 100 ms after the eye movement caused by the perturbation. To contrast these responses a few neurons were also tested during eye movements induced by large-field visual motion. The preferred neuronal response was in the direction opposite to the optimal SPEM response. Under these conditions virtually all neurons responded before the step-ramp and perturbation-induced eye movements. The results indicate that MSTd neurons probably do not play a major role in the initiation of the perturbation responses during SPEM; however, they could contribute to SPEM control during maintained tracking.

METHODS

Three monkeys (*Macaca mulatta*, 5–7 kg), born in captivity at the Yerkes National Primate Research Center (Atlanta, GA), were prepared for chronic eye-movement and single-unit recordings. All surgical procedures were performed in compliance with National Institutes of Health *Guide for the Care and Use of Laboratory Animals* and protocols were reviewed and approved by the Institutional Animal Care and Use Committee at Emory University. Surgical procedures were performed in a dedicated facility using aseptic techniques under isoflurane anesthesia (1.25–2.5%). Vital signs including blood pressure, heart rate, blood oxygenation, body temperature, and CO_2 in expired air were monitored with a Surgivet instrument (Waukesha, WI) and maintained within normal physiological limits. Postsurgical analgesia (buprenorphine, 0.01 mg/kg, administered intramuscularly [im]) and antiinflammatory (banamine, 1.0 mg/kg, im) treatment were delivered every 6 h for several days, as indicated. To permit single-unit recording, we used stereotaxic methods to implant a titanium head-stabilization post and a titanium recording chamber (Crist Instrument, Hagerstown, MD) over MST cortex (posterior, 5 mm; lateral, 15 mm). In the same surgery, a scleral search coil for measuring eye movements (Fuchs and Robinson 1966) was implanted underneath the conjunctiva of one eye using the technique of Judge et al. (1980).

Behavioral paradigms

During the experiments monkeys were seated in a primate chair (Crist Instrument) with their head fixed in the horizontal stereotaxic plane in a completely dark room to which they were customized. The room was sealed with darkroom tape and light traps to ensure no ambient light entered the room. This was verified by having a trained observer sit in the room for 30 min in complete darkness and attempt to find light leaks. Power to visual stimulus projector bulbs and to the laser diode, which provides the tracking target, were extinguished during blink testing. Neurons in MSTd were tested during smooth-pursuit and visual motion. All visual stimuli were rear-projected onto a tangent screen (Stewart Film Screen, Torrance, CA) at 57-cm distance. Stimuli were delivered using computer-controlled two-axis mirror galvanometers (General Scanning, Watertown, MA) and appropriate optics and hardware. Stimulus motion was controlled with custom LabVIEW software and National Instruments hardware (Austin, TX).

Localization of MSTd

We verified that our neurons were located in MSTd by functional (e.g., SPEM response continues during a target blink and large visual receptive fields), histological, and magnetic resonance imaging (MRI; T1-weighted, fast spin-echo; Siemens, 3-T magnet) criteria. Structural MRI was obtained from both monkeys while they were under surgical levels of inhalation anesthesia (described earlier). We confirmed the location of our recording sites histologically in one of the monkeys; the other monkeys are still being used in other studies. At the conclusion of our recording experiments, the first monkey was deeply anesthetized and perfused with physiological saline followed by 4% paraformaldehyde, as described in detail elsewhere (Mustari et al. 1994). Frozen sections were cut at 50 μm and every section was mounted on microscope slides and stained for Nissl substance to allow histological reconstruction of representative electrode tracks.

Visual stimuli

We searched for units in MSTd that were modulated during smooth-pursuit or visual motion in the frontal plane. We used either circular motion of a large-field visual stimulus or motion in eight cardinal directions, separated by 45° to determine neuronal direction preference. Visual stimuli were either large-field (35 × 35°) random dot patterns, small-field (5 × 5°) random dot patterns, or small-diameter (2°) spots. Random-dot patterns had light and dark contours with a mean luminance of 100 cd/m^2. Contrast of the light and dark contours was set at 50%. Circular motion was produced by driving the horizontal and vertical galvanometers 90° out of phase (±5–10°; 0.25–1.0 Hz). This circular motion stimulus produces constant-speed motion of all scene components across the full extent of the pattern. Smooth-pursuit direction preference was tested as using either circular motion (±10°; 0.25–0.5 Hz) or motion along eight cardinal directions

(U, up; D, down; L, left; R, right and the oblique directions: UL, UR, DL, DR) of a small-diameter (0.2°) target spot. The target was a rear-projected red spot produced with a light-emitting diode laser (Melles Griot, Rochester, NY). We maintained the target 1.0 log unit above the dark background, as measured with calibrated neutral density filters (Melles Griot). The optimal responses for smooth-pursuit tracking and large-field visual stimulation during fixation were usually in opposite directions. Except for the visual stimuli the monkey was in complete darkness. The following stimulus conditions were applied.

1) SPEM. The laser spot first stepped away from the center position and then moved at constant velocities from 5 to 20°/s in the preferred direction. The initial step was arranged so that the target crossed the center position after 130 ms. The constant-velocity part lasted 1,500–1,800 ms.

2) Large-field (LF) visual motion response. The monkey fixated a small target spot located at the center of gaze. The target was turned off coincident with the start of LF stimulus motion at constant velocity (5–20°/s) for 2,000 ms. This stimulus consistently leads to following eye movements (optokinetic response [OKR]).

3) Perturbation. During both SPEM and LF stimulation a visual perturbation consisting of one sinusoidal cycle (5 Hz, ±10°/s), with the first half-cycle increasing the stimulus velocity (peak-first perturbation; Churchland and Lisberger 2002), was introduced during the constant-velocity phase (600–800 ms after stimulus onset).

4) Blinking. Extraretinal modulation of neuronal response during SPEM was tested by blinking the target during ongoing pursuit for 100–200 ms. Trials with and without blinking were randomly interleaved (Ono and Mustari 2006). During the blink all visual stimuli were extinguished, leaving the monkey in complete darkness.

Visual receptive fields

Visual receptive fields (RFs) of neurons were mapped by moving a probe stimulus in the preferred and antipreferred directions at regularly spaced eccentricities across the visual field. The probe stimulus for RF mapping was a white rectangle (2 × 2°) oscillating at 0.5–3 Hz (±1°). RF size was taken as the area in which the neuron was modulated by the oscillating stimulus. Responses of our MSTd neurons were in agreement with known discharge properties of MSTd neurons (Komatsu and Wurtz 1988). Receptive fields were large and had their center in the contralateral hemifield. For most neurons RF size exceeded 30° and for many neurons it was >60°. None of the neurons had RFs <15° and they were not restricted to the central 15° around the fovea, as might be expected for other regions of MST (e.g., MSTl). Some neurons extended their RF into the ipsilateral hemifield, but generally not >20°. Larger extensions into the ipsilateral hemifield were always combined with increasing RF sizes. For 63% of the neurons the RF included the fovea. There was no difference in RF sizes for neighboring visual only and visual-smooth pursuit neurons.

Data collection

Eye movements were detected with standard electromagnetic methods using scleral search coils (Fuchs and Robinson 1966) and precision hardware (CNC Electronics, Seattle, WA). For calibration the monkey was required to fixate stationary targets at known eccentricities. Monkeys were rewarded with juice for maintaining fixation within a window of ±1.5°. Single-unit activity was recorded from neurons in MSTd using customized epoxy-coated tungsten microelectrodes (FHC, Bowdoin, ME) with an impedance of 1–3 MΩ. Single-unit action potentials were detected with either a hardware window discriminator (Bak Electronics, Mount Airy, MD) or template-matching algorithm (Alpha-Omega, Alpharetta, GA) and were registered at high precision as an event mark in our data-acquisition system (CED Power 1401, Cambridge Electronic Design, Cambridge, UK). Eye and target position feedback signals were processed with antialiasing filters at 200 Hz using six-pole Bessel filters before digitization at 1 kHz with 16-bit precision.

Data analysis

The recorded eye position traces were filtered with a Gaussian low-pass (cutoff frequency: 10 Hz) and three-point differentiated to obtain the velocity traces. Saccades were detected and removed with a slow-phase estimation algorithm as described previously (Ladda et al. 2007). Briefly, an estimate of the slow-phase component (SPC) was initialized to zero and iteratively improved in each step. The difference between the actual eye velocity trace and the current SPC served as an estimate of the fast-phase component (FPC). When the FPC exceeded a threshold (100°/s in the first step, 20°/s in the second step), a saccade was detected. The SPC was then computed by linear interpolation of the eye velocity across saccades and subsequent filtering with a Gaussian low-pass (cutoff frequency: 1 Hz in the first step, 10 Hz in the second step). Neuronal response was represented as a spike density function that was generated by convolving spike times with a 15-ms Gaussian function. Eye-movement and spike density functions corresponding to each trial were extracted and averaged over corresponding conditions.

To determine the eye-movement onset latency (EMOL) (Fig. 1), the mean and SD of the eye velocity during the initial fixation period were calculated. The point in time at which the eye velocity trace crosses the threshold of this mean + 3SD yields the EMOL, relative to target step-ramp onset ($t = 0$). The perturbation response latency (PRL), which describes the delay of the ocular response to target perturbation, was determined by the maximum of eye velocity in a time interval ≤400 ms after target perturbation. The difference of this maximum to the subsequent minimum of eye velocity yields the perturbation response modulation (PRM). For statistical assessment of these parameters, outliers deviating >3SD from the mean response were removed.

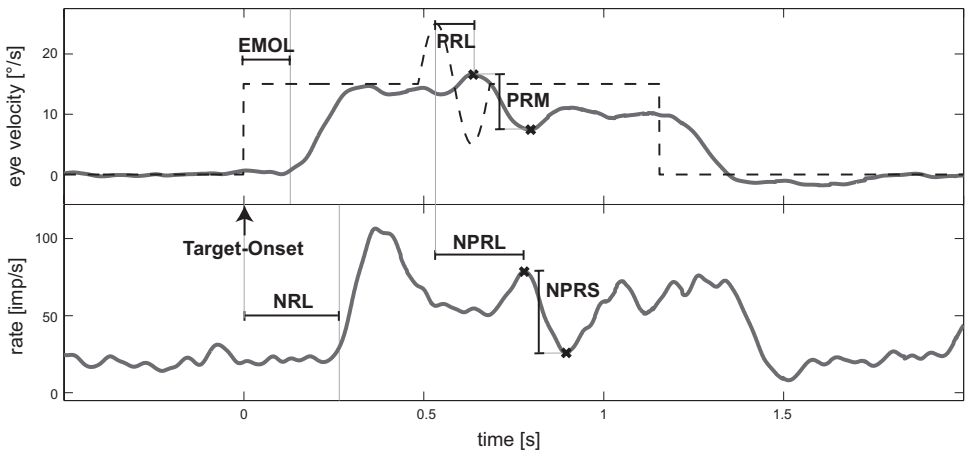

FIG. 1. Eye velocity (*A*) and neuronal parameters (*B*) measured. *A*: EMOL, eye-movement onset latency; PRL, perturbation response latency; PRM, perturbation response modulation. *B*: NRL, neuronal response latency; NPRL, neuronal perturbation response latency; NPRS, neuronal perturbation response sensitivity. Dashed line in *A* marks target velocity.

The neuronal response latency (NRL) denominates the delay of the increase in neural activity after target step-ramp onset. It was determined by the time when the response exceeds the mean + 3SD of the initial activity. The neuronal response sensitivity is the ratio of the mean spike density in a time interval between 500 and 600 ms after target step-ramp onset minus the mean initial spike density during fixation divided by the mean eye velocity in that time interval.

In the analysis associated with a blinking target the neuronal activity was compared with control trials without a blink. The blink response latency was defined as the point of minimal eye velocity in a period ≤400 ms after the start of blink. The time interval for determination of the response ratio consisted of a 200-ms period around this latency plus the neuronal latency with respect to the eye movements.

Data analysis of neuronal perturbation response

To decide whether a neuronal response shows modulation to a target perturbation, a confidence region was defined as a 3SD value around the Gaussian low-pass filtered (cutoff frequency: 2 Hz) spike density function of the control trials. When the spike density during the perturbation trials exceeded this confidence region in a time interval ≤550 ms after start of target perturbation, the neuronal response was declared to show a perturbation response.

If present, the delay of a neuronal modulation response to the perturbation of the visual target stimulus is described by the neuronal perturbation response latency (NPRL) (Fig. 1). It was determined by the maximum of spike density in a time interval ≤350 ms after target perturbation. The neuronal perturbation response sensitivity determines the ratio of the difference between this maximum and the subsequent minimum of spike density divided by twice the amplitude of the target perturbation.

We further analyzed whether a detectable perturbation response would be expected from the data by predicting the perturbation response based on the control trials. We first fitted a linear regression model with the regressor variables eye velocity (v) and eye acceleration (a) to the spike density function (sdf) of each neuron, according to

$$\text{sdf} = \beta_0 + \beta_1 \text{v} + \beta_2 \text{a}$$

Trial mean values were used for each target velocity from 500 ms before target onset until target offset. The lag of the neuronal response with respect to eye movement (NRL − EMOL) was taken into account by varying the delay in steps of 1 ms and searching for the best fit (maximal R^2). Using this model, we then predicted the neuronal response of the perturbation trials based on eye velocity and eye acceleration of these trials. The predicted response was then entered into the perturbation analysis described in the preceding paragraph. Thus neurons could fall in four classes (data responsive or not responsive; prediction responsive or not responsive), depending on whether a perturbation response was expected from the control responses.

RESULTS

In general, the majority (65%) of neurons encountered in the MSTd region responded only to visual motion. They will not be considered in the following text. For the present study, only SPEM-related MSTd neurons were included (n = 61). They were recorded in the right hemisphere of three monkeys (HZ, n = 48; UJ, n = 7; OY, n = 6 neurons) and were optimally modulated during SPEM in a preferred direction. Fifty-five of those also responded to visual motion, the remaining six only during SPEM. Generally, the preferred direction for visual motion and smooth pursuit was in opposite directions as reported previously (Newsome et al. 1988). All neurons were spontaneously active with a low and irregular firing rate.

SPEM perturbation responses

EYE MOVEMENTS. The perturbation (5 Hz, ±10°/s) during ongoing pursuit led in all instances to a change in eye velocity (Figs. 1, 2, and 3). We interleaved perturbation and normal step-ramp trials to prevent the monkey from anticipating a perturbation event. There was a tendency that trials with

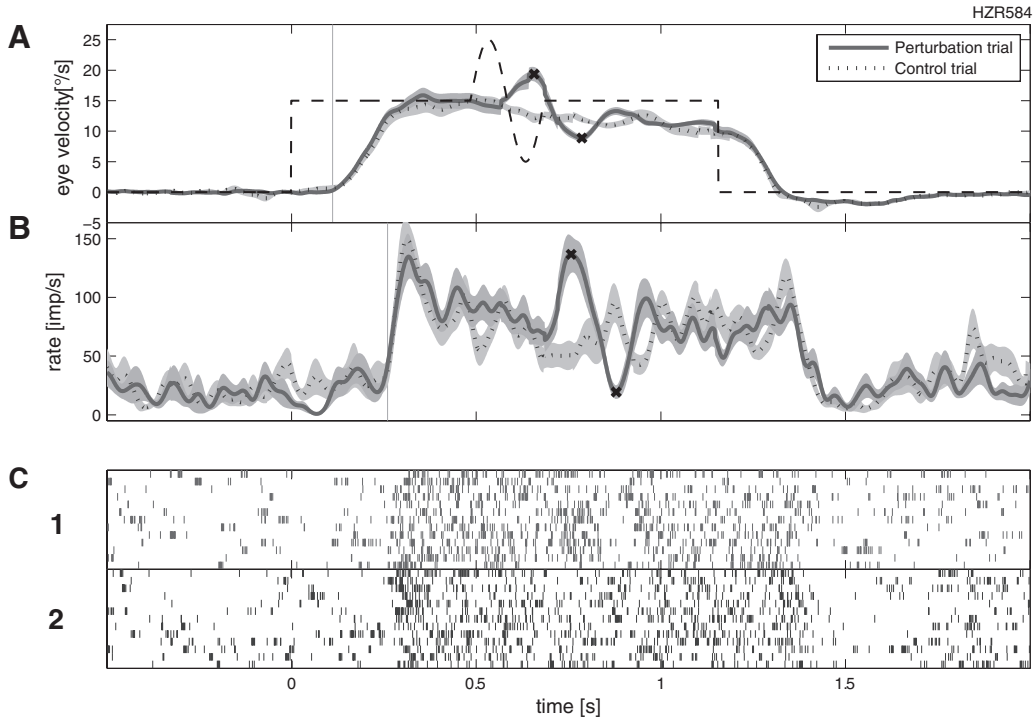

FIG. 2. MSTd (dorsal division of the medial superior temporal area) neuron during step-ramp smooth-pursuit eye movement (SPEM) and target perturbation. *A*: target and eye velocity. *B*: averaged neuronal activity from the individual traces shown in *C*. Continuous lines and *C1* refer to perturbation trials, dotted lines and *C2* to controls. Gray areas in *A* and *B* indicate SD of eye velocity and neuronal activity, respectively. Step-ramp stimulation leads to SPEM, followed by an increase in neuronal activity. The initial neuronal acceleration increase is followed by a constant velocity component. The perturbation (one cycle 5 Hz, ±10°/s) during the step-ramp stimulation leads to eye velocity changes and is also followed by a modulation of neuronal activity. Maximum and minimum of the eye and the neuronal perturbation response are marked by the analysis algorithm (METHODS), onset of SPEM (EMOL), and neuronal activity increase (NRL) (gray vertical line) as well. Time refers to stimulus onset.

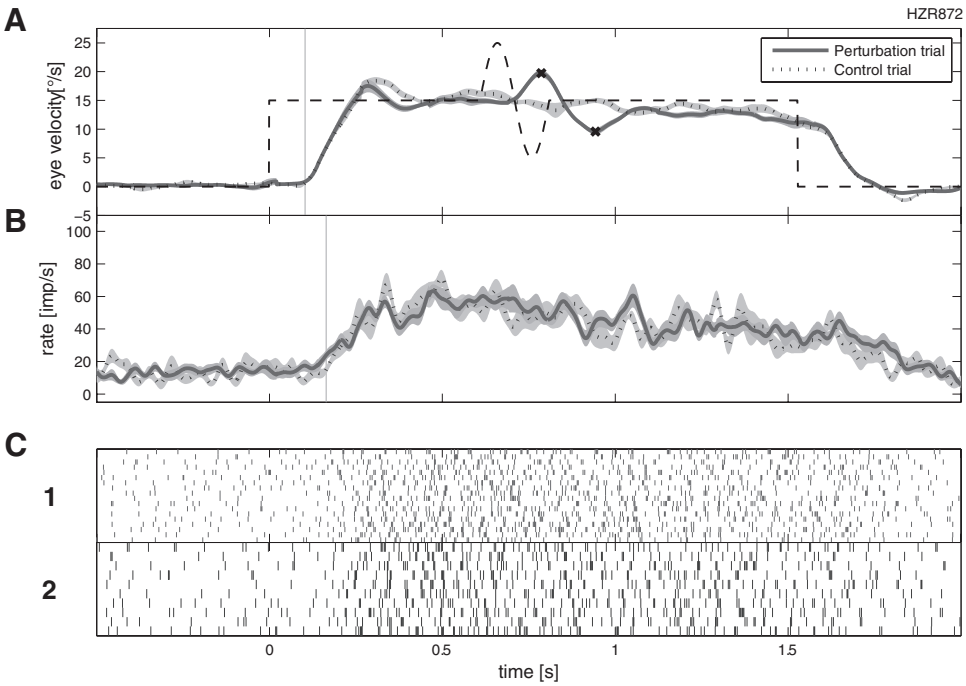

FIG. 3. MSTd neuron, which is modulated during SPEM, but not in relation to eye-movement perturbation. For further explanation see Fig. 1.

perturbation were contaminated by saccades that led to the elimination of these trials. The underlying constant eye velocity during ramp stimulation had a clear effect on the perturbation response in terms of both latency and response modulation (Fig. 4, *A* and *B*).

The mean latency (PRL; see Fig. 1) monotonically decreased from 121 ms at 5°/s ramp velocity to 94 ms at 20°/s ramp velocity. This decrease was highly significant [one-way ANOVA, four levels corresponding to four target velocities: $F(3,158) = 14.99$; $P < 0.0001$] and different from the latency pattern seen in response to the standard step-ramp stimulation. Here stimulus velocity had little effect on latency (see following text; Fig. 4*C*).

In contrast to perturbation latency, the magnitude of the perturbation response (PRM; see Fig. 1) continuously increased from 6.3°/s at 5°/s ramp velocity to 9.3°/s at 20°/s ramp velocity (Fig. 4*B*). This increase was also highly significant [one-way ANOVA, four levels corresponding to four target velocities: $F(3,158) = 12.29$; $P = < 0.0001$]. Both latency and magnitude reflect dynamic gain control with values similar to those described previously (Churchland and Lisberger 2005a).

NEURONAL RESPONSE. Based on the criteria described earlier (METHODS) 22 of 61 neurons (36%) showed some modulation during perturbation, whereas most neurons (64%; HZ, $n = 31$; UJ, $n = 6$; OY, $n = 2$) were not modulated.

A modulated neuron is shown in Fig. 2. Neuronal activity during SPEM started 150 ms after eye movement onset (260 ms after stimulus onset). After a modest phasic response associated with eye acceleration the remaining response was related to eye velocity. The perturbation during pursuit led to an eye-movement response after 121 ms, which was followed 100 ms later by a modulation in neuronal activity (Fig. 2). This sequence of events was the case in virtually all instances. The neuronal activity followed the eye-movement perturbation response on average by 101.6 ms (SD = ±46.1 ms) (Fig. 5*A*). This latency was slightly shorter than the onset of neuronal activity for step-ramp stimulation of the same trials (average

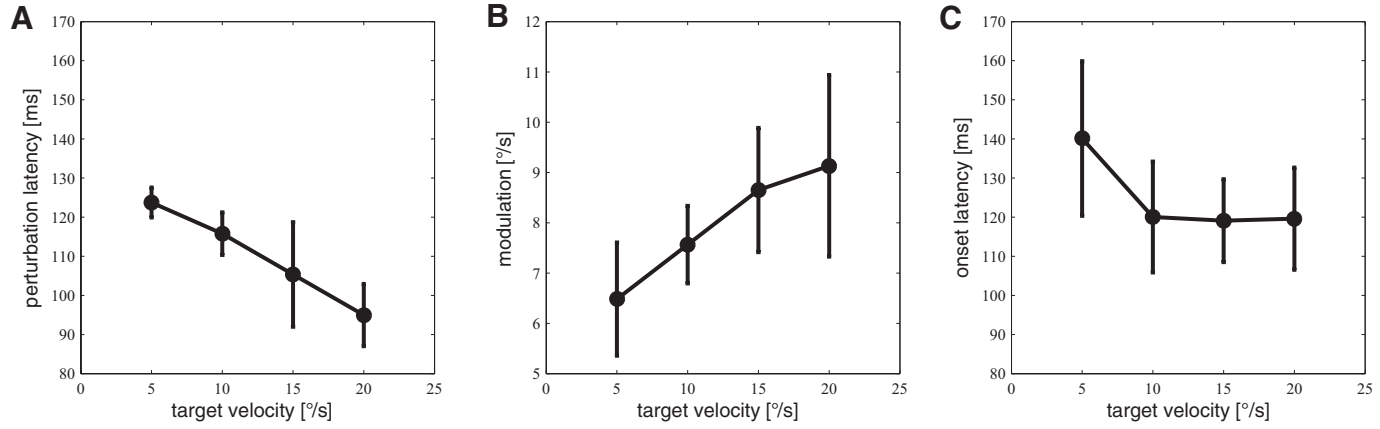

FIG. 4. Perturbation eye-movement latency (*A*) and modulation (*B*) at different underlying constant (ramp) velocities. Increasing ramp velocities lead to a significant decrease in latency and an increase in modulation (gain), which reflects dynamic gain control. *C*: the eye-movement latency to step-ramp stimulation with little effect of target velocity. Vertical lines: SD.

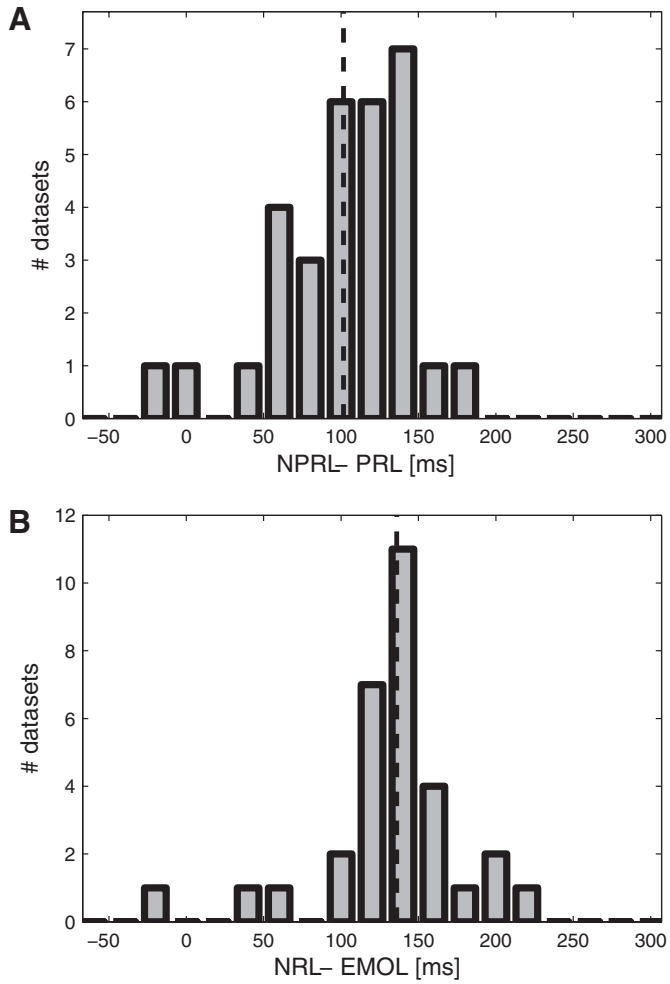

FIG. 5. Neuronal perturbation response latency (NPRL) relative to ocular perturbation response latency (PRL) (*A*) and for the same data sets neuronal response latency after step-ramp target onset (NRL) relative to eye-movement onset latency (EMOL) (*B*). One data set is the neuronal response at a given stimulus velocity. In *A* and *B* neuronal activity starts on average >100 ms after the eye movement. Stippled lines in *A* and *B* show average values.

127.3; SD = ±55.5 ms) (Fig. 5*B*). The mean perturbation latency (NPRL − PRL) decreased with target velocity from 118 ms at 5°/s to 67 ms at 20°/s (Fig. 6*B*). However, this decrease was not significant [one-way ANOVA, four levels corresponding to four target velocities: $F(3,27) = 1.06$; $P = 0.381$]. In general neurons were tested at more than one stimulus velocity, yielding 61 data sets for these 22 neurons. (The term "data set" refers to the neuronal response at one stimulus velocity.) Whereas 6 neurons (HZ, $n = 6$; UJ, $n = 0$; OY, $n = 0$) were modulated under all conditions ($n = 9$), the remaining 16 neurons (HZ, $n = 11$; UJ, $n = 1$; OY, $n = 4$) were not modulated at all stimulus velocities (modulation in 22 of 55 conditions).

As mentioned earlier, most neurons ($n = 39$) did not respond to perturbation at any stimulus velocity (131 conditions). For the example shown in Fig. 3, target perturbation leads to a clear eye-movement modulation (Fig. 3*A*), but not to a modulation of neuronal activity (Fig. 3*B*). Thus although the perturbation led consistently to an eye-movement modulation, most MSTd neurons were not affected.

SPEM step-ramp responses

EYE MOVEMENTS. After the step the eyes started to move with a latency of 120–140 ms with little effect of stimulus velocity (Fig. 4*C*). The timing of the step-ramp prevented in nearly all cases an initial catch-up saccade. The final constant velocity was reached after another 200 ms (Figs. 1–3). Constant eye velocity increased with stimulus velocity, with gain values ranging from 0.85 to 0.95, which reflects normal behavior.

NEURONAL RESPONSES. Preferred directions were equally distributed across the tested directions. Neuronal activity started to increase in nearly all instances after the beginning of smooth pursuit. There was only one neuron that started to discharge 28 ms before eye-movement onset. The average latency (NRL − EMOL; see Fig. 1) for all MSTd neurons ranged from 151 ms at 10°/s to 135 ms at 20°/s target velocity (Fig. 6*A*). Thus there was a small, but not significant effect of stimulus velocity on neuronal latency [one-way ANOVA, four levels corresponding to four target velocities: $F(3,158) = 2.55$; $P = 0.058$]. We found that 75% of the neurons had activity increases, which started >120 ms after stimulus onset. The distribution of latencies for those neurons, in which the perturbation led to neuronal activity changes (Fig. 5*B*), was not different from the nonresponding neurons. During the constant-velocity period activity increased with eye velocity. However, the average sensitivity in relation to eye velocity remained nearly constant.

Relationship between neuronal step-ramp and perturbation responses

With respect to neuronal response latency (NRL), there was no difference between modulated and unmodulated MSTd neurons during perturbation. Responding neurons did not appear to be clustered in certain regions of MSTd. The ratio of phasic (initial) to tonic (constant-velocity) activity was on average slightly higher for the responsive (1.96) than that for the unresponsive (1.71) neurons. Also the constant-velocity sensitivity was slightly higher (3.11 impulses$\cdot s^{-1}\cdot deg^{-1}\cdot s^{-1}$) for responsive neurons compared with 2.46 impulses$\cdot s^{-1}\cdot deg^{-1}\cdot s^{-1}$ for unresponsive neurons (average). Both differences did not become significant (relation phasic vs. tonic: $P = 0.090$, constant-velocity sensitivity: $P = 0.081$; Student's *t*-test). However, although the difference in neuronal sensitivity was modest, it turned out to be critical for understanding why only some neurons had clear responses to the perturbation (see following text).

As shown earlier, the eye-movement perturbation response modulation (PRM) increased with higher constant velocities (Fig. 4*B*). This modulation, however, was not reflected in more responsive data sets at higher stimulus velocities. In contrast, the percentage of responsive data sets decreased with stimulus velocity. Whereas 33% of the data sets were responsive at 5°/s, this number decreased to 23% (10°/s), 21% (15°/s), and 9% (3 of 32) at 20°/s stimulus velocity. This initially surprising finding was also seen with our regression analysis (see following text).

To further investigate why neurons did not show detectable modulation in response to target perturbation, we predicted the neuronal responses in perturbation trials based on the averaged control trials using a linear regression approach (see METHODS). We

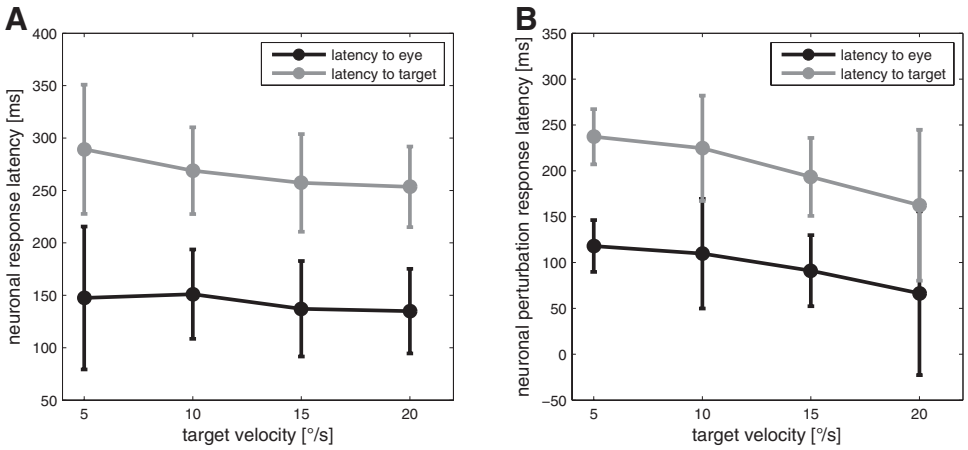

FIG. 6. The effect of target velocity on neuronal latency (*A*) and neuronal perturbation response latency (*B*). Gray: latency to target onset, equivalent to NRL (*A*) and NPRL (*B*), respectively; black: latency relative to eye-movement onset, equivalent to NRL − EMOL (*A*) and NPRL − PRL (*B*), respectively. In *A* target velocity has little effect on neuronal latencies. Neurons are lagging target onset by 250–300 ms. In *B*, both neuronal perturbation response latency with respect to eye and target onset show a small but not significant decrease.

first fitted the neuronal responses in control trials using a combination of eye velocity and eye acceleration. In general, this regression approach provided a good fit of the neural response during control trials, with an average R^2 value of 0.61 ± 0.20 (see Fig. 7 for examples of a responsive and a nonresponsive neuron). Furthermore, the fit of the neuronal control data confirmed that the MSTd neurons basically encode eye velocity with a small eye acceleration component (velocity factor: 2.4 ± 1.6 impulses·s^{-1}·deg^{-1}·s^{-1}; acceleration factor: 0.06 ± 0.16 impulse·s^{-1}·deg^{-1}·s^{-2}). For 64% of the data sets the acceleration component was negligible (<0.001 impulse·s^{-1}·deg^{-1}·s^{-2}). Adding a mixed term (velocity × acceleration) improved the average R^2 to only 0.63 and was therefore not used.

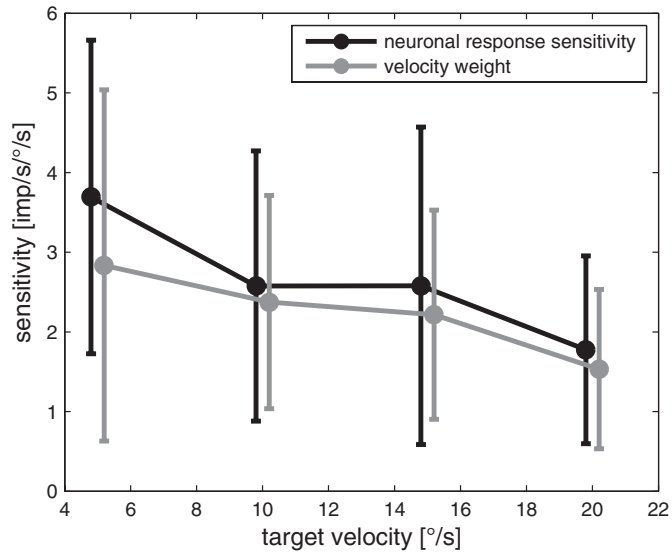

FIG. 7. Prediction of neuronal response to target perturbation. Dashed curve in *A1* shows the averaged neuronal response during a control trial of an MSTd neuron that shows modulation to target perturbation (*A2*). The stippled curve illustrates the result of a curve fitting using a weighted combination of eye velocity, acceleration, and a constant part. The estimated parameters of that regression analysis are used to predict a neuronal response to the eye movements of the perturbation trials, plotted in *A2* as a stippled curve. The gray band in the *bottom panel* illustrates the confidence region, which is used to classify the neuronal responses. To decide whether a neuronal response shows modulation to the target perturbation, a confidence region is defined as 3SD around the Gaussian low-pass filtered spike density function of the control trials. When the firing rate of the perturbation trials exceeds this confidence region in a time interval ≤550 ms after start of target perturbation, this neuronal response is declared to show a perturbation response. Furthermore, the averaged neuronal response during a perturbation trial is plotted as dashed line. Here, both measured and predicted neuronal responses leave the confidence region and show modulation to the target perturbation. Accordingly, these examples are classified as "responsive." A "nonresponsive" neuron that does not show modulation to the target perturbation is illustrated in *B*. The measured and predicted neuronal responses do not leave the confidence region (*B2*).

The perturbation analysis of the *predicted* neuronal response, using the same confidence region as that for the measured perturbation data, revealed that for the majority of data sets (68%), prediction and data were in accordance (20% responsive, 48% nonresponsive). For the remaining data, prediction and measurement did not match (prediction: response − measured: no response: 19%; prediction: no response − measured: response: 13%). In other words, our analysis showed that, based on the response properties of the neurons during step-ramp control trials and the eye movement during perturbation trials, for most nonresponsive neurons a detectable perturbation response was not expected, since the noise level in relation to the velocity weight was too high.

The regression analysis also showed that the predicted neuronal responses were related to target velocity. Whereas at 5°/s 63% of the data sets were predicted as responsive, this percentage decreased to 38% at 10°/s, 32% at 15°/s, and 19% at 20°/s. Thus both the measured (see earlier text) and the predicted responsive data sets decreased with target velocity. This result was not due to an increase of the confidence region (noise) in relation to target velocity (5°/s: 45.5 impulses/s; 10°/s: 56.7 impulses/s; 15°/s: 56.3 impulses/s; 20°/s: 49.5 impulses/s). There was also no difference between responsive and nonresponsive data sets. However, the neuronal sensitivity decreased with target velocity, which can be seen for both the neuronal data and the regression analysis (Fig. 8). In both measures the decrease amounts to a factor of 2 and is significant [neuronal response sensitivity: one-way ANOVA, four levels corresponding to four target velocities, $F(3,158) = 5.5636$; $P = 0.0012$; velocity weight: one-way ANOVA, four levels corresponding to four target velocities, $F(3,158) = 3.7794$; $P = 0.0121$]. The decrease was similar for responsive and nonresponsive data sets. On the other hand, the eye movement perturbation response modulation (PRM) increased with a factor of about 1.5 (see Fig. 4*B*). Thus the effect of decreas-

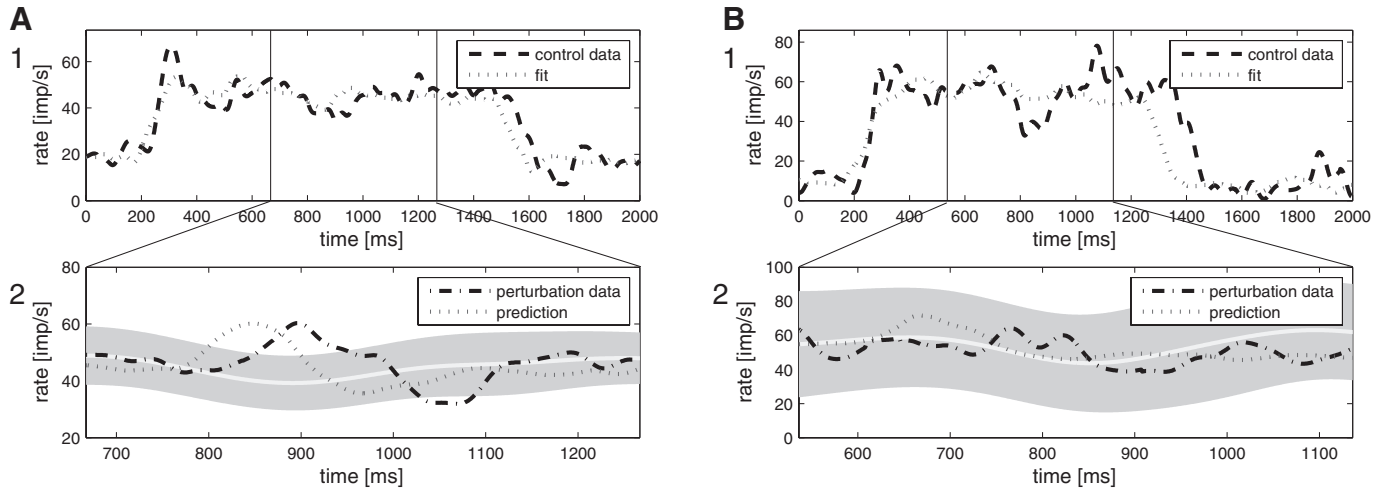

FIG. 8. Dependence of neuronal response sensitivity (black) and regression weight for eye velocity (gray) on target velocity. Both measures decrease with increasing target velocity by a factor of 2. Compare with Fig. 4*B*, which shows that the eye-movement modulation increases by a factor of only about 1.5.

ing neuronal perturbation response with higher target velocity prevails over the effect of increasing ocular perturbation response, which can explain the lower number of responsive data sets with increasing target velocity.

LF motion responses

The main emphasis of this study is on the neuronal responses during smooth-pursuit perturbation. Since virtually all MSTd neurons responding during SPEM also responded during LF visual motion (in the opposite direction), some examples ($n = 15$) were taken to underline the difference in the response characteristics. Values were taken from neurons tested at 15°/s stimulus velocity ($n = 12$). The remaining neurons were tested at 20°/s ($n = 2$) and 5°/s ($n = 1$) with similar results.

LF perturbation responses

EYE MOVEMENTS ASSOCIATED WITH LF MOTION. The LF stimulus consistently led to changes in eye velocity following the perturbation (Fig. 9). For an underlying stimulus velocity of 15°/s, the perturbation (5 Hz, ±10°/s) response latency (PRL) was 88 ± 7.4 ms, slightly shorter than that during SPEM. The eye-movement response modulation (PRM) with 10.5 ± 2.1°/s (corresponding to a gain of 0.53) was also comparable to the value during SPEM.

NEURONAL RESPONSE. All neurons ($n = 15$), except for one, were clearly modulated by the LF perturbation. The sensitivity ranged from 1.01 to 4.77 impulses·s^{-1}·deg^{-1}·s^{-1} and was on average 2.25 impulses·s^{-1}·deg^{-1}·s^{-1}. In contrast to the late onset of smooth-pursuit perturbation responses, neuronal activity following LF motion led the eye-movement response (NPRL, Fig. 9) by 34.1 ms for most neurons (12 of 15). For

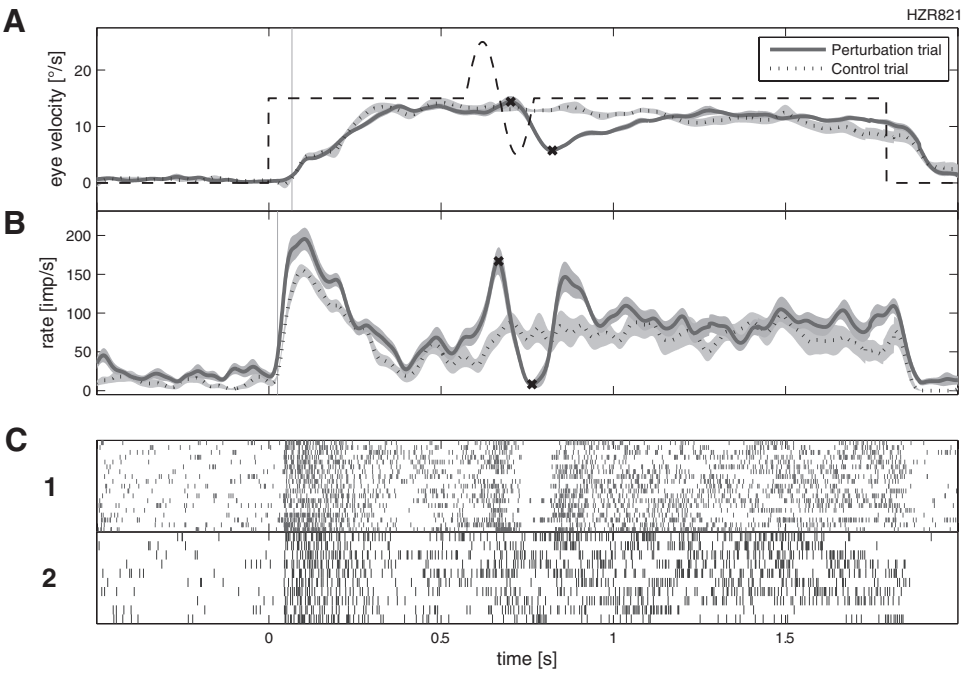

FIG. 9. Response of an MSTd neuron to large-field (LF) visual motion with (straight line) and without (dotted line, control) perturbation. For further details see Figs. 1 and 2. During LF stimulation and perturbation the neuronal response starts before the eye movements.

two neurons activity lagged both for ramp (see following text) and for perturbation. The remaining neuron lagged only during perturbation.

LF ramp responses

EYE MOVEMENTS. The LF stimulus induced eye movements with a latency (EMOL) of 76 ± 20.1 ms, which was much shorter than the 120 ms obtained during SPEM stimulation. Eye velocity at 200 ms poststimulus onset reached 12.3°/s (average) with a 15°/s stimulus.

NEURONAL RESPONSES. In general the neuronal response latency during ramp stimulation (NRL) was short (Fig. 9) except for two neurons with a latency of 209 and 241 ms after stimulus onset. All other neurons (including those tested at 5 and 20°/s) had short latencies (average 42 ± 14 ms) with respect to stimulus onset and started on average 34 ms before the eye movement. This is in sharp contrast to the SPEM situation, during which the neurons responded on average 135 ms following the eye-movement onset.

The sensitivity of the neurons tested with LF stimulation was variable. Some neurons ($n = 4$ of 12) had small steady-state responses (<0.5°/s) but a large initial response, which might reflect the different amount of retinal slip during stimulation. The remaining neurons ($n = 8$) had an average sensitivity of 3.19 impulses$\cdot s^{-1}\cdot deg^{-1}\cdot s^{-1}$.

Responses during target blinking

To confirm the dependence of the smooth-pursuit–related response on extraretinal signals, 22 of the SPEM-related neurons were additionally tested during step-ramp stimulation, with the target blinked for 100 ms during ongoing pursuit (Ono and Mustari 2006). For the tested neurons the neuronal activity started 131 ms (average) after pursuit onset (see earlier text). During the target blink the eye movement continued as smooth pursuit with only a small transient decline in velocity. The minimum in eye velocity was reached 215 ms (average) after blink onset. The gain decreased on average to 0.69 compared with the control gain of 0.90 for the population of tested neurons. The neuronal activity was not significantly affected by the blink. The relation of neuronal activity to eye velocity during the blink analysis period was 109% compared with the 100% for the controls—thus even slightly higher than that under control conditions. It is known that neuronal responses related to *visual motion* (e.g., in area MT) show a pronounced activity decrease during the target blink (Newsome et al. 1988). Thus the continuous response during the target blink supports the nonretinal origin of the responses during SPEM.

DISCUSSION

Our study shows that the characteristic changes in eye movement due to dynamic gain control can be easily demonstrated in accordance with earlier studies (Churchland and Lisberger 2005a,b). With higher ongoing SPEM velocities the perturbation response increases and the latency decreases (Fig. 4). In general the perturbation response latency (PRL) appeared shorter than the SPEM onset latency (EMOL) during step-ramp stimulation, although it has to be kept in mind that the methods for determining SPEM (onset) and perturbation (peak-to-peak) latencies were different (see Fig. 1 and METHODS).

Despite prominent eye-movement changes with perturbation, this was only poorly reflected in the SPEM response of MSTd neurons. Our MSTd neurons had a good sensitivity during pursuit, but a perturbation-related response could be detected for only a minority (36%). Even for the modulated neurons, the perturbation response was not detectable at all stimulus velocities. Interestingly the percentage of responsive data sets decreased with higher stimulus velocities (see RESULTS). This most likely seems to be related to the decrease of neuronal sensitivity with increasing stimulus velocity (Fig. 8), which appears to be higher than the increase of the eye-movement perturbation response (PRM, Fig. 4*B*).

For the classification of neurons, the noise level plays an important role. We chose 3SDs to judge whether a neuronal response shows responsiveness. A higher criterion tends to miss weak responses; a lower one might classify noise as a perturbation response. Our subsequent regression analysis showed that for 68% of our data sets the presence or absence of a neuronal perturbation response was a direct consequence of the dynamic properties of the neurons. The large proportion of nonresponsive neurons is thus explained by the fact that the neuronal discharge is mainly determined by eye velocity and, in these neurons, the expected perturbation modulation was too small compared with the noise level. The remaining 32% fall into two categories: for 13% the measured perturbation response was even larger than predicted, which could be explained by the observation that phasic responses were usually underestimated by our regression model. The remaining 19% of the data sets were expected to show a detectable modulation based on the control data, but the measurement failed to reveal the expected perturbation response.

The relatively late onset of the perturbation-related response seems to argue against participation of MSTd neurons in generation of the perturbation response. However, MSTd neurons could provide a signal that carries a delayed efference copy of eye movements (also see the following text), which is needed to reconstruct a signal representing target velocity in space from a similarly delayed retinal slip signal. From earlier studies it is known that onset of the SPEM component of MSTd neurons often starts >100 ms after eye-movement onset (Newsome et al. 1988). In our sample the average delay was 127 ms. Similarly, the perturbation response occurred 102 ms after the eye movement. MSTd could thus monitor the state of the SP system. The highly direction specific nature and SPEM dependence of responses suggest that MSTd neurons could play a role in maintenance of pursuit (Ono and Mustari 2006). A direct involvement of MSTd in dynamic gain control, however, seems unlikely.

Origin of the nonretinal component

Maintenance of SPEM critically depends on feedback mechanisms providing information about eye velocity (Krauzlis and Lisberger 1994; Nuding et al. 2008; Robinson et al. 1988). One possible source could be the thalamus, where SPEM-related activity has recently been encountered (Tanaka 2005). Here, neuronal activity lags SPEM initiation on average by 30 ms, which is still considerably shorter than the 100–130 ms encountered for our MSTd neurons and found in earlier studies (Newsome et al. 1988). MSTd also receives an input from FEF

(Tusa and Ungerleider 1988), where SPEM-related activity is present as well. Neuronal activity in FEF typically leads SPEM (Tanaka and Fukushima 1998), but there are late-responding neurons, which could account for the delay seen in MSTd.

Recently eye-position–related activity has been discovered in the somatosensory cortex, probably reflecting proprioception (Wang et al. 2007). Although these signals have an average delay of 80 ms after saccade onset (Zhang et al. 2008), they are not appropriate, since MSTd neurons encode gaze rather than eye velocity (Ono and Mustari 2006). Thus the thalamic signal seems adequate, although an explanation is missing as to how the long delay seen in MSTd neurons is generated.

Where does the dynamic gain control take place?

Current studies show that at least two cortical structures are involved in the generation and control of SPEM. Evidence exists to show that the FEF participates more in SPEM initiation and MST more in SPEM maintenance (Nuding et al. 2008), but the roles of these areas and their pontine target areas are not completely separated. Several studies point toward a prominent role of FEF in dynamic gain control. For example, electrical stimulation in FEF enhances a perturbation response (Tanaka and Lisberger 2001). Recently it was shown using transcranial magnetic stimulation (TMS) in humans that the FEF is directly involved in dynamic gain control during SPEM (Nuding et al. 2008). Potentially, dynamic gain control could be the result of some interaction between FEF and MST. However, our data do not support a role for MSTd in such interaction. The MSTd smooth-pursuit signals are too late to allow a substantial contribution to the very reliable eye-movement signals as a result of dynamic gain control. Similar conclusions were drawn in an earlier study (Churchland and Lisberger 2005b) that did not directly investigate neuronal activity during perturbation. Currently, it cannot be excluded that the dynamic gain control results from interaction with other parietooccipital areas, such as MT or MSTl, which so far have not been thoroughly investigated with this question in mind. However, it also seems quite possible that the dynamic gain control results from some local interactions within FEF, where not only SPEM-related but also visual responses are encountered (Fukushima et al. 2002). Alternatively, short-latency visual and eye motion signals in cortical-ponto-cerebellar circuits might all contribute to dynamic gain control.

What is the functional meaning of the extraretinal component of MSTd neurons?

Before considering this question, it has to be emphasized that virtually all MSTd neurons possess large visual-motion–sensitive receptive fields. Importantly, the large majority of neurons has opposite preferred directions for visual and nonretinal components, as described previously (Newsome et al. 1988; Shenoy et al. 2002). In our study LF visual motion induced an OKR response with a short latency (average 76 ms) and the perturbation response during OKR showed a similar latency (average 88 ms). For virtually all neurons LF visual motion and perturbation were accompanied by neuronal activity changes. In contrast to the extraretinal pursuit component, these activity changes occurred much earlier before the eye movement for both ramp and perturbation stimulation (average lead: 34 ms). This general pattern leads to a number of interpretations.

Several studies have put forward the suggestion that extraretinal signals play an important role in pursuit maintenance (Newsome et al. 1988; Nuding et al. 2008; Ono et al. 2009). This is quite plausible despite the large delay of the extraretinal component in MSTd neurons. Interestingly, this neuronal delay (127 ms) and the delay of pursuit onset with respect to target motion (120–140 ms) exhibit similar values. The similarity of temporal delays together with simulations of our nonlinear pursuit model incorporating delays (Brostek et al. 2009) suggest that the extraretinal pursuit signal of MSTd neurons may serve to reconstruct target velocity in space, which then could be represented in MSTl, as suggested previously (Ilg and Thier 2003). The representation of the perturbation response in our MSTd neurons is compatible with this idea, since it reflects what was predicted from our modeling of the step-ramp responses.

One important argument against this hypothesis is that MSTd responses found during LF visual motion do not reflect delayed eye velocity. Thus other roles for the extraretinal signals have to be considered. For example, MST has been shown to be involved in decoding movement through the environment (Duffy and Wurtz 1991). It is thus possible that late-responding MSTd pursuit neurons might be involved in spatial orientation and navigation (Chen et al. 2008). Based on these ideas, a possible hypothesis for the signal coded by our MSTd neurons is that they represent gaze velocity in a spatial reference frame, given that large-field visual motion may be interpreted as self-motion at the processing stage of MSTd.

Ocular following

There have been a number of studies relating MSTd activity to the generation of ocular following. With LF visual motion ocular following occurs 55–60 ms after stimulus onset (Miles et al. 1986). Visual MSTd activity recorded under these conditions started before the eye movements (Kawano et al. 1994). It has been concluded that this visual signal is transferred to the brain stem and the cerebellum to generate the eye-movement response (Kawano 1999). In our study LF visual motion led to comparable results. However, since most MSTd neurons with an extraretinal signal have a preferred direction opposite to the visual response, it appears unlikely that the response of these neurons is used only to drive the ocular following response. Although parietooccipital lesions including MSTd affect the ocular following response (Takemura et al. 2007), specific regions of MST may serve different functions.

Optic flow

Recent reports focus on the responses of MSTd neurons to optic flow (Britten 2008; Shenoy et al. 2002). Furthermore, at least some MSTd neurons compensate for pursuit speed during optic flow, which provides critical information for the computation of self-motion (Shenoy et al. 2002). The authors in this study also determined the smooth-pursuit response of the MSTd neurons, which—as it is known from previous studies—had a preferred direction opposite to the optimal laminar flow direction.

Interestingly, Inaba et al. (2007) found that the visual motion response of MSTd neurons is affected by smooth pursuit even if the neurons do not respond during smooth pursuit per se. This applied to >70% of the MSTd neurons tested. These results also support a role of MSTd in self-motion perception.

Conclusions

Only a minority of smooth-pursuit–related MSTd neurons show detectable modulation in response to short perturbations of the visual stimulus. The responding neurons were modulated on average >100 ms after the eye movement. The small number of responsive neurons can be explained by the discharge properties of MSTd neurons derived from step-ramp responses. Based on these findings it is unlikely that MSTd neurons play a significant role in dynamic gain control. However, the SPEM and perturbation results are still compatible with models, in which MSTd is involved in smooth-pursuit maintenance (Dicke and Thier 1999; Nuding et al. 2008).

If one takes into account that virtually all MSTd neurons with extraretinal signals encode gaze velocity, have large-field motion-sensitive receptive fields, and show visual responses with opposite preferred directions, other functional interpretations have to be considered. In accordance with earlier studies (Shenoy et al. 1999) LF motion could be interpreted as being caused by self-motion in space. Accordingly, SPEM-responsive MSTd neurons could then represent gaze velocity in a spatial reference frame.

GRANTS

This work was supported by National Institutes of Health Grants EY-013308 and RR-00166 and Bernstein Center for Computational Neuroscience Grant BMBF 011GQ0440.

REFERENCES

Britten KH. Mechanisms of self-motion perception. *Annu Rev Neurosci* 31: 389–410, 2008.

Brostek L, Ono S, Mustari MJ, Nuding U, Büttner U, Glasauer S. Neuronal responses in the cortical area MSTd during smooth pursuit and ocular following eye movements. *BMC Neurosci* 10, *Suppl.* 1: P367, 2009.

Büttner U, Büttner-Ennever JA. Present concepts of oculomotor organization. *Prog Brain Res* 151: 1–42, 2006.

Chen CW, Gu Y, Takahashi K, Angelaki DE, DeAngelis GC. Clustering of self-motion selectivity and visual response properties in macaque area MSTd. *J Neurophysiol* 100: 2669–2683, 2008.

Churchland AK, Lisberger SG. Gain control in human smooth-pursuit eye movements. *J Neurophysiol* 87: 2936–2945, 2002.

Churchland AK, Lisberger SG. Discharge properties of MST neurons that project to the frontal pursuit area in macaque monkeys. *J Neurophysiol* 94: 1084–1090, 2005a.

Churchland AK, Lisberger SG. Relationship between extraretinal component of firing rate and eye speed in area MST of macaque monkeys. *J Neurophysiol* 94: 2416–2426, 2005b.

Dicke PW, Thier P. The role of cortical areas MST in a model of combined smooth eye-head pursuit. *Biol Cybern* 80: 71–84, 1999.

Distler C, Mustari MJ, Hoffmann KP. Cortical projections to the nucleus of the optic tract and dorsal terminal nucleus and to the dorsolateral pontine nucleus in macaques: a dual retrograde tracing study. *J Comp Neurol* 444: 144–158, 2002.

Duffy CJ, Wurtz RH. Sensitivity of MST neurons to optic flow stimuli. I. A continuum of response selectivity to large-field stimuli. *J Neurophysiol* 65: 1329–1345, 1991.

Fuchs AF, Robinson DA. A method for measuring horizontal and vertical eye movement chronically in the monkey. *J Appl Physiol* 21: 1068–1070, 1966.

Fukushima K, Yamanobe T, Shinmei Y, Fukushima J. Predictive responses of periarcuate pursuit neurons to visual target motion. *Exp Brain Res* 145: 104–120, 2002.

Ilg UJ, Thier P. Visual tracking neurons in primate area MST are activated by smooth-pursuit eye movements of an "imaginary" target. *J Neurophysiol* 90: 1489–1502, 2003.

Inaba N, Shinomoto S, Yamane S, Takemura A, Kawano K. MST neurons code for visual motion in space independent of pursuit eye movements. *J Neurophysiol* 97: 3473–3483, 2007.

Judge SJ, Richmond BJ, Chu FC. Implantation of magnetic search coils for measurement of eye position: an improved method. *Vision Res* 20: 535–538, 1980.

Kawano K. Ocular tracking: behavior and neurophysiology. *Curr Opin Neurobiol* 9: 467–473, 1999.

Kawano K, Shidara M, Watanabe Y, Yamane S. Neural activity in cortical area MST of alert monkey during ocular following responses. *J Neurophysiol* 71: 2305–2323, 1994.

Komatsu H, Wurtz RH. Relation of cortical areas MT and MST to pursuit eye movements. I. Localization and visual properties of neurons. *J Neurophysiol* 60: 580–603, 1988.

Krauzlis RJ. Recasting the smooth pursuit eye movement system. *J Neurophysiol* 91: 591–603, 2004.

Krauzlis RJ, Lisberger SG. Temporal properties of visual motion signals for the initiation of smooth pursuit eye movements in monkeys. *J Neurophysiol* 72: 150–162, 1994.

Ladda J, Eggert T, Glasauer S, Straube A. Velocity scaling of cue-induced smooth pursuit acceleration obeys constraints of natural motion. *Exp Brain Res* 182: 343–356, 2007.

Leigh RJ, Zee DS. *The Neurology of Eye Movements*. New York: Oxford Univ. Press, 2006.

Maunsell JHR, Van Essen DC. The connections of the middle temporal visual area (MT) and their relationship to a cortical hierarchy in the macaque monkey. *J Neurosci* 3: 2563–2586, 1983.

Miles FA, Kawano K, Optican LM. Short-latency ocular following responses of monkey. I. Dependence on temporospatial properties of visual input. *J Neurophysiol* 56: 1321–1354, 1986.

Mustari MJ, Fuchs AF, Kaneko CRS, Robinson FR, Kaneko CR. Anatomical connections of the primate pretectal nucleus of the optic tract. *J Comp Neurol* 349: 111–128, 1994.

Mustari MJ, Fuchs AF, Wallman J. Smooth-pursuit-related units in the dorsolateral pons of the rhesus macaque. *J Neurophysiol* 60: 664–686, 1988.

Newsome WT, Wurtz RH, Komatsu H. Relation of cortical areas MT and MST to pursuit eye movements. II. Differentiation of retinal from extraretinal inputs. *J Neurophysiol* 60: 604–620, 1988.

Nuding U, Ono S, Mustari MJ, Büttner U, Glasauer S. A theory of the dual pathways for smooth pursuit based on dynamic gain control. *J Neurophysiol* 99: 2798–2808, 2008.

Ono S, Das VE, Mustari MJ. Gaze-related response properties of DLPN and NRTP neurons in the rhesus macaque. *J Neurophysiol* 91: 2484–2500, 2004.

Ono S, Mustari MJ. Extraretinal signals in MSTd neurons related to volitional smooth pursuit. *J Neurophysiol* 96: 2819–2825, 2006.

Ono S, Mustari MJ. Smooth pursuit-related information processing in frontal eye field neurons that project to the NRTP. *Cereb Cortex* 19: 1186–1197, 2009.

Rashbass C. The relationship between saccade and smooth tracking eye movements. *J Physiol* 159: 326–338, 1961.

Robinson DA, Gordon JL, Gordon SE. A model of the smooth pursuit eye movement system. *Biol Cybern* 55: 43–57, 1988.

Schwartz JD, Lisberger SG. Initial tracking conditions modulate the gain of visuo-motor transmission for smooth pursuit eye movements in monkeys. *Vis Neurosci* 11: 411–424, 1994.

Shenoy KV, Bradley DC, Andersen RA. Influence of gaze rotation on the visual response of primate MSTd neurons. *J Neurophysiol* 81: 2764–2786, 1999.

Shenoy KV, Crowell JA, Andersen RA. Pursuit speed compensation in cortical area MSTd. *J Neurophysiol* 88: 2630–2647, 2002.

Suzuki DA, Yamada T, Yee RD. Smooth-pursuit eye-movement-related neuronal activity in macaque nucleus reticularis tegmenti pontis. *J Neurophysiol* 89: 2146–2158, 2003.

Takemura A, Murata Y, Kawano K, Miles FA. Deficits in short-latency tracking eye movements after chemical lesions in monkey cortical areas MT and MST. *J Neurosci* 27: 529–541, 2007.

Tanaka M. Involvement of the central thalamus in the control of smooth pursuit eye movements. *J Neurosci* 25: 5866–5876, 2005.

Tanaka M, Fukushima K. Neuronal responses related to smooth pursuit eye movements in the periarcuate cortical area of monkeys. *J Neurophysiol* 80: 28–47, 1998.

Tanaka M, Lisberger SG. Regulation of the gain of visually guided smooth-pursuit eye movements by frontal cortex. *Nature* 409: 191–194, 2001.

Thier P, Koehler W, Buettner UW. Neuronal activity in the dorsolateral pontine nucleus of the alert monkey modulated by visual stimuli and eye movements. *Exp Brain Res* 70: 496–512, 1988.

Tusa RJ, Ungerleider L. Fiber pathways of cortical areas mediating smooth pursuit eye movements in monkeys. *Annu Rev Neurosci* 23: 174–183, 1988.

Wang X, Zhang M, Cohen IS, Goldberg ME. The proprioceptive representation of eye position in monkey primary somatosensory cortex. *Nat Neurosci* 10: 640–646, 2007.

Zhang M, Wang X, Goldberg ME. Monkey primary somatosensory cortex has a proprioceptive representation of eye position. *Prog Brain Res* 171: 37–45, 2008.

frontiers in
COMPUTATIONAL NEUROSCIENCE

METHODS ARTICLE
published: 30 March 2011
doi: 10.3389/fncom.2011.00015

An information-theoretic approach for evaluating probabilistic tuning functions of single neurons

Lukas Brostek[1,2]*, Thomas Eggert[3], Seiji Ono[4], Michael J. Mustari[4], Ulrich Büttner[2,5] and Stefan Glasauer[1,2,5]

[1] Clinical Neurosciences, Ludwig-Maximilians-Universität München, Munich, Germany
[2] Bernstein Center for Computational Neuroscience, Munich, Germany
[3] Department of Neurology, Ludwig-Maximilians-Universität München, Munich, Germany
[4] Washington National Primate Research Center, University of Washington, Seattle, WA, USA
[5] Integrated Center for Research and Treatment of Vertigo, Ludwig-Maximilians-Universität München, Munich, Germany

Edited by:
Karen A. Moxon, Drexel University, USA

Reviewed by:
Karim Oweiss, Michigan State University, USA
Alessandro Scaglione, Drexel University, USA

***Correspondence:**
Lukas Brostek, Department of Neurology, Ludwig-Maximilians-Universität München, Marchioninistraße 23, 81377 Munich, Germany.
e-mail: lukas.brostek@lrz.uni-muenchen.de

Neuronal tuning functions can be expressed by the conditional probability of observing a spike given any combination of explanatory variables. However, accurately determining such probabilistic tuning functions from experimental data poses several challenges such as finding the right combination of explanatory variables and determining their proper neuronal latencies. Here we present a novel approach of estimating and evaluating such probabilistic tuning functions, which offers a solution for these problems. By maximizing the mutual information between the probability distributions of spike occurrence and the variables, their neuronal latency can be estimated, and the dependence of neuronal activity on different combinations of variables can be measured. This method was used to analyze neuronal activity in cortical area MSTd in terms of dependence on signals related to eye and retinal image movement. Comparison with conventional feature detection and regression analysis techniques shows that our method offers distinct advantages, if the dependence does not match the regression model.

Keywords: information theory, mutual information, neuronal tuning, neuronal latency, MSTd

1 INTRODUCTION

Defining the dependence of neuronal activity on certain variables, e.g., presented stimuli, is often the major aim of studies attempting to define neural mechanisms supporting sensory-motor behavior. A neuronal tuning function defines the functional relation between the spiking activity and uni- or multivariate explanatory variables. Virtually every sensory system, from the vertebrate visual cortex to wind-detecting neurons in the cricket cercal system, has been characterized in this way (Rieke et al., 1997; Dayan and Abbott, 2001).

One common approach to determine the dependence of neurons on these variables is regression analysis, in which the spike density function is approximated by one or multiple explanatory variables using linear or other models (Ilg et al., 2004; Ono et al., 2004; Wu et al., 2006). It remains questionable, however, what model assumptions can be made when analyzing neuronal data.

Another difficulty in the analysis of neuronal data is the accurate estimation of latencies between any given variable and associated neuronal activity (Seal et al., 1983; Friedman and Priebe, 1998; Bollimunta et al., 2007). For example, when visual information arrives in cortical area MSTd, which is the dorsal part of the medial superior temporal cortex, it has passed a number of processing stages resulting in a considerable delay with respect to the stimulus. Depending on the properties of the visual input, retinal delay alone accounts for a latency of up to 50 ms (Schmolesky et al., 1998). On the way through thalamus and primary visual areas, the signal propagates with a velocity on the order of 10–100 m/s. Additionally, synaptic transmission produces delays of several milliseconds. Therefore, a proper model of this system has to account for the fact that neuronal activity is a delayed function of the input variables.

Here, we present a novel approach for evaluating neuronal tuning functions. Using a probabilistic tuning function description, we propose a model-free alternative to regression analysis. By maximizing the mutual information between the neuronal activity and any combination of explanatory variables, the presented method allows the estimation of neuronal latency and gives a measure for the dependence of neuronal activity on different combinations of the explanatory variables. This stands in contrast with typical applications of information-theoretic techniques in neural data analysis (see, e.g., Rieke et al., 1997), which investigate the relevance of spike timing or the influence of correlations in neural populations.

In the following, we demonstrate the application of this novel method on data from MSTd and show that neuronal activity in this cortical area is determined by combinations of retinal (e.g., image velocity) and extraretinal variables (e.g., eye velocity and position).

2 METHODS

2.1 EVALUATING PROBABILISTIC TUNING FUNCTIONS

The method proposed here consists of two components: first, a Bayesian approach for the determination of probabilistic tuning functions, and second, an information-theoretic technique for evaluating these tuning functions by estimating neuronal latencies and selecting those variables that show the greatest dependence on the neuronal activity.

2.1.1 Bayesian approach for tuning function determination

Let S be a binary random variable for the observation of a spike or non-spike, with $p_S(s)$ denoting the probability mass function of spike occurrence. The discrete random variable V denotes the observation of a specific combination of explanatory variables with

associated probability mass function $p_V(v)$. Then, $p_{S|V}(s|v)$ expresses the conditional probability of observing a spike given any combination of variable values. By multiplying with the sampling rate, this probability translates directly into an expectation value of the rate of spiking activity, and therefore describes a neuronal tuning function. Using Bayes' theorem, $p_{S|V}(s|v)$ can be expressed as the quotient of the joint probability mass function $p_{V,S}(v,s)$ divided by $p_V(v)$:

$$p_{S|V}(s \mid v) = \frac{p_{V,S}(v,s)}{p_V(v)}.$$

The normalization on $p_V(v)$ allows the estimation of the tuning function in unbalanced designs (i.e., unequal number of observations across explanatory variables). **Figure 1** demonstrates this principle for the two-dimensional case.

Estimates of $p_V(v)$ and $p_{V,S}(v,s)$ can be attained by generating histograms of the experimental data. Note that the joint probability mass function $p_{V,S}(v,s)$ critically depends on the assumed neuronal latency. For estimating the optimal number of bins, with which each variable is discretized, we adapted an algorithm proposed by Knuth (2006). According to this, the optimal bin width is defined by the Bayesian estimate of the number of segments of a piecewise constant probability function that is limited to a fixed interval. The most probable solution is determined by a balance between the likelihood function, which describes the probability that a data point can be assigned to a specific bin, and the prior probability that decreases with an increasing number of bins. For smoothing the resulting histograms, we used a symmetrical Gaussian low-pass filter with a SD of two bin widths.

The amount of data needed for generating reasonably fine-grained histograms increases exponentially with the number of dimensions. However, the duration one single neuron can be recorded is restricted due to experimental and physiological constraints. Hence, there is a practical limitation on the number of variables that can be modeled or included in this Bayesian approach for tuning function determination.

2.1.2 Mutual information maximization

Entropy H is a measure of the uncertainty of a single random variable. The reduction in uncertainty due to another random variable is called mutual information I (Cover and Thomas, 1991). Mutual information is a measure of the dependence between two random variables. It is symmetric, non-negative, and equal to zero only if both random variables are mutually independent. Mutual information captures all dependencies between random variables, not just second order dependencies which are indicated, for example, by the covariance.

When applied to the two random variables V and S from the previous section, the mutual information $I(V;S)$ can be stated as

$$I(V;S) = H(S) - H(S \mid V)$$

with $H(S)$ being the entropy of S and $H(S|V)$ the conditional entropy of S given V, also referred to as noise entropy. These are defined by

$$H(S) = -\sum_s p_S(s) \log p_S(s)$$

$$H(S \mid V) = -\sum_v p_V(v) \sum_s p_{S|V}(s \mid v) \log p_{S|V}(s \mid v),$$

where $p_S(s)$ denotes the probability mass function of spike occurrence. The conditional probability $p_{S|V}(s|v)$ denotes the tuning function, determined by the Bayesian approach mentioned in the previous section. This probability and thus $H(S|V)$ as well depend on both the choice of variables analyzed and the choice of latencies between these variables and the neuronal activity.

Maximizing the mutual information between V and S provides an unbiased estimator for the neuronal latency. A proof based on the data-processing inequality theorem in information theory (Cover and Thomas, 1991) is given in the Section "Appendix." The proof requires only the moderate assumption that a constant delay exists between stimulus and neuronal activity.

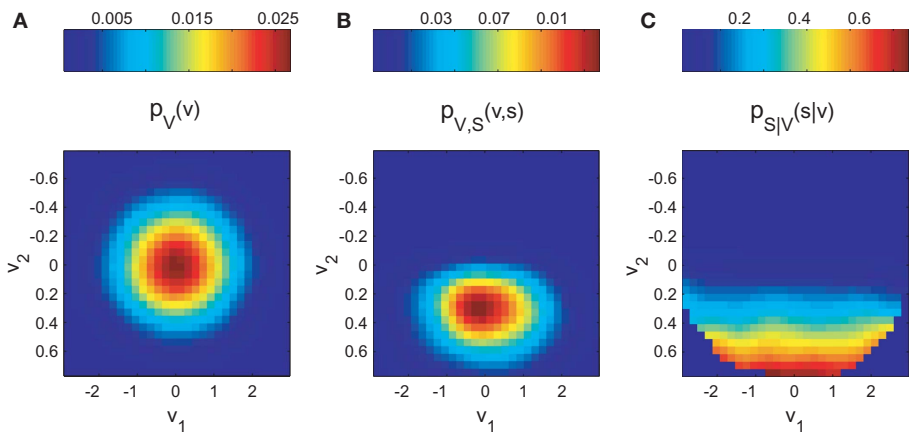

FIGURE 1 | Bayesian approach for tuning function determination demonstrated for simulated two-dimensional data. The synthetic dataset is 10K samples long and includes 264 spikes. **(A)** illustrates the probability mass function $p_V(v)$ of the occurrence of combinations of mutual independent variables v_1 and v_2. The joint probability mass function $p_{V,S}(v,s)$ of coincident variable and spike occurrence is shown in **(B)**. Dividing $p_{V,S}(v,s)$ by $p_V(v)$ yields the conditional probability $p_{S|V}(s|v)$ of observing a spike given any combination of the variables **(C)**.

As $H(S)$ is defined by the neuronal activity alone, the maximization of $I(V;S)$ is achieved by minimizing the noise entropy $H(S|V)$. In the limit case of $H(S|V) = 0$, S and V are one-to-one related and the probability of spike occurrence is uniquely defined by the explanatory variables.

Due to the limitation mentioned in the previous section, the dimension of the tuning function is constrained by the amount of data recorded. Estimating the entropy from a finite number of samples is prone to systematic errors. This so called sampling bias problem is described in Panzeri et al. (2007). Put shortly, the noise entropy tends to be underestimated, as finite sampling makes the neuronal response seem less variable than it really is. In our case, the length of each dataset was around 500K samples. The typical number of bins per dimension was less than 20. Hence, the average amount was more than 1250 samples per stimulus condition for the case of two-dimensional tuning functions. To avoid errors due to an insufficient amount of samples, we limited the analysis to this case. Bins containing less than 32 samples were omitted in the analysis.

To investigate the dependence of a spike on more than two explanatory variables, we determined the tuning functions of a single neuron for any pairwise selection V_k of those variables. For each of these pairs neuronal latencies of both variables were estimated by maximizing the mutual information $I(V_k;S)$. As $I(V_k;S)$ quantifies the dependence of the spike on the selected pair of variables, those two variables that are most related to the spiking activity can be determined by comparing the maximal mutual information of the two-dimensional tuning functions.

The mutual information depends on the number of bins used to discretize the variables. Using the algorithm of Knuth (2006; see previous section) an optimal number of bins was estimated for each pair of variables. The average of these optimal numbers of bins was determined and used for comparing the different pairs of variables. For each neuron, this average number of bins was determined separately.

2.2 OTHER METHODS

2.2.1 Regression analysis

Regression analysis is a common approach to estimate both the latency and the dependence of neuronal activity on explanatory variables. Spiking activity was represented as a spike density function (sdf), generated by convolving the spike pulses with a Gaussian window function (σ = 100 ms). To allow a comparison with the two-dimensional analysis in previous section, the linear regression model consisted of the two regressor variables v_1 and v_2 according to

$$sdf = \beta_0 + \beta_1 \cdot v_1 + \beta_2 \cdot v_2 + r,$$

where r represents the Gaussian noise term. The model was fit to the whole dataset. Neuronal latencies were estimated by shifting the variables in steps of 10 ms and searching for the best fit (maximal R^2). Furthermore, maximal R^2 values were compared for all pairs of variables.

2.2.2 Simulation of synthetic datasets

For each dataset the two explanatory variables image velocity ($v_1(t)$) and eye velocity ($v_2(t)$) were generated as 10 s long band-limited (<20 Hz) white noise random signal, sampled at 1 kHz. The mean was zero and the SD was the same as in the example MSTd neuron dataset. Both variables were perfectly uncorrelated.

For the simulation of neuronal activity, we used a Poisson process model as described in Rieke et al. (1997). The Poisson model is characterized by the statistical independence of events in disjoint time intervals. The probability distribution for k events in the time interval Δ is

$$P_\lambda(k) = \frac{(\Delta\lambda(t))^k}{k!} e^{-(\Delta\lambda(t))},$$

where $\lambda(t)$ denotes the time-dependent firing rate. To simulate a neuron that resembles the two-dimensional tuning function $p_{S|V}(s|v)$, $\lambda(t)$ was set to

$$\lambda(t) = p_{S|V_1,V_2}(s \mid v_1(t-\tau_1), v_2(t-\tau_2)) \cdot f_s,$$

with sampling rate f_s and $v_1(t)$ and $v_2(t)$ being time shifted by the estimated neuronal latencies τ_1 and τ_2.

2.3 APPLICATION

The data reported in this paper were recorded in cortical area MSTd from two behaving monkeys (*Macaca mulatta*, 5–7 kg). The experiments were performed at the Yerkes National Primate Research Center (Atlanta, GA, USA) in compliance with National Institutes of Health *Guide for the Care and Use of Laboratory Animals* and protocols were reviewed and approved by the Institutional Animal Care and Use Committee at Emory University. For verifying MSTd location we used functional, histological, and MRI criteria. During the experiments monkeys were seated in a primate chair with their head fixed in the horizontal stereotaxic plane in a completely dark room. Only those neurons that showed significant response to moving visual stimuli were analyzed. Visual receptive fields of neurons were mapped by moving a probe stimulus at regularly spaced eccentricities across the visual field. Most receptive fields were large (>30°) and had their center in the contralateral hemifield in accordance with known MSTd properties. Experimental procedures are explained in detail in Ono et al. (2010).

2.3.1 Visual stimuli

Visual large field (LF) stimuli (35° × 35° random dot patterns) were rear projected on a tangent screen. Data were acquired only for those movement directions that were previously identified to be the preferred direction of the neuron, i.e., the direction which elicits maximal spiking activity for a moving LF stimulus in the analyzed neuron.

For each neuron two kinds of paradigms were tested:

(1) Fixation during moving LF stimulus: The monkey fixated a small target spot located at the center of gaze. After some random time the LF stimulus started to move with constant velocity (5–20°/s) in the neuron's preferred direction for a period between 1000 and 1800 ms. During presentation of the visual motion the monkey still fixated the laser spot, though LF stimulation always produces a slight optokinetic nystagmus (<2°/s; see **Figure 2A**).
(2) Optokinetic response: As (1) with the difference that the laser spot was turned off when the LF stimulus began to move. In this case, the monkey's eye movements followed the motion (see **Figure 2B**).

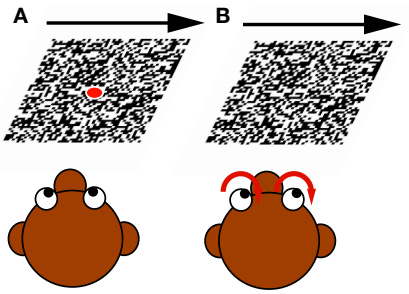

FIGURE 2 | The two different paradigms used: (A) Fixation during moving large field (LF) stimulus. The monkey fixated a centered target spot while the LF stimulus started to move with constant velocity in the neuron's preferred direction. **(B)** Optokinetic response. When the LF stimulus began to move, the monkey's eye movements followed the motion.

During both (1) and (2) the constant velocity phase of LF motion was interrupted (600–800 ms after stimulus onset) in some trials by a perturbation of target speed consisting of one sinusoidal cycle (5 Hz, ±10°/s), which increased the range of image and eye velocity (as in Ono et al., 2010).

This combination of two different paradigms has the advantage of yielding a large range of values for both retinal image velocity during fixation trials, as well as eye velocity in the optokinetic response trials.

2.3.2 Data collection and preparation

Single unit activity was analyzed from 49 neurons. Action potentials were detected with both a hardware window discriminator and template matching algorithm.

Eye movements were detected with standard electro-magnetic methods using scleral search coils (Fuchs and Robinson, 1966). Eye and target position feedback signals were processed with anti-aliasing filters at 200 Hz using 6-pole Bessel filters (latency 5 ms) before digitization at 1 kHz with 16-bit precision. The recorded eye position traces were filtered with an acausal zero phase Gaussian low-pass (cutoff frequency 30 Hz) and three-point differentiated to obtain the velocity traces. Saccades were detected and removed with a slow-phase estimation algorithm as described in Ladda et al. (2007).

We related the neuronal activity to variables supposed to be coded in MSTd during moving LF stimulation (Newsome et al., 1988; Bremmer et al., 1997; Hamed et al., 2003). Retinal variables were image velocity and acceleration, whereas extraretinal variables were eye position, velocity, and acceleration.

3 RESULTS

In this section we demonstrate the analysis of neuronal recordings from MSTd using different methods. Neuronal latency is estimated first using a feature detection technique. We then apply the previously described information-theoretic method on the same data to determine both neuronal latency and dependence of neuronal activity on certain variables. Furthermore we analyze the example MSTd neuron using linear regression analysis. To compare the performance in latency estimation, we simulated 100 neuronal recordings of the example MSTd neuron and analyzed this synthetic datasets using both the information-based method and regression analysis. Finally, we end this section with the population results for 49 MSTd neurons.

3.1 ANALYSIS OF AN EXAMPLE MSTd NEURON

We begin with the detailed analysis of an example neuron. The 763 s long dataset contained 19452 detected spikes. The explanatory variables were slightly correlated, with a maximal Pearson correlation coefficient of 0.23 for the pair of variables (image velocity and eye position).

3.1.1 Feature detection technique

Detecting certain features of averaged data from multiple trials associated with a given stimulus is an often used approach for estimating the latency between some signal, e.g., a stimulus variable, and the neuronal activity. **Figure 3** shows the mean eye movement traces and spike density function of an example MSTd neuron during optokinetic response to a moving LF stimulus. Signal onset was defined as the time when the trace increased above the 99% confidence limit during the preceding fixation period. Latency of the neuronal activity with respect to any explanatory variable was defined as time interval between adjacent onsets of that signal and neuronal activity. Retinal image velocity is the difference between target and eye velocity. As can be seen in **Figure 3**, neuronal latency in regard to target, as well as image velocity, was 45 ms. Regarding the eye velocity signal, neuronal activity was leading (in the following denoted as negative latency) by 20 ms.

3.1.2 Mutual information maximization method

Next we analyze data from the same neuron using our information-based approach. Due to the practical limit of number of variables mentioned in Section 2, we determined the tuning functions for pairwise selections of explanatory variables. Neuronal latencies were also estimated for each pair separately. **Figure 4** demonstrates this for the pair [image velocity & eye velocity] in more detail. The noise entropy $H(S|V)$ is plotted against different latencies for both variables. As can be seen in **Figure 4**, minimal noise entropy (0.1577 bits) is achieved by delaying image velocity by 50 ms and eye velocity by −80 ms relative to spiking activity. With $H(S) = 0.1712$ bits, the mutual information $I(V;S) = H(S) - H(S|V)$ accounted for 0.0136 bits. This information contained in the spiking activity was the maximum that could be explained by the information of that pair of variables. Note that this value depends on the number of bins used to discretize the variables. Here, each explanatory variable was discretized in 22 bins of equal width. The dependence of the estimated latencies on the number of bins is shown in **Figure 5**. For both image and eye velocity the latency estimate is robust for a wide range of chosen number of bins.

In the same way the neuronal tuning functions were determined for all variable pairs (**Figure 6**). Comparing all pairwise selections of considered variables, the mutual information $I(V;S)$ for the pair [image velocity & eye velocity] was maximal. Hence, this pair was most related to spiking activity. As can be seen, the expected rate of spiking activity increased primarily with higher image velocity values. Within a certain range of image velocity, the rate additionally increased with eye velocity, yielding a non-linear dependence of spiking activity on both variables. Estimated latencies of image

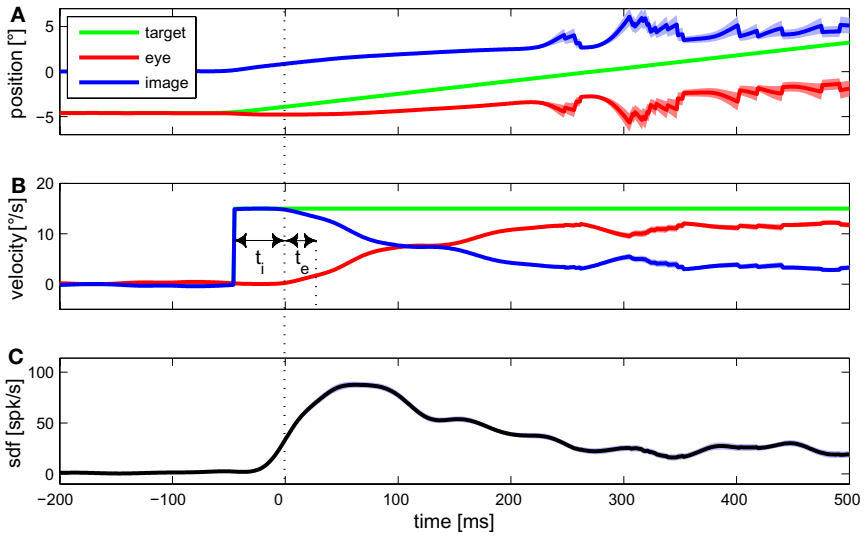

FIGURE 3 | Mean eye movement traces and spike density function (sdf) of an example MSTd neuron during optokinetic response to a moving large field stimulus. In **(A)** the mean traces for target, eye, and retinal image position are plotted. Target and eye position refer to world coordinates, image position to retina based coordinates. The (desaccaded) velocities of target, eye, and retinal image are shown in **(B)**. **(C)** Shows the mean sdf, generated by convolving each spike event trace with a Gaussian window function (σ = 15 ms) and averaging over the 105 trials. Light colored bands around the traces indicate SE. For this condition, feature detection indicated a neuronal latency regarding image velocity of t_i = 45 ms, and regarding eye velocity of t_e = –20 ms.

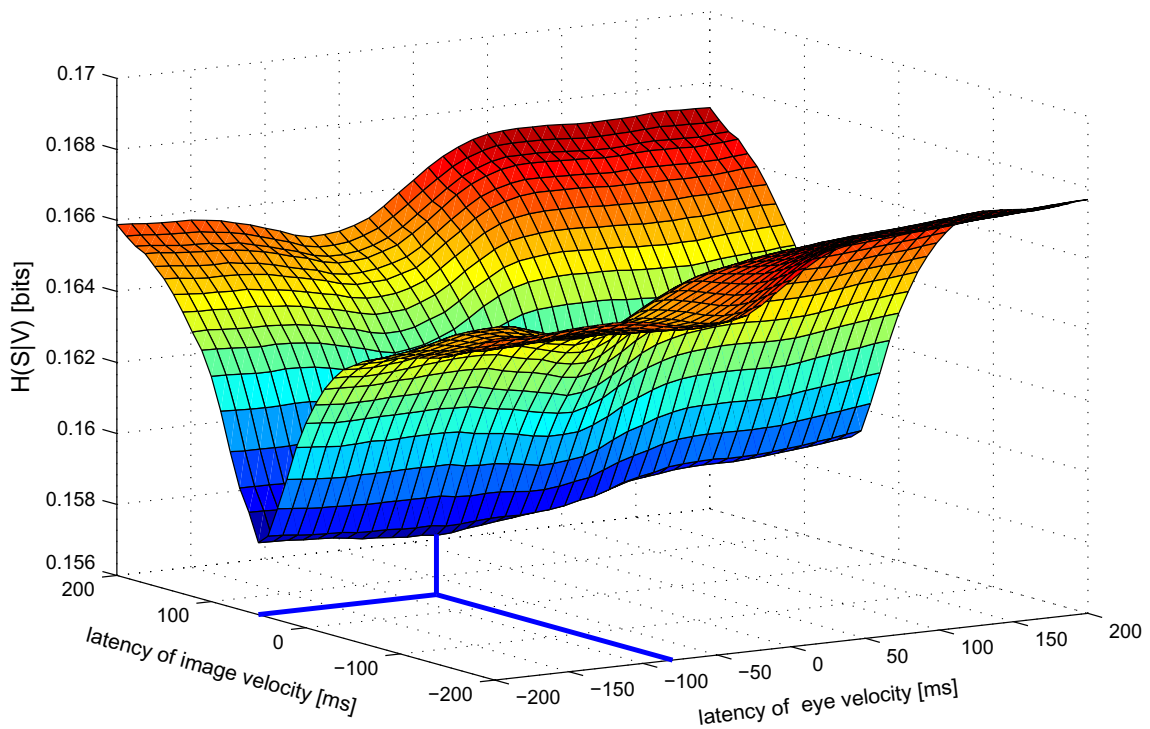

FIGURE 4 | Noise entropy $H(S|V)$ against different latencies of image and eye velocity for the example MSTd neuron. Both variables were shifted in the range between –200 and +200 ms relative to spiking activity. The noise entropy $H(S|V)$ was minimal for an image velocity latency of +50 ms and eye velocity latency of –80 ms. At this point (marked by thick lines) the mutual information $I(V,S)$ between the probability distributions of input variables and spike occurrence was maximized.

velocity, eye velocity, and eye position depended little on which pair was analyzed. In contrast, estimated latencies of eye acceleration and image acceleration depended strongly on the variable they were paired with. This is primarily due to the low dependence of spiking activity on eye and image acceleration in this specific neuron, as can be seen in **Figure 6**.

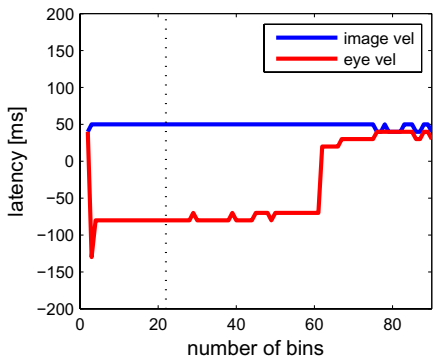

FIGURE 5 | Dependence of the estimated latency on the choice of number of bins, which were used to discretize each dimension. Estimated latencies of image velocity (blue) and eye velocity (red) are plotted. The dotted line indicates the optimal number of 22 bins. Especially for eye velocity, the latency estimate becomes unstable with a very low number or when exceeding more than 60 bins. For more than 90 bins per dimension there are less than 100 samples per bin on average, resulting in errors due to the sampling bias (see Section 2).

3.1.3 Regression analysis

Analogous to the result of the information-based approach, linear regression analysis determined the pair [image velocity & eye velocity] as being most related to spiking activity (R^2=0.40). The estimated neuronal latencies, however, differed from the previous results. The best fit was obtained for delaying image velocity by 70 ms and eye velocity by 170 ms.

3.2 ANALYSIS OF SYNTHETIC DATASETS

To further compare the performances of latency estimation for both the information-based and the regression approach, we simulated 100 neuronal recordings based on the non-linear tuning function for [image velocity & eye velocity] of the example MSTd neuron (details are explained in Section 2.2.2). This allowed the *a priori* definition of the neuronal latency, which was set to the previously estimated values of 50 and −80 ms, respectively.

Results for both approaches are shown in **Figure 7**. Linear regression analysis was not able to correctly estimate the latencies of 50 and −80 ms. The broad distributions of estimates around 67 (±68) and −61 (±110) ms for image and eye velocity, respectively, demonstrate that a linear model is insufficient for analyzing this example neuron. The information-based approach, on the other hand, was capable of estimating the proper latencies for both variables in all datasets.

3.3 MSTd POPULATION RESULTS

We applied our information-theoretic approach to 49 cells recorded in area MSTd. The mean recording length per neuron was about 500 s, with an average spike count of approximately 18K. The explanatory variables were slightly correlated. The combination [image velocity & eye velocity] for instance exhibited an average Pearson correlation coefficient of −0.23 ± 0.11.

3.3.1 Mutual information maximization method

The pairs of variables [image velocity & eye velocity], [image velocity & eye position], [image velocity & eye acceleration], and [eye velocity & eye position] showed maximal mutual information in 20 (41%), 15 (30%), 13 (27%), and 1 (2%) neurons, respectively. The tuning functions of those 20 neurons in which [image velocity & eye velocity] showed maximum $I(V;S)$ are illustrated in **Figure 8**. The tuning to these variables was highly non-linear and differed across the neurons.

Figure 9 shows the estimated latencies of the variables image velocity and eye velocity. To ensure that for each variable only those neurons were selected, in which this variable was actually related to the activity of that neuron, only those cells were considered that belonged to the pair that showed maximum $I(V;S)$. Each histogram contains the latencies of the neurons for which the corresponding variable belonged to this optimal combination. For instance, image velocity was one of the optimal pair in 20 + 15 + 13 = 48 neurons. Average estimated latencies for image velocity, and eye velocity were 52.5, and −37.1 ms, respectively. For image velocity the SD within the population was very small (11.2 ms). For eye velocity it was larger (50.6 ms).

3.3.2 Regression analysis

For comparison with our previous results we show the results for linear regression analysis of the same MSTd population data.

The pairs of variables [image velocity & eye velocity], [image velocity & eye position], [image velocity & eye acceleration], and [eye velocity & eye position] showed maximal R^2 in 23 (47%), 14 (29%), 9 (18%), and 3 (6%) neurons, respectively. Therefore, both approaches, information maximization, and linear regression, agreed in concluding that a combination of an image velocity and an eye movement variable is most related to spiking activity in MSTd.

Figure 9 shows the results of latency estimation, using an analogous selection criterion as previous section. Instead of maximal $I(V;S)$, those combinations were selected that showed maximum R^2 of all combinations. For both variables image and eye velocity the SD was much larger in the regression estimates than with the information-based approach.

4 DISCUSSION

We showed that our novel information-theoretic approach is capable of estimating and evaluating probabilistic neuronal tuning functions. By maximizing the mutual information between the probability distributions of spike occurrence and the variables, their neuronal latency can be estimated and the dependence of neuronal activity on different combinations of variables can be measured. In the following we discuss the various techniques for neuronal latency estimation. Finally, we compare our method with other information-theoretic approaches for analyzing neuronal data.

4.1 ESTIMATION OF NEURONAL LATENCY

Numerous methods for estimating the latency of spiking activity relative to some variable on a trial-by-trial basis have been published (e.g., Seal et al., 1983; Friedman and Priebe, 1998; Bollimunta et al., 2007). Because the latency can vary for each trial, such detailed analysis is often necessary and might yield better results than the feature detection technique based on averaging as used here. Nonetheless, averaging techniques are widely used in the neurophysiological literature, and many applications, for instance tuning function determination as presented here, require the estimation of a distinct latency for each neuron.

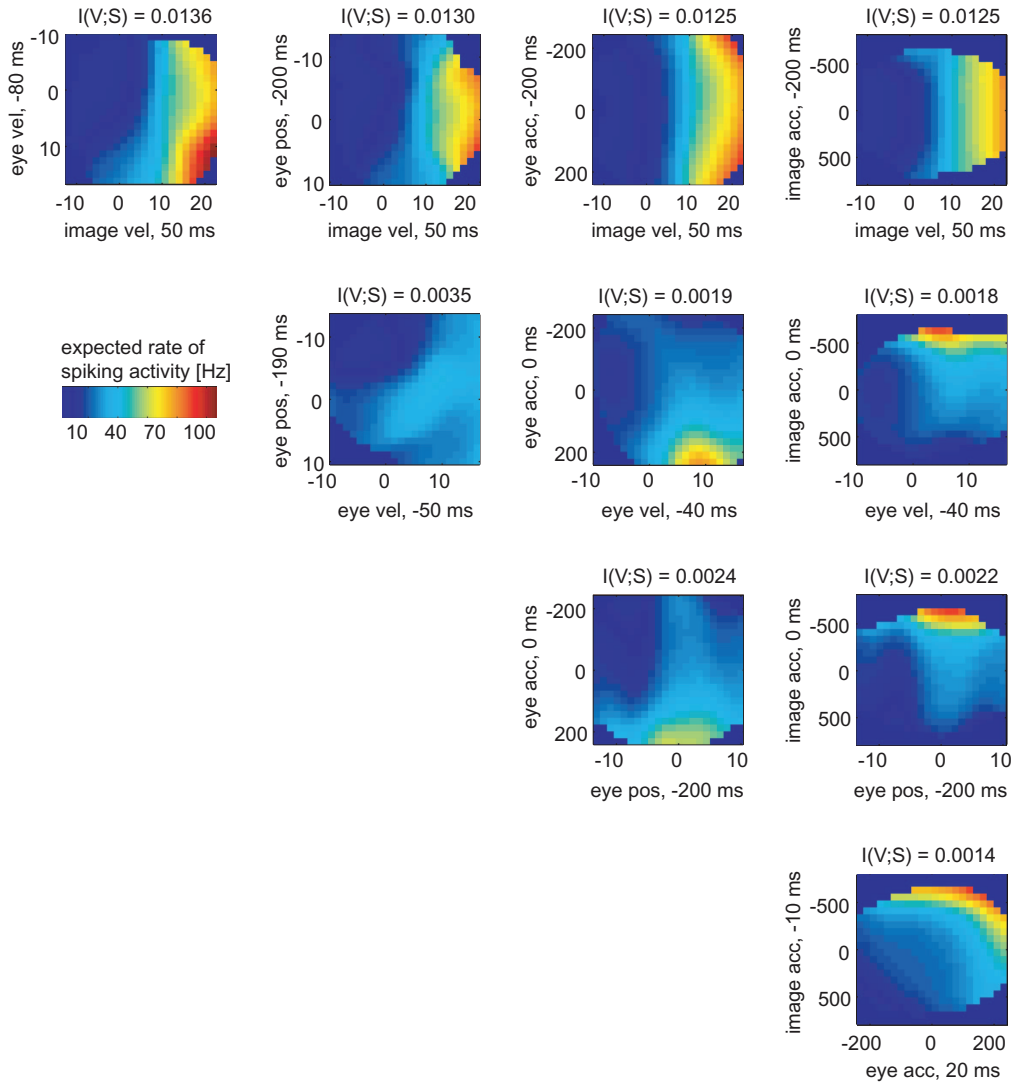

FIGURE 6 | Two-dimensional tuning functions of the example MSTd neuron for all pairs of variables. Colors indicate the expected rate of spiking activity, which results by multiplying the conditional probability $p_{S|V}(s|v)$ with the sample rate of 1 kHz. The dark blue bins were omitted in the analysis due to lack of data. Each axis is labeled by respective variable and the estimated latency in regard to the neuronal activity. The mutual information $I(V,S)$ was maximal for the pair [image velocity & eye velocity]. The expected rate of spiking activity in this neuron increased with both higher image and eye velocity values in a non-linear way.

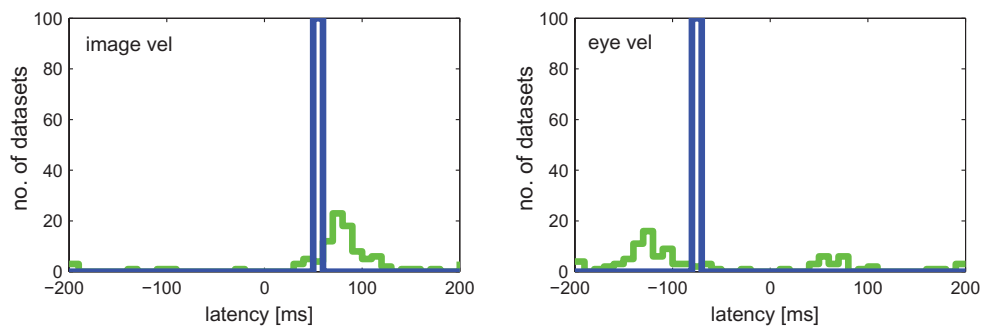

FIGURE 7 | Estimated latencies of image and eye velocity for 100 simulated neuronal recordings based on the estimated tuning function for [image velocity & eye velocity] of the example MSTd neuron. The information-based approach (blue line) estimated in all datasets the proper neuronal latencies of 50 and –80 ms for image and eye velocity, respectively. In contrast, linear regression analysis (green line) yields a wide distribution of estimated latencies for both variables.

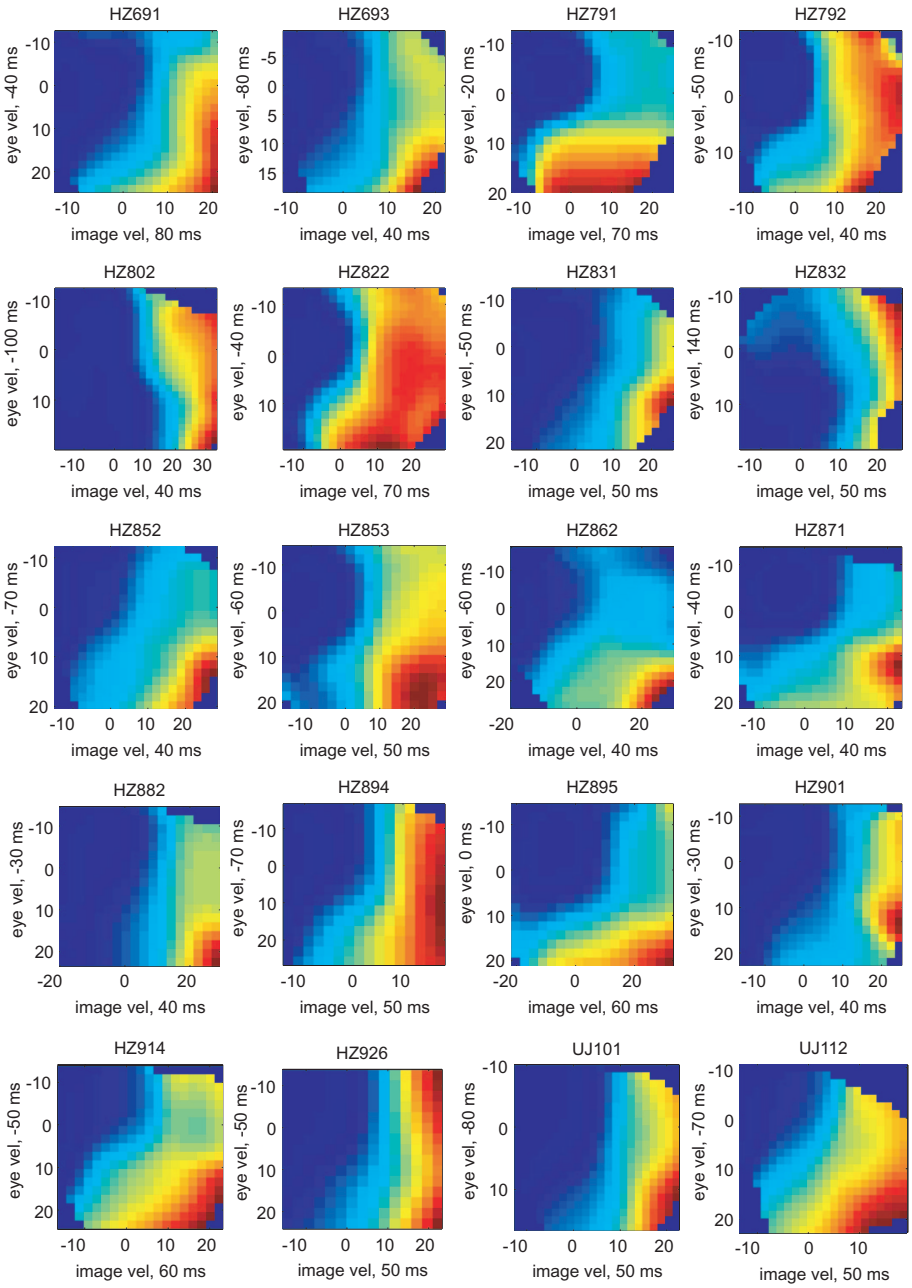

FIGURE 8 | Tuning functions for [image velocity & eye velocity] of those 20 neurons where this pair of variables showed maximal mutual information. The labeling is analog to **Figure 6.** The expected rate of spiking activity increased in general with higher image and eye velocity values. However, the shape of the tuning functions differed remarkably in each neuron.

Feature detection is an intuitive approach for estimating a distinct neuronal latency. Using this technique, the estimated latency for image velocity was about the same as with our information-theoretic approach in the example neuron. For eye velocity there was a discrepancy of 60 ms between feature detection (−20 ms latency) and our method (−80 ms latency). However, a shift that maximizes the mutual information between two random variables does not necessarily align the on- and offsets of these signals.

While our information-based method considers temporal mean values, a method like feature detection might be better suited, when the primary goal is estimating the actual onset time of a signal. Such an approach requires temporal matching between distinct features in stimulus and response, as for example given by the sudden onset of acceleration in a ramp stimulus. Whenever this is not achievable, this method cannot be applied and temporal averaging methods such as regression analysis or our information-based technique are more appropriate.

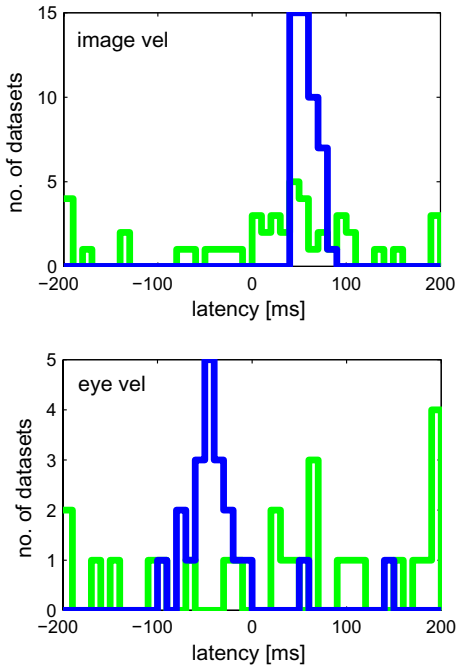

FIGURE 9 | Estimated latencies of image and eye velocity for a population of 49 MSTd neurons using the mutual information maximization method (blue) and linear regression analysis (green). Only those neurons were considered where the variable was actually related to the activity of that neuron. Compared to the results of our information-based approach, the distribution of estimated latencies is much wider when using regression analysis.

Regression analysis can be applied on a virtually arbitrary number of variables. However, the results strongly depend on the model assumptions. The results shown here demonstrated that a simple linear model is insufficient when analyzing neuronal data. As **Figure 6** illustrates, the versatility and non-linear character of neuronal tuning functions means that it can be difficult to find adequate general models.

For image velocity, estimated latencies of the population averaged 20 (±101) ms using linear regression. In contrast, our information-based method yielded a much sharper distribution of latencies averaging 53 (±11) ms. This result equals previous studies that were using feature detection techniques to estimate latencies in MSTd neurons: Kawano et al. (1994) found a latency of 47 (±7) ms to moving LF stimuli; Ono et al. (2010) determined a similar value of 42 (±14) ms.

A signal such as eye velocity is the output of a non-linear dynamic system with a large number of different input signals and recurrent connections. Neuronal activity in MSTd resembles some intermediate stage embedded in this network. Hence, assuming that the activity in MSTd can be explained using a single non-linearity with fixed delayed input variables may oversimplify conditions extant in a complex system. Nevertheless, our method yields consistent and plausible latency estimation under these conditions.

4.2 COMPARISON WITH OTHER INFORMATION-THEORETIC APPROACHES

In recent years various information-theoretic approaches have been used to analyze neuronal data (for reviews see, e.g., Rieke et al., 1997; Borst and Theunissen, 1999; Victor, 2006; Quiroga and Panzeri, 2009). Several of these studies examined the mutual information between stimulus variables and the neuronal response (e.g., Eckhorn and Pöpel, 1974; Optican and Richmond, 1987; Kjaer et al., 1994; Panzeri and Treves, 1996; Golomb et al., 1997; Rolls et al., 1997; Strong et al., 1998; Butts, 2003; Nirenberg and Latham, 2003; Osborne et al., 2004). Sharpee et al. (2004, 2006) maximized the mutual information between neuronal responses and certain subspaces of the high-dimensional stimulus. Similarly, our approach maximizes the mutual information between pairwise selected variables.

However, these studies analyze the neuronal response, single or multi-unit recordings, to quantify either the information due to spike patterns or the information due to correlations between neurons. Those methods estimate the probabilities of certain spiking patterns in the neuronal response given specific stimuli. These probabilities are usually determined by pooling over a large number of trials, where the same stimulus was presented many times.

Our method, on the other hand, estimates for each sample the probability of spike occurrence given certain stimuli, not caring for certain spiking patterns. This probability is determined by pooling the whole dataset over time. Therefore, our method does not depend on recording a large number of similar trials. In this sense, it rather presents a model-free alternative to the model-based regression analysis.

Previous approaches that were determining the mutual information between stimulus and response were, to our knowledge, less concerned about neuronal latency estimation. When using static stimuli (Optican and Richmond, 1987; Kjaer et al., 1994; Rolls et al., 1997), there is no need for exact knowledge of the neuronal latency. Also, it might be negligible if latencies are relatively short, for instance in data from peripheral neurons in insects (Rieke et al., 1997). When, in contrast, large latencies have to be considered, determining neuronal tuning functions depends critically on estimating these latencies. In such cases, an approach as presented here is required.

Our approach for evaluating neuronal tuning functions is analogous to a method used for the alignment or registration of medical images: the relative position and orientation of two different images is adjusted by transforming one of the images until the mutual information between both intensity distributions is maximized (Collignon et al., 1995; Wells and Viola, 1996). Similar techniques have been used for instance for object detection in computer vision (Shams et al., 2000). Analogous to the spatial alignment used in these approaches, our method performs temporal alignment of two random variables by maximizing the mutual information.

5 CONCLUSION

We present a novel method for determining and evaluating multi-dimensional probabilistic tuning functions. Our Bayesian approach allows the identification of arbitrary neuronal tuning functions. It can be applied in unbalanced designs and allows quantification of any possible dependence of the neuronal activity on the explanatory variables. However, the dimension of the tuning function is limited by the length of the neuronal recording.

Maximizing the mutual information allows estimation of neuronal latency and comparison of the coherence between spiking activity and different variable combinations. This information-based approach does not require parametric modeling of the tuning function and is an appropriate tool for evaluating probabilistic tuning functions defined in the Bayesian framework.

Model-based approaches like regression analysis critically depend on the validity of model assumptions. As demonstrated here, simple approaches, such as the linear model evaluated above, are often insufficient for analyzing neuronal data.

By applying this novel technique to data from MSTd neurons, we show that they are tuned for non-linear combinations of retinal image and eye movement signals. Though latencies are quite consistent across neurons, single neurons differ remarkably in their individual response properties to the same variables. For this reason, the model-free approach proposed here is particularly suitable for this analysis.

ACKNOWLEDGMENTS

This work was supported by the German Federal Ministry of Education and Research Grants 01 GQ 0448, 01 EO 0901, and National Institutes of Health Grants EY013308, RR000166.

REFERENCES

Bollimunta, A., Knuth, K. H., and Ding, M. (2007). Trial-by-trial estimation of amplitude and latency variability in neuronal spike trains. *J. Neurosci. Methods* 160, 163–170.

Borst, A., and Theunissen, F. E. (1999). Information theory and neural coding. *Nat. Neurosci.* 2, 947–957.

Bremmer, F., Ilg, U. J., Thiele, A., Distler, C., and Hoffmann, K.-P. (1997). Eye position effects in monkey cortex. i. Visual and pursuit-related activity in extrastriate areas MT and MST. *J. Neurophysiol.* 77, 944–961.

Butts, D. A. (2003). How much information is associated with a particular stimulus? *Network* 14, 177–187.

Collignon, A., Maes, F., Delaere, D., Vandermeulen, D., Suetens, P., and Marchal, G. (1995). Automated multi-modality image registration based on information theory. *Inf. Process. Med. Imaging* 3, 263–274.

Cover, T. M., and Thomas, J. A. (1991). *Elements of Information Theory*. Hoboken, NJ: Wiley-Interscience.

Dayan, P., and Abbott, L. F. (2001). *Theoretical Neuroscience*. Cambridge, MA: MIT Press.

Eckhorn, R., and Pöpel, B. (1974). Rigorous and extended application of information theory to the afferent visual system of the cat. i. basic concepts. *Kybernetik* 16, 191–200.

Friedman, H. S., and Priebe, C. E. (1998). Estimating stimulus response latency. *J. Neurosci. Methods* 83, 185–194.

Fuchs, A. F., and Robinson, D. A. (1966). A method for measuring horizontal and vertical eye movement chronically in the monkey. *J. Appl. Physiol.* 21, 1068–1070.

Golomb, D., Hertz, J., Panzeri, S., Treves, A., and Richmond, B. (1997). How well can we estimate the information carried in neuronal responses from limited samples? *Neural Comput.* 9, 649–665.

Hamed, S. B., Page, W., Duffy, C., and Pouget, A. (2003). MSTd neuronal basis functions for the population encoding of heading direction. *J. Neurophysiol.* 90, 549–558.

Ilg, U. J., Schumann, S., and Thier, P. (2004). Posterior parietal cortex neurons encode target motion in world-centered coordinates. *Neuron* 43, 145–151.

Kawano, K., Shidara, M., Watanabe, Y., and Yamane, S. (1994). Neural activity in cortical area MST of alert monkey during ocular following responses. *J. Neurophysiol.* 71, 2305–2324.

Kjaer, T. W., Hertz, J. A., and Richmond, B. J. (1994). Decoding cortical neuronal signals: network models, information estimation and spatial tuning. *J. Comput. Neurosci.* 1, 109–139.

Knuth, K. H. (2006). *Optimal Data-based Binning for Histograms*. ArXiv Physics e-prints.

Ladda, J., Eggert, T., Glasauer, S., and Straube, A. (2007). Velocity scaling of cue-induced smooth pursuit acceleration obeys constraints of natural motion. *Exp. Brain Res.* 182, 343–356.

Newsome, W. T., Wurtz, R. H., and Komatsu, H. (1988). Relation of cortical areas MT and MST to pursuit eye movements. ii. Differentiation of retinal from extraretinal inputs. *J. Neurophysiol.* 60, 604–620.

Nirenberg, S., and Latham, P. E. (2003). Decoding neuronal spike trains: how important are correlations? *Proc. Natl. Acad. Sci. U.S.A.* 100, 7348–7353.

Ono, S., Brostek, L., Nuding, U., Glasauer, S., Büttner, U., and Mustari, M. J. (2010). The response of MSTd neurons to perturbations in target motion during ongoing smooth-pursuit eye movements. *J. Neurophysiol.* 103.

Ono, S., Das, V. E., Economides, J. R., and Mustari, M. J. (2004). Modeling of smooth pursuit-related neuronal responses in the DLPN and NRTP of the rhesus macaque. *J. Neurophysiol.* 93, 108–116.

Optican, L. M., and Richmond, B. J. (1987). Temporal encoding of two-dimensional patterns by single units in primate inferior temporal cortex. iii. Information theoretic analysis. *J. Neurophysiol.* 57, 162–178.

Osborne, L. C., Bialek, W., and Lisberger, S. G. (2004). Time course of information about motion direction in visual area MT of macaque monkeys. *J. Neurosci.* 24, 3210–3222.

Panzeri, S., Senatore, R., Montemurro, M. A., and Petersen, R. S. (2007). Correcting for the sampling bias problem in spike train information measures. *J. Neurophysiol.* 98, 1064–1072.

Panzeri, S., and Treves, A. (1996). Analytical estimates of limited sampling biases in different information measures. *Network* 7, 87–107.

Quiroga, R. Q., and Panzeri, S. (2009). Extracting information from neuronal populations: information theory and decoding approaches. *Nat. Rev. Neurosci.* 10, 173–185.

Rieke, F., Warland, D., de Ruyter van Steveninck, R., and Bialek, W. (1997). *Spikes: Exploring the Neural Code*. Cambridge, MA: MIT Press.

Rolls, E. T., Treves, A., Tovee, M. J., and Panzeri, S. (1997). Information in the neuronal representation of individual stimuli in the primate temporal visual cortex. *J. Comput. Neurosci.* 4, 309–333.

Schmolesky, M. T., Wang, Y., Hanes, D. P., Thompson, K. G., Leutgeb, S., Schall, J. D., and Leventhal, A. G. (1998). Signal timing across the macaque visual system. *J. Neurophysiol.* 79, 3272–3278.

Seal, J., Commenges, D., Salamon, R., and Bioulac, B. (1983). A statistical method for the estimation of neuronal response latency and its functional interpretation. *Brain Res.* 278, 382–386.

Shams, L. B., Brady, M. J., and Schaal, S. (2000). Graph matching vs mutual information maximization for object detection. *Neural Netw.* 14, 345–354.

Sharpee, T., Rust, N. C., and Bialek, W. (2004). Analyzing neural responses to natural signals: maximally informative dimensions. *Neural Comput.* 16, 223–250.

Sharpee, T. O., Sugihara, H., Kurgansky, A. V., Rebrik, S. P., Stryker, M. P., and Miller, K. D. (2006). Adaptive filtering enhances information transmission in visual cortex. *Nature* 439, 936–942.

Strong, S. P., Koberle, R., de Ruyter van Steveninck, R. R., and Bialek, W. (1998). Entropy and information in neural spike trains. *Phys. Rev. Lett.* 80, 197–200.

Victor, J. D. (2006). Approaches to information-theoretic analysis of neural activity. *Biol. Theory* 1, 302–316.

Wells, W. M., and Viola, P. (1996). Multimodal volume registration by maximization of mutual information. *Med. Image Anal.* 1, 35–51.

Wu, M. C.-K., David, S. V., and Gallant, J. L. (2006). Complete functional characterization of sensory neurons by system identification. *Annu. Rev. Neurosci.* 29, 477–505.

Conflict of Interest Statement: The authors declare that the research was conducted in the absence of any commercial or financial relationships that could be construed as a potential conflict of interest.

Received: 22 October 2010; accepted: 07 March 2011; published online: 30 March 2011.

Citation: Brostek L, Eggert T, Ono S, Mustari MJ, Büttner U and Glasauer S (2011) An information-theoretic approach for evaluating probabilistic tuning functions of single neurons. Front. Comput. Neurosci. ***5****:15. doi: 10.3389/fncom.2011.00015*

6 APPENDIX

Here it is shown that maximizing the mutual information between V and S, as defined in Section 2, provides an unbiased estimator for the neuronal latency. Our proof is based on the data-processing inequality theorem in information theory (Cover and Thomas, 1991): If three random variables X, Y, and Z form a Markov chain, so that X and Z are conditionally independent given Y

$$p_{X,Z|Y}(x,z\,|\,y) = p_{X|Y}(x\,|\,y)\cdot p_{Z|Y}(z\,|\,y),$$

then

$$I(X;Y) \geq I(X;Z).$$

The mutual information between neighboring states is larger or equal to the mutual information of non-neighboring states.

Next we show that this theorem can be applied to our case under certain conditions concerning the properties of these random variables. Let V_τ be the random variable with a distinct latency τ for which the relation between the spiking activity S and V_τ is given by

$$s(t) = f(v_\tau(t+\tau)) + r,$$

where r represents some unknown noise. V_λ denotes the random variable with a differing latency $\lambda \neq \tau$. Herefrom follows that the tuning function $p_{S|V_\tau}(s\,|\,v_\tau)$ is independent of V_λ, and we have

$$p_{S|V_\tau,V_\lambda}(s\,|\,v_\tau,v_\lambda) = p_{S|V_\tau}(s\,|\,v_\tau).$$

With this, the joint probability of s and v_λ given v_τ can be transformed as follows

$$\begin{aligned} p_{S,V_\lambda|V_\tau}(s,v_\lambda\,|\,v_\tau) &= \frac{p_S(s)\cdot p_{V_\tau|S}(v_\tau\,|\,s)\cdot p_{V_\lambda|V_\tau,S}(v_\lambda\,|\,v_\tau,s)}{p_{V_\tau}(v_\tau)} \\ &= \frac{p_S(s)\cdot p_{V_\tau|S}(v_\tau\,|\,s)\cdot p_{V_\lambda|V_\tau}(v_\lambda\,|\,v_\tau)}{p_{V_\tau}(v_\tau)} \\ &= p_{S|V_\tau}(s\,|\,v_\tau)\cdot p_{V_\lambda|V_\tau}(v_\lambda\,|\,v_\tau) \end{aligned}$$

This shows that the spiking activity S and the shifted variable V_λ are conditionally independent, given the variable with the proper latency V_τ, which is the condition for applying the data-processing inequality theorem. The conditional independence yields

$$I(S;V_\lambda\,|\,V_\tau) = 0.$$

On the other hand, we have

$$\begin{aligned} I(S;V_\tau\,|\,V_\lambda) &= H(S\,|\,V_\lambda) - H(S\,|\,V_\tau,V_\lambda) \\ &= H(S\,|\,V_\lambda) - H(S\,|\,V_\tau) > 0, \end{aligned}$$

for $p_{S|V_\tau}(s\,|\,v_\tau) \neq p_{S|V_\lambda}(s\,|\,v_\lambda)$.

By the chain rule for information, we can expand mutual information in two different ways:

$$\begin{aligned} I(S;V_\lambda,V_\tau) &= I(S;V_\lambda) + I(S;V_\tau\,|\,V_\lambda) \\ &= I(S;V_\tau) + I(S;V_\lambda\,|\,V_\tau). \end{aligned}$$

With $I(S;V_\lambda|V_\tau) = 0$ and $I(S;V_\tau|V_\lambda) > 0$ we get

$$I(S;V_\tau) > I(S;V_\lambda).$$

Thus, the mutual information between the spiking activity S and the variable V is maximal for the variable V_τ with proper latency.

A Method for Evaluating Tuning Functions of Single Neurons based on Mutual Information Maximization

Lukas Brostek[*], Thomas Eggert[†], Seiji Ono[**], Michael J. Mustari[**], Ulrich Büttner[*] and Stefan Glasauer[*]

[*]*Clinical Neurosciences and Bernstein Center for Computational Neuroscience, Ludwig-Maximilians-Universität, Munich, Germany*
[†]*Department of Neurology, Ludwig-Maximilians-Universität, Munich, Germany*
[**]*Regional Primate Center, University of Washington, Seattle, WA, USA*

Abstract. We introduce a novel approach for evaluation of neuronal tuning functions, which can be expressed by the conditional probability of observing a spike given any combination of independent variables. This probability can be estimated out of experimentally available data. By maximizing the mutual information between the probability distribution of the spike occurrence and that of the variables, the dependence of the spike on the input variables is maximized as well. We used this method to analyze the dependence of neuronal activity in cortical area MSTd on signals related to movement of the eye and retinal image movement.

Keywords: Neuroscience, Mutual Information, Neuronal Tuning, Neuronal Latency
PACS: 87.19.lo, 87.19.L-

INTRODUCTION

Neurons code the information they transmit using a binary code. The so called action potentials, or spikes, are the only form of neuronal membrane potential fluctuation that can propagate over long distances. It is usually assumed that the information is conveyed in the rate of spiking activity [1, 2].

Neuronal tuning functions are typically defined by the functional relation between the rate of spiking activity and uni- or multivariate independent variables. Tuning functions have provided a first-order description of virtually every sensory system, from orientation colums in the vertebrate visual cortex up to wind-detecting neurons in the cricket cercal system [2, 3, 4].

A difficulty in the analysis of neuronal data is the estimation of proper latency values between any of the variables and the neuronal activity. Appropriate estimation of neuronal latencies is important, since the choice of these latency values has great influence on the tuning function [5, 6].

A common approach to the problem of latency estimation is minimizing the residual error in regression analysis using a linear, quadratic, or any other model [7, 8, 9]. To overcome the limitations of model-based system identification we developed an information based approach for evaluating the dependence of neuronal activity of single cells on combinations of one or multiple independent variables.

The proposed approach is similar to a method used for the registration of medical images: the relative position and orientation of two different images is adjusted by transforming one of the images until the mutual information between both intensity distributions is maximized [10, 11]. Analogous to the spatial alignment used in this methods, our method performs temporal alignment of two random variables by maximizing the mutual information.

THE MAXIMUM MUTUAL INFORMATION METHOD

Basically, our approach consists of two components: first, a method for the determination of a neuronal tuning function, and second, an information-theoretic technique for estimating neuronal latencies and selecting those variables that show the greatest dependence on the neuronal activity.

Tuning function determination

A neuronal tuning function describes the rate of spiking activity in a neuron depending on one or multiple independent variables. This dependence is ideally expressed by the conditional probability $p_{S|V}(s|v)$ of observing a spike given any combination of the variables. By multiplying with the sampling rate, this probability translates directly into an expectation value of the rate of spiking activity. Using Bayes' theorem, $p_{S|V}(s|v)$ can be expressed as the quotient of the joint probability mass function $p_{V,S}(v,s)$ divided by $p_V(v)$:

$$p_{S|V}(s|v) = \frac{p_{V,S}(v,s)}{p_V(v)},$$

where $p_V(v)$ is the marginal probability mass function of observing any combination of variables. The normalization on $p_V(v)$ allows the estimation of the tuning function in unbalanced designs (unequal number of observations across independent variables).

Estimates of $p_V(v)$ and $p_{V,S}(v,s)$ can be attained by histogramming the experimental data. Note, that the joint probability mass function $p_{V,S}(v,s)$ critically depends on the assumed neuronal latency. For optimal bin width estimation we adapted an algorithm proposed by Knuth [12]. According to this, the optimal bin width is defined by the Bayesian estimate of the number of segments of a piecewise constant probability function that is limited to a fixed interval. For smoothing the histogramms, we used a symmetrical Gaussian low-pass filter with a standard deviation of two bin widths. Bins containing a number of values less than 0.5 percent of total spike count were omitted in the analysis.

The amount of data needed for histogramming increases exponentially with the number of dimensions. However, the duration one single neuron can be recorded is restricted due to experimental and physiological constraints. Hence, there is a limitation in the number of variables this method for tuning function determination can be applied on.

Mutual information maximization

Applied to the two random variables V and S from previous section, the mutual information $I(V;S)$ can be stated as

$$I(V;S) = H(S) - H(S|V).$$

with $H(S)$ being the entropy of S and $H(S|V)$ the conditional entropy of S given V, also referred to as noise entropy. These are defined by

$$H(S) = -\sum_s p_S(s) \log p_S(s)$$

$$H(S|V) = -\sum_v p_V(v) \sum_s p_{S|V}(s|v) \log p_{S|V}(s|v),$$

where $p_S(s)$ denotes the probability mass function of spike occurence. The conditional probability $p_{S|V}(s|v)$ denotes the tuning function, determined by the method mentioned in the previous section. This probability and herewith $H(S|V)$ depend on both, the choice of variables analyzed, and the choice of latencies between these variables and the neuronal activity.

The proposed approach chooses the latency in such a way, that the dependence of the neuronal activity on the independent variables is maximized by maximizing the mutual information between V and S. As $H(S)$ is defined by the neuronal activity alone, the maximization is achieved by minimizing the noise entropy $H(S|V)$.

We define the mutual information rate

$$IR(V;S) = \frac{I(V;S)}{H(S)}.$$

This measure specifies the percentage of information about S that can be gathered by knowledge of V.

Due to the limitation in the number of variables mentioned in previous section, in practice the dimension of the tuning function will not exceed values of two or three. To investigate the dependence of a spike on a higher number of independent variables, we determined the tuning functions of a single neuron for any pairwise selection V_k of those variables. For each of these pairs neuronal latencies of both variables were estimated by maximizing the mutual information $I(V_k;S)$. As $I(V_k;S)$ quantifies the dependence of the spike on the selected pair of variables, those two variables that are most related to the spiking activity can be determined by comparing the maximal mutual information rates of the two-dimensional tuning functions.

APPLICATION

The data presented in this paper consists of a 400 s long extracellular recording in cortical area MSTd from a behaving monkey (Macaca mulatta, 5-7 kg), born in captivity at the Yerkes National Primate Research Center (Atlanta, GA). Experimental procedures

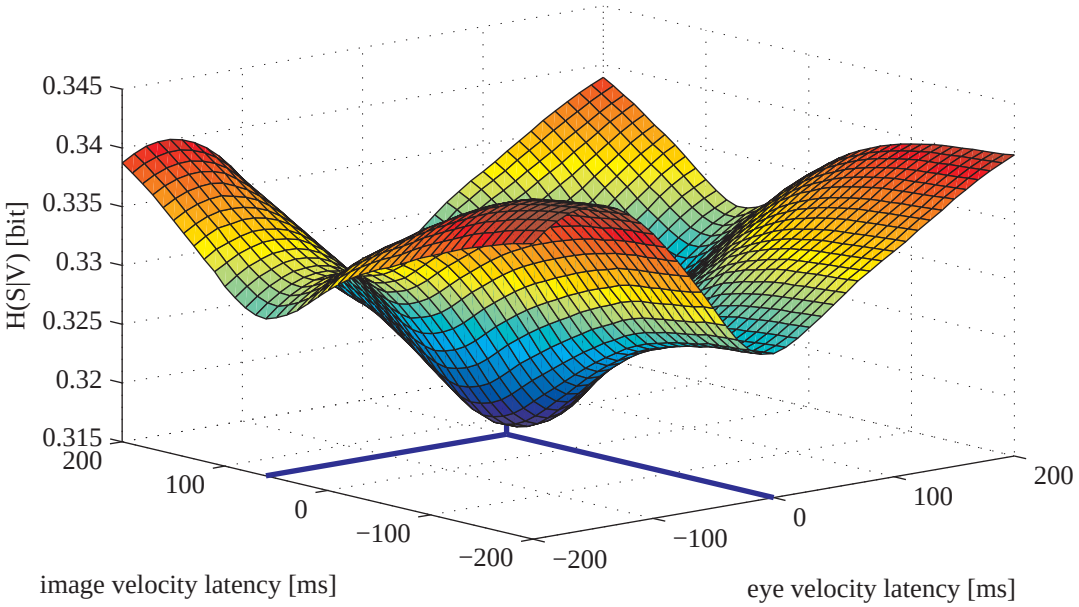

FIGURE 1. Noise entropy $H(S|V)$ against various latencies of image and eye velocity.

are explained in detail in [13]. During the experiments the monkey was seated in a primate chair with his head fixed in the horizontal stereotaxic plane in a completely dark room. Single unit activity was recorded with customized epoxy-coated tungsten microelectrodes. Using a hardware window discriminator a total number of 26015 action potentials was detected and sampled at 1 kHz. Eye movements were detected with standard electro-magnetic methods using scleral search coils [14]. The recorded eye position traces were filtered with a Gaussian low-pass (cutoff frequency 10 Hz) and three-point differentiated to obtain the velocity traces. Saccades were detected and removed with a slow-phase estimation algorithm as described in [15].

The stimulus consisted of a moving large field (35° x 35°) random dot pattern. For optimal coverage of the value range, we used quasi random motion with a flat frequency spectrum (white noise) with maximal eccentricity of 25° and velocity up to $100°/s$. During presentation of the visual motion the monkey had to fixate a small target spot at the center of gaze, though large-field stimulation always produces slight optokinetic eye movements.

We related the neuronal activity to variables, supposed to be potentially coded in MSTd during visual stimulation [16, 17, 18]. The retinal variables consisted of image velocity and acceleration, whereas the group of extraretinal variables contained eye position, velocity and acceleration. Data were acquired only for those movement directions that were previously identified to be the preferred direction of the neuron. This means, the direction which elicits maximal spiking activity for a moving large field stimulus in the analyzed neuron.

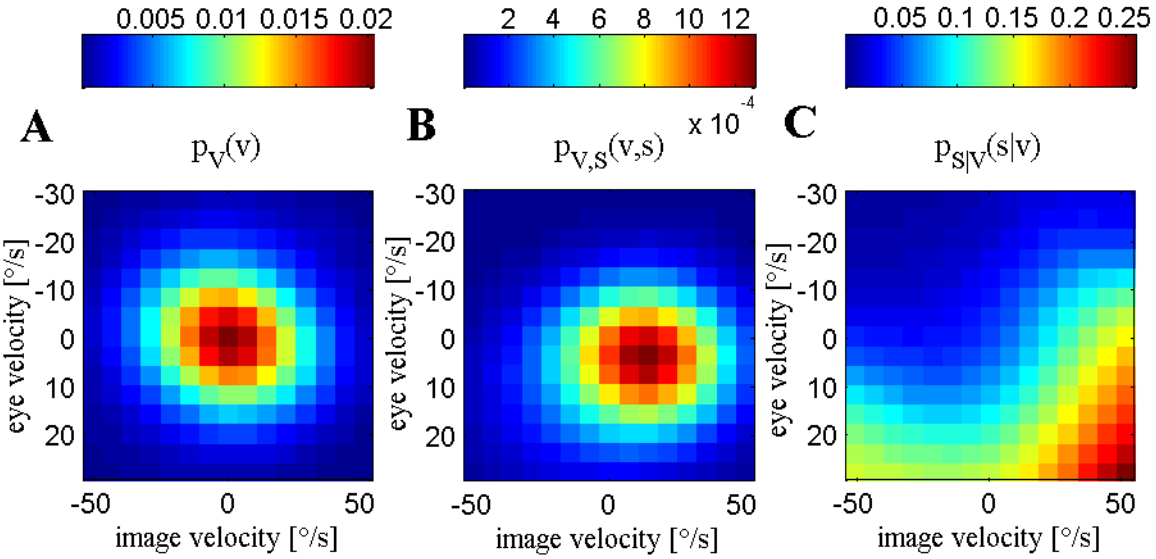

FIGURE 2. Tuning function determination. Dividing $p_{V,S}(v,s)$ (B) by $p_V(v)$ (A) yields the conditional probability $p_{S|V}(s|v)$ of observing a spike given any combination of the variables (C).

RESULTS

Figure 1 shows the noise entropy $H(S|V)$ against various latencies of the variables retinal image velocity and eye velocity. Both variables were shifted in the range between -200 and +200 ms relative to spiking activity, with negative and positive delay meaning backwards and forwards shifts, respectively. For the image velocity latency of +60 ms and eye velocity latency of 0 ms $H(S|V)$ had a minimum of 0.3268 bits. With $H(S) = 0.3456$ bits, the mutual information $I(V,S)$ accounted for 0.0189 bits for these estimates of neuronal latency. The mutual information rate $IR(V,S)$ was 5.46 %, meaning that this portion of information contained in the spiking activity was the maximum that could be explained by the information of that variable pair.

Figure 2 demonstrates the determination of the neuronal tuning function for the variable pair image velocity & eye velocity by application of Bayes' rule. The estimated probability mass function $p_V(v)$ of the occurrence of combinations of the independent variables image velocity and eye velocity is plotted in Fig. 2A. Figure 2B shows the estimated joint probability mass function $p_{V,S}(v,s)$ of coincident variable and spike occurrence. Note that both variables were shifted relative to the neuronal activity according to the estimated neuronal latencies. Dividing $p_{V,S}(v,s)$ by $p_V(v)$ yields the conditional probability $p_{S|V}(s|v)$ of observing a spike given any combination of the variables (Fig. 2C).

In the same way the neuronal tuning functions were determined for all variable combinations (Fig. 3). Neuronal activity in area MSTd is non-linearly related to combinations of the considered eye movement and retinal image movement variables. In the analyzed

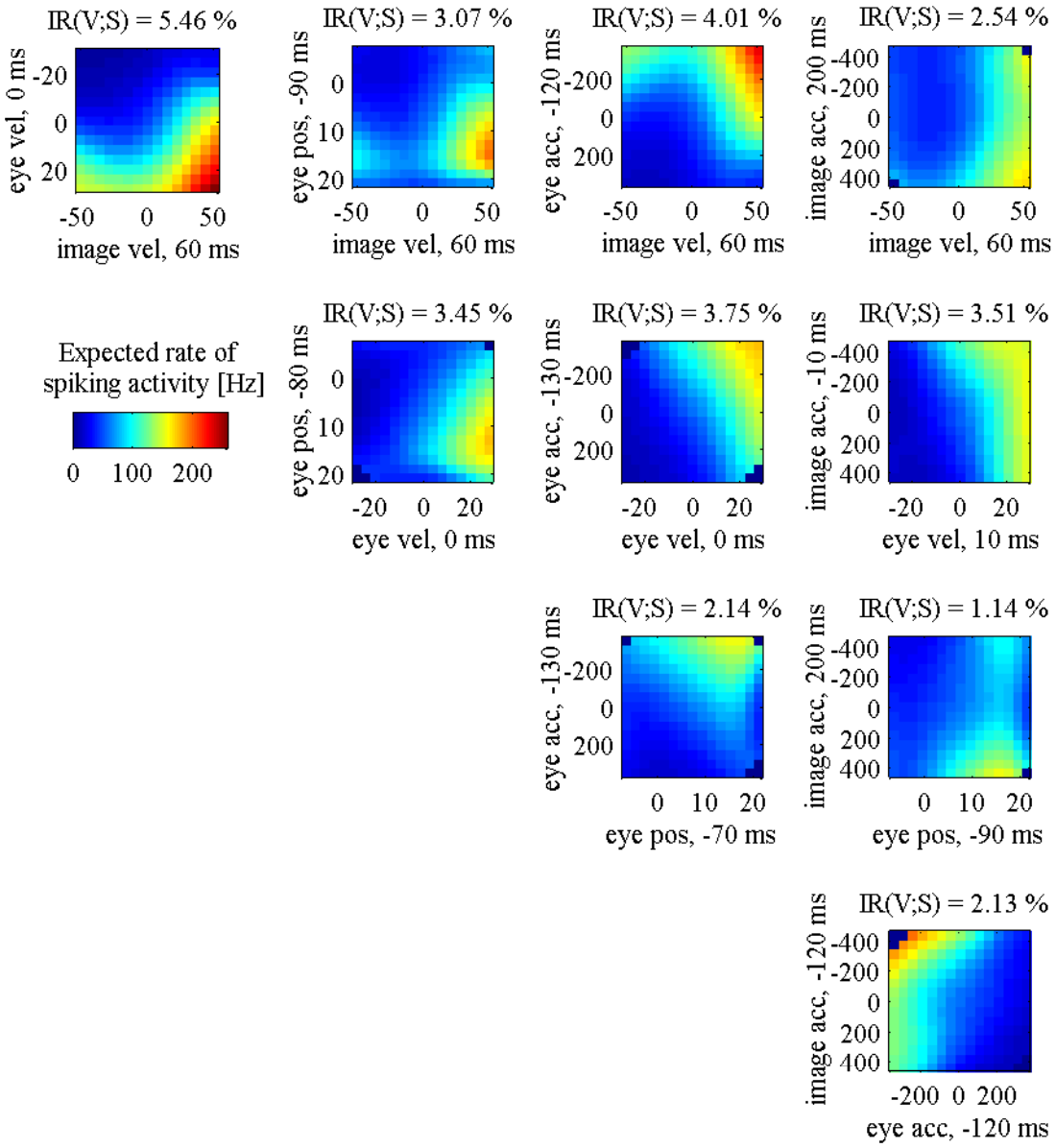

FIGURE 3. Two-dimensional tuning functions for all pairs of analyzed variables. Here, colors indicate the expected rate of spiking activity, which results by multiplying the conditional probability $p_{SV}(s|v)$ with the sample rate of 1 kHz. Each axis is labeled by respective variable and the estimated latency in regard to the neuronal activity.

neuron the mutual information rate $IR(V,S)$ for the variable combination image velocity & eye velocity was larger then any other combination. Hence, this combination was most related to spiking activity. The estimated latencies agree well with results based on other approaches [16, 19]. The latencies of all variables depended only little on the combination, except that of image acceleration. This is related to the low dependence of spiking activity on image acceleration, also apparent in the respective tuning functions.

CONCLUSIONS

The proposed method for tuning function determination allows the identification of any neuronal tuning function. It can be applied in unbalanced designs and allows quantification of any possible dependence of the neuronal activity on the independent variables. However, the dimension of the tuning function is limited by the length of the neuronal recording.

Analyzing the mutual information is the adequate tool for evaluating tuning functions defined in this probabilistic framework. This method is independent of model assumptions. Maximizing the mutual information allows estimation of neuronal latency and comparison of the coherence between spiking activity and different variable combinations. Since neuronal tuning functions can be versatile and highly non-linear, the proposed method is especially suitable for analyzing these.

ACKNOWLEDGMENTS

This work was supported by the Bernstein Center for Computational Neuroscience Grant BMBF 011GQ0440 and NIH Grants EY013308, RR00166.

REFERENCES

1. E. D. Adrian, *J. Physiol.* **61** (1926).
2. P. Dayan, and L. F. Abbott, *Theoretical Neuroscience*, MIT Press, 2001.
3. F. Rieke, D. Warland, R. de Ruyter van Steveninck, and W. Bialek, *Spikes: Exploring the Neural Code*, MIT Press, 1999.
4. D. A. Butts, and M. S. Goldman, *PLoS Biol* **4**, 639–646 (2006).
5. J. Seal, D. Commenges, R. Salamon, and B. Bioulac, *Brain Research* **278**, 382–386 (1983).
6. H. S. Friedman, and C. E. Priebe, *J. Neurosc. Methods* **83**, 185–194 (1998).
7. S. Ono, V. E. Das, J. R. Economides, and M. J. Mustari, *J. Neurophysiol.* **93**, 108–116 (2004).
8. U. J. Ilg, S. Schumann, and P. Thier, *Neuron* **43**, 145–151 (2004).
9. M. C.-K. Wu, S. V. David, and J. L. Gallant, *Annu. Rev. Neurosci.* **29**, 477–505 (2006).
10. A. Collignon, F. Maes, D. Delaere, D. Vandermeulen, P. Suetens, and G. Marchal, *Information Processing in Medical Imaging* **3**, 263–274 (1995).
11. W. M. Wells, and P. Viola, *Med. Image Anal.* **1**, 35–51 (1996).
12. K. H. Knuth, *ArXiv Physics e-prints* (2006), `arXiv:physics/0605197`.
13. S. Ono, L. Brostek, U. Nuding, S. Glasauer, U. Büttner, and M. J. Mustari, *J. Neurophysiol.* **103** (2010).
14. A. F. Fuchs, and D. A. Robinson, *J. Appl. Physiol.* **21**, 1068–1070 (1966).
15. J. Ladda, T. Eggert, S. Glasauer, and A. Straube, *Exp. Brain Res.* **182**, 343–356 (2007).
16. W. T. Newsome, R. H. Wurtz, and H. Komatsu, *J. Neurophysiol.* **60** (1988).

17. F. Bremmer, U. J. Ilg, A. Thiele, C. Distler, and K.-P. Hoffmann, *J. Neurophysiol.* **77**, 944–961 (1997).
18. S. B. Hamed, W. Page, C. Duffy, and A. Pouget, *J. Neurophysiol.* **90**, 549–558 (2003).
19. K. Kawano, M. Shidara, Y. Watanabe, and S. Yamane, *J. Neurophysiol.* **71**, 2305–2324 (1994).

Cerebral Cortex
doi:10.1093/cercor/bhs146

Neuronal Variability of MSTd Neurons Changes Differentially With Eye Movement and Visually Related Variables

Lukas Brostek[1,3], Ulrich Büttner[1,2], Michael J. Mustari[4] and Stefan Glasauer[1,2,3]

[1]Clinical Neurosciences, [2]Integrated Center for Research and Treatment of Vertigo, [3]Bernstein Center for Computational Neuroscience, Ludwig-Maximilians-University, Munich, Germany and [4]Department of Ophthalmology and Washington National Primate Research Center, University of Washington, Seattle, WA, USA

Address correspondence to Lukas Brostek, Bernstein Center for Computational Neuroscience, Marchioninistr. 23, 81377 Munich, Germany. Email: lukas.brostek@lrz.uni-muenchen.de

Neurons in macaque cortical area MSTd are driven by visual motion and eye movement related signals. This multimodal characteristic makes MSTd an ideal system for studying the dependence of neuronal activity on different variables. Here, we analyzed the temporal structure of spiking patterns during visual motion stimulation using 2 distinct behavioral paradigms: fixation (FIX) and optokinetic response. For the FIX condition, inter- and intra-trial variability of spiking activity decreased with increasing stimulus strength, complying with a recent neurophysiological study reporting stimulus-related decline of neuronal variability. In contrast, for the optokinetic condition variability increased together with increasing eye velocity while retinal image velocity remained low. Analysis of stimulus signal variability revealed a correlation between the normalized variance of image velocity and neuronal variability, but no correlation with normalized eye velocity variance. We further show that the observed difference in neuronal variability allows classifying spike trains according to the paradigm used, even when mean firing rates (FRs) were similar. The stimulus-dependence of neuronal variability may result from the local network structure and/or the variability characteristics of the input signals, but may also reflect additional timing-based mechanisms independent of the neuron's mean FR and related to the modality driving the neuron.

Keywords: Coefficient of variation, Fano factor, Metric-space approach, MST, Spiking irregularity

Introduction

A great amount of knowledge about neuronal information processing has been gained by relating the mean neuronal firing rate (FR) to any variables supposed to be coded in the analyzed area. Besides the mean rate, however, there are more features of neural responses that may depend systematically on certain stimuli. One of these is the regularity of neuronal activity.

Neuronal variability can be measured in various ways. The Fano factor (FF), for instance, measures the variability of the spike count *across* trials that were recorded during identical conditions (Fano 1947). Other measures such as the coefficient of variation (CV) analyzes the variability of the inter-spike interval (ISI) *within* a single trial, which may be independent of the across trial variability (Cox and Lewis 1966).

The functional meaning of changing neuronal variability has been related to a broad range of factors, as, for instance, attention (Mitchell et al. 2007) or motor-preparation (Steinmetz and Moore 2010). In a recent meta-study, Churchland et al. (2010) examined the trial-to-trial variability in various cortical areas. Since each area needs appropriate stimulation to increase spiking activity, a variety of paradigms was used. As a common principle, the authors found that trial-to-trial variability in general declined during stimulation in comparison to pre-stimulus conditions.

Previous studies have analyzed neuronal variability dependence on a single stimulus variable only. However, many areas of the brain do not just code for a single stimulus variable and neuronal variability may thus depend on the stimulus dimension. The medial superior temporal (MST) cortex is such a multimodal area: it is involved in processing visual motion stimuli, but also receives extra-retinal input about eye movements (Komatsu and Wurtz 1988; Newsome et al. 1988). Neurons in the dorsal subpart (MSTd) have large receptive fields and respond to rotating, expanding and planar large-field (LF) motion (Duffy and Wurtz 1991). Many neurons show extra-retinal, eye movement related activity during smooth pursuit eye movements (Newsome et al. 1988; Ono and Mustari 2006; Ono et al. 2010). Also during LF stimulation, neuronal response in MSTd neurons has been shown to be modulated by oculomotor signals (Bradley et al. 1996; Page and Duffy 1999; Ben Hamed et al. 2003; Bremmer et al. 2010; Brostek et al. 2011).

This combination of both visual motion and eye movement related activity makes MSTd an ideal system for analyzing neuronal activity in dependence on different stimulus dimensions. In the following, we measured the inter- and intra-trial variability of the spiking activity in MSTd neurons using 2 different paradigms and related it to the visual and oculomotor signals. We found that both variables, image and eye velocity, differentially affected neuronal variability. Spiking irregularity decreased when image velocity increased and eye velocity was kept low, but increased with increasing eye velocity and low image velocity.

Methods

Data were recorded in cortical area MSTd from 2 behaving monkeys (*Macaca mulatta*, 5–7 kg). The experiments were performed at the Yerkes National Primate Research Center (Atlanta, GA, United States of America) in compliance with National Institutes of Health Guide for the Care and Use of Laboratory Animals. The protocols were reviewed and approved by the Institutional Animal Care and Use Committee at Emory University. For verifying MSTd location we used functional, histological, and magnetic resonance imaging criteria. During the experiments, monkeys were seated in a primate chair with their head fixed in the horizontal stereotaxic plane in a completely dark room, except during visual stimulation (see below). Only those neurons that showed significant response to large moving visual stimuli were analyzed. Visual receptive fields of neurons were mapped by moving a probe stimulus at regularly spaced eccentricities

across the visual field while the monkey fixated a stationary target spot. Most receptive fields were large (>30°) and had their center in the contralateral hemifield in accordance with known MSTd properties. Some of the data reported here were also used for other studies (Ono et al. 2010; Brostek et al. 2011). All experimental procedures are explained in detail in Ono et al. (2010).

Visual Stimuli

Visual LF stimuli (35° × 35° random dot patterns) were rear projected on a tangent screen 57 cm distant. Data were acquired only for those movement directions that were previously identified to be the preferred direction of the neuron, that is the direction which elicits maximal spiking activity for a moving LF stimulus in the analyzed neuron. Two kinds of paradigms were tested:

1. Fixation (FIX) with visual stimulation: The monkey fixated a small target spot located at the center of the screen. After some random time the LF stimulus started to move with constant velocity (5, 10, 15, 20, or 30°/s) in the neuron's preferred direction for a period between 1000 and 1800 ms. During presentation of the visual motion the monkey still fixated the laser spot, though this LF stimulation is known to produce a slight (<2°/s) optokinetic nystagmus (Komatsu and Wurtz 1988).
2. Optokinetic response (OKR): The stimulus for the OKR was the same as in the FIX task, with the difference that the laser spot was turned off when the LF stimulus began to move. In this case, the monkey's eye movements followed the motion.

Between trials there was a 1200 ms long period during which the monkey fixated the laser spot with the LF stimulus still visible but not moving (zero velocity condition).

Each neuron was tested with both paradigms at different velocities. One dataset comprised all trials tested for 1 specific neuron, paradigm, and velocity. In total, 325 datasets were recorded (on average 5.8 per neuron). The mean number of trials per dataset was 31 ± 10 (mean ± std. dev.).

FIX datasets with mean eye velocity greater than 5°/s (2.5% of all FIX datasets) and OKR datasets with retinal image velocity greater than 5°/s (5.8% of all OKR datasets) were discarded for analysis. In this way, we could ensure that in FIX datasets eye velocity was close to zero, and in OKR datasets retinal image velocity was close to zero. Both variables, which are otherwise coupled by stimulus velocity, could therefore be compared quasi independently of each other.

In some trials, the constant velocity phase of LF motion was interrupted by a short high-frequency perturbation of stimulus velocity (Ono et al. 2010) consisting of 1 sinusoidal cycle (5 Hz, 10°/s amplitude). We included these trials to our analysis, as it did not affect the observed dependence of neuronal variability on image and eye velocity (Supplementary Fig. S1).

Data Collection and Preparation

Action potentials were detected using both a hardware window discriminator (Bak Electronics, MD, United States of America) and template matching algorithm (Alpha-Omega, Israel). Eye movements were recorded with standard electro-magnetic methods using scleral search coils (CNC Engineering, Seattle, WA, United States of America). Eye and target position feedback signals were processed with anti-aliasing filters at 200 Hz using 6-pole Bessel filters (latency 5 ms) before digitization at 1 kHz with 16-bit precision using a CED 1401 hardware interface. The recorded eye position traces were filtered with a Gaussian low-pass (cut-off frequency 30 Hz) and 3-point differentiated to obtain the velocity traces. Saccades were detected and removed from the eye movement traces with an algorithm as described in Ladda et al. (2007). Neuronal response was represented as a FR by convolving spike times with a Gaussian function ($\sigma = 15$ ms) and averaging over corresponding trials.

Measures of Neuronal Variability

We used 3 different measures for determining neuronal discharge irregularity:

First: The FF was calculated for time windows of 100 ms length according to

$$\mathrm{FF} = \frac{\mathrm{Var}[\mathrm{SC}]}{E[\mathrm{SC}]},$$

with E and Var symbolizing mean and variance, respectively, and $\mathrm{SC} = \langle \mathrm{sc}_1, \mathrm{sc}_2, \ldots, \mathrm{sc}_n \rangle$ denoting the spike counts of the n trials.

Discharge irregularity tends to decrease with higher FRs due to the refractory period after each spike. To control for a possible effect of variable FRs on the FF, we applied in some analysis the mean-matching algorithm by Churchland et al. (2010) using the Matlab toolbox provided by the authors (http://www.stanford.edu/~shenoy/GroupCodePacks.htm) with a window size of 50 ms. The algorithm computes the mean spike counts for all datasets. For each analyzed time point the algorithm determines a common distribution of mean spike counts across all datasets. The analyzed distribution of datasets for each time is then matched to this common distribution by randomly discarding datasets. The FF is computed for the remaining distribution of datasets by calculating the slope of the regression relating the variance to the mean of the spike counts of the analyzed datasets. This process is repeated 50 times, and the results are averaged to control for variation due to the randomness of the procedure. As the size of the analyzed distribution of datasets decreases with greater number of analyzed time points, we constrained this analysis to 100 ms steps. Due to the great difference in the FR before and during stimulation, our data had a relatively heterogeneous structure. As a result, only 13 and 18% of datasets were preserved in the mean-matched distribution for the FIX and OKR paradigms, respectively. Nevertheless, the difference between mean matched and raw FF, averaged over all datasets, was marginal (see Results).

Second: The "variance of the conditional expectation" (VarCE) is another measure of trial-to-trial variability that also intends the suppression of possible effects due to differing mean FRs. This method has been proposed by Churchland et al. (2011). According to this method, the total measured variance is divided into 2 components: the "point process variance", which is produced by a renewal process with a given rate, and the residual VarCE. Assuming renewal process characteristics (see Results), VarCE can be estimated as

$$\mathrm{VarCE} = \mathrm{Var}[\mathrm{SC}] - \phi E[\mathrm{SC}],$$

with ϕ being a quantity characterizing the underlying point process. For each neuron, ϕ was obtained by the minimum value of the measured FF, which was typically shortly after stimulus motion onset (see Fig. 2).

Third: The CV^2 was determined as

$$\mathrm{CV}^2 = \frac{\mathrm{Var}[\mathrm{ISI}]}{E[\mathrm{ISI}]^2},$$

with $\mathrm{ISI} = \langle \mathrm{isi}_1, \mathrm{isi}_2, \ldots, \mathrm{isi}_n \rangle$ denoting the ISIs of each analyzed spike train.

Metric-Space Analysis

For an information-theoretic analysis of our data, we used the metric-space approach developed by Victor and Purpura (1996, 1997). This method determines the extent to which experimentally measured neural responses cluster in a systematic fashion using an information-theoretic measure. The measure of clustering indicates the extent to which this candidate distance is sensitive to features of spike trains that convey stimulus-specific information. The formal structure of this approach is an embedding of spike trains into a "metric space". These spaces have well-defined distances but do not require the assumption of a linear structure. To measure the difference between 2 spike trains in terms of the arrangement of spikes in time, we used the so-called D^{spike} metric here. The analysis is performed for different *a priori* defined temporal precision values. These determine the maximal distance of how far the spikes in 1 trial can be displaced to match the temporal arrangement of spikes in another

trial. Each displacement of a spike is accounted by a "cost" proportional to the distance. Also the adding or deleting of a spike has a certain "cost".

We applied the algorithm by using a Matlab toolbox (http://neuroanalysis.org) provided by the Weill Medical College of the Cornell University (Ithaca, NY, United States of America). All parameters were set to standard values; the clustering exponent was −2. For the original data, the standard error of transmitted information was estimated using the Jackknife method. Classifying the spike trains into different categories was considered to be feasible, when the transmitted information of the original data exceeded the range of the mean plus 2 standard deviations information of the shuffled data.

Simulated Data

To illustrate the dependence of intra-trial and inter-trial variability on the distribution of ISIs of the underlying spiking process, synthetic spike trains were generated. This was done by sampling ISIs independently and identically distributed from a gamma distribution

$$f(x;k;s) = x^{k-1}\frac{e^{-x/s}}{s^k\Gamma(k)},$$

with shape parameter k and scale parameter s. Γ denotes the gamma function. The scale parameter was adjusted to a constant FR of 20 Hz (Maimon and Assad 2009).

Results

We analyzed single-unit recordings of 56 MSTd neurons from 2 monkeys. They were stimulated with a LF random dot pattern moving with different velocities in the preferred direction of each neuron. During this stimulation, the monkeys had to either fixate a small non-moving target spot (FIX) or follow the visual movement by OKR.

FF During FIX and OKR

Figure 1 shows visual and oculomotor variables, FR and FF traces, averaged across all neurons and tested stimulus velocities for both paradigms. To equalize mean FRs of both conditions during the subsequently used testing interval between 300 and 1000 ms after stimulus onset, some datasets were discarded from this analysis. Retinal image velocity is the difference between the velocity of the moving stimulus and eye velocity. In the FIX paradigm, retinal image velocity increased with the onset of stimulus movement and remained constant during the whole trial, whereas eye velocity stayed at a minimal level (A1). For OKR, eye velocity increased gradually until about 300 ms after stimulus onset, whereas image velocity showed an initial peak and remained low after eye velocity reached its constant level (B1). In both paradigms, the averaged FR traces had transient components right after stimulus onset and sustained responses of about 40 Hz (A2, B2). The FF, however, differed remarkably between both paradigms: Both traces had values between 2.2–3 (FIX) and 1.8–2.4 (OKR) before stimulus motion onset, and a significant decrease to a value of 0.7 for FIX and 0.9 for OKR right after stimulus onset. For the FIX paradigm the FF retained this low level until the end of the trial (A3). For OKR, the FF did not sustain the low level but increased again to a level around 2 after 300 ms (B3). Thus, despite the ongoing stimulation, the trial-by-trial variability was comparable to the pre-stimulus variability.

To compensate for possible effects of temporally changing FRs, the FF was also determined using the mean-matching algorithm by Churchland et al. (2010). This procedure computes the mean spike counts for all datasets and determines a common distribution of mean spike counts across all time points. The analyzed distribution of datasets is then matched to this common distribution by randomly discarding datasets (see Methods). The raw FF, which was not mean matched but determined from all data, differed only marginally.

FF Dependence on Visual and Oculomotor Variables

Figure 2 shows spike raster plots of an example neuron for 2 different conditions during the testing interval (Fig. 1 light gray area). In this interval, all analyzed variables were almost constant for both paradigms. Whereas for FIX spiking was quite regular, the same neuron showed bursty activity in the

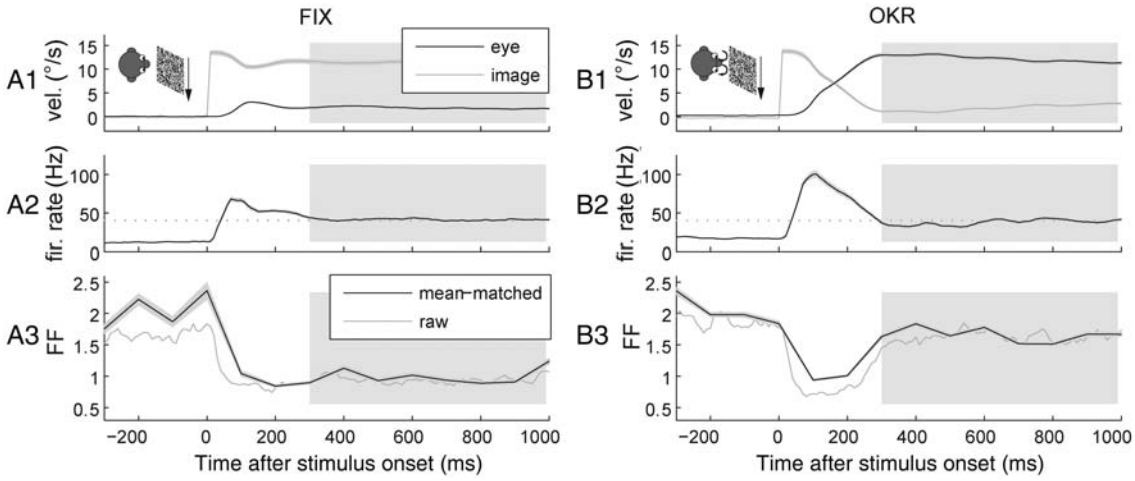

Figure 1. Mean traces of image and eye velocity, firing rate (FR), and Fano factor (FF) of the analyzed MSTd population for fixation (FIX) and optokinetic response (OKR) during large-field visual stimulation. A fraction of datasets (FIX: 20%; OKR: 15%) was discarded to match the averaged firing rates of both conditions during the testing interval. Data were aligned to the onset of stimulus movement (0 ms) in the preferred direction of each neuron. (*A*1) Desaccaded eye and retinal image velocity, averaged across all tested velocities (5, 10, 15, 20, and 30°/s) and 56 neurons, during FIX. (*A*2) Averaged firing rate. Dotted gray line marks the average firing rate (40 Hz) during the testing interval. (*A*3) Raw and mean-matched FF. Latter is constrained to 100 ms steps (see Methods). (*B*1–*B*3) show the corresponding traces for OKR. Flanking traces mark standard errors. The light gray area marks the testing interval between 300 and 1000 ms after stimulus onset, which was used for subsequent analysis.

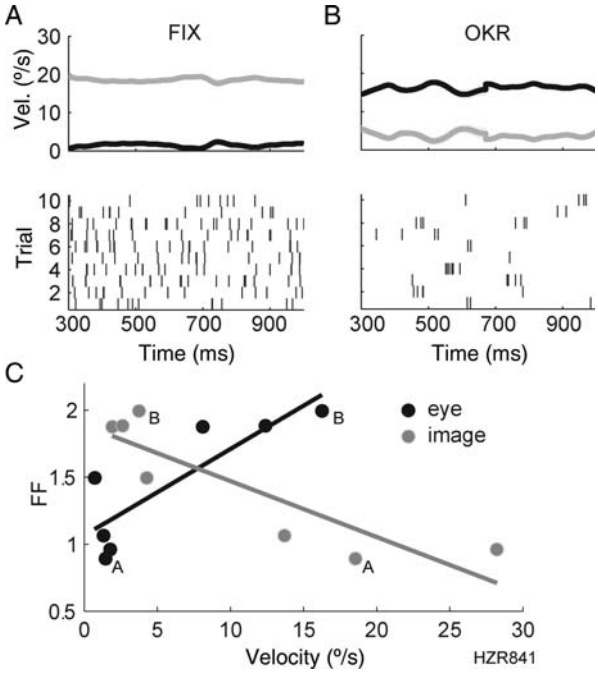

Figure 2. Fano factor (FF) of an example neuron for different image and eye velocities. (*A*) Eye (black) and image (gray) velocity during the testing interval for FIX with visual stimulation at 20°/s. The corresponding spike raster plot of this dataset shows quite regular activity (FF = 0.9, $CV^2 = 1.0$) (*B*) Same neuron for OKR with stimulus velocity of 20°/s. In this case, spiking activity was much more irregular (FF = 2.0, $CV^2 = 1.6$) (*C*) Each dot marks FF and image or eye velocity of one dataset. The 2 example conditions are indicated by letters. All measures were averaged across the testing interval (300–1000 ms after stimulus onset). In this example neuron, FF correlates negatively with image velocity and positively with eye velocity. Linear regression lines were least squares fitted.

OKR paradigm. For further analysis, we determined Pearson's correlation coefficient ρ between retinal image velocity and FF, and eye velocity and FF, respectively. The FIX paradigm with visual stimulation at different stimulus velocities yielded datasets with high image and low eye velocities, whereas the OKR paradigm yielded datasets with different low image and high eye velocity. We determined FF and both variables for each dataset, which comprised all trials, tested for 1 specific neuron, paradigm and velocity, and averaged all measures over the testing interval. The comparison of all datasets from this example neuron indicated negative correlation between FF and image velocity ($\rho_{\text{image vel, FF}} = -0.88$, $P < 0.01$) and positive correlation between FF and eye velocity ($\rho_{\text{eye vel, FF}} = 0.85$, $P < 0.01$), as shown in Figure 2*C*.

The results for all 56 MSTd neurons are shown in Figure 3*A*. In 48 neurons (86%), the FF correlated negatively with image velocity and positively with eye velocity. Figure 3*B* shows the mean FF dependence on both variables. In the FIX paradigm, the average FF decreased from 1.5 for small image velocity to a level of about 0.8 during high velocity. For OKR, the FF increased from 1.5 for small eye velocity to 2.1 during high eye velocity. Both changes were statistically significant (linear regression analysis: $\beta = -0.03$, $P < 0.01$ and $\beta = 0.02$, $P < 0.01$). Note that the change in FF was not task-dependent, as the FF had identical levels at small stimulus velocities for both paradigms. Both findings, decrease of neuronal variability with the visual variable, and increase of neuronal variability with the oculomotor variable, however, only apply for cases in which one of the 2 variables is close to zero. The average FF for all FIX datasets was 1.05 ± 0.43 (mean ± std. dev.), for OKR it was 1.78 ± 0.67. The mean FF, averaged across all datasets, was 1.47 ± 0.69.

The dependency of the mean FR on image and eye velocity is shown in Figure 4. In contrast to neuronal variability, mean FR increased with increasing stimulus velocities for both paradigms (see also Brostek et al. 2011). Linear correlation analysis between FR and FF revealed slight negative correlation ($\rho = -0.17$, $P = 0.04$) for FIX, and slight positive correlation ($\rho = 0.16$, $P = 0.03$) for OKR. We will address the apparent unexpected relationship between FF and FR in the Discussion.

Variance of the Conditional Expectation

Similar to the FF, the VarCE (Churchland et al. 2011) measures the trial-to-trial variability of spike counts. It reflects the residual variability after subtracting the component that would be produced by some point process with given mean FR. As with the mean-matching algorithm (see Fig. 1), possible effects due to differing mean FRs are compensated. This technique, however, does not discard datasets from analysis. Figure 3*C* and *D* shows the dependence between VarCE and the visual and eye movement variables. In 43 neurons (77%), VarCE correlated negatively with image velocity and positively with eye velocity. For FIX, the mean VarCE showed significant decrease from a level of about 3.9 for small image velocities, to 1.7 for high image velocities (linear regression analysis: $\beta = -0.11$, $P < 0.05$). For OKR, the mean VarCE increased from 3.9 to a value of 7.0 for high eye velocities ($\beta = 0.10$, $P = 0.08$). The average VarCE for FIX datasets was 2.32 ± 2.91, for OKR it was 4.75 ± 4.81. The mean VarCE, averaged across all datasets, was 3.71 ± 4.27.

Coefficient of Variation

The CV measures the variability of ISIs *within* a single trial. For a stationary renewal process, in which ISIs are assumed to be independent and identically distributed, it holds that FF = CV^2 for the limit of long observations (Cox 1962; Cox and Lewis 1966). In the following, we used the CV^2 to allow the evaluation of the renewal process hypothesis. In each dataset, CV^2 was determined for the testing interval and then averaged over all trials. The dependence between CV^2 and both variables is shown in Figure 3*E* and *F*. In 47 neurons (84%) CV^2 correlated negatively with image velocity and positively with eye velocity. As with FF, the mean CV^2 decreased significantly (linear regression analysis: $\beta = -0.04$, $P < 0.01$) with retinal image velocity. In the OKR paradigm, CV^2 showed increasing tendency ($\beta = 0.02$, $P = 0.09$) with eye velocity. This means that spiking irregularity did not only change in dependence on visual and oculomotor variables *across* the trials, as indicated by FF. Also *within* a single trial, ISIs tended to be more regular with increasing image velocity, and more irregular with an increase in eye velocity, as indicated by CV^2. The average CV^2 for FIX datasets was 1.12 ± 0.49, for OKR it was 1.93 ± 1.05. The mean CV^2 across all datasets was 1.58 ± 0.93.

Dependencies between the analyzed measures are shown in Figure 5. There was positive correlation between all 3 measures. In particular, the correlation between FF and CV^2 was quite strong. Regression analysis using a linear, zero offset model, yielded $CV^2 = 1.06$ FF, which is in good agreement with the assumption of renewal process characteristic.

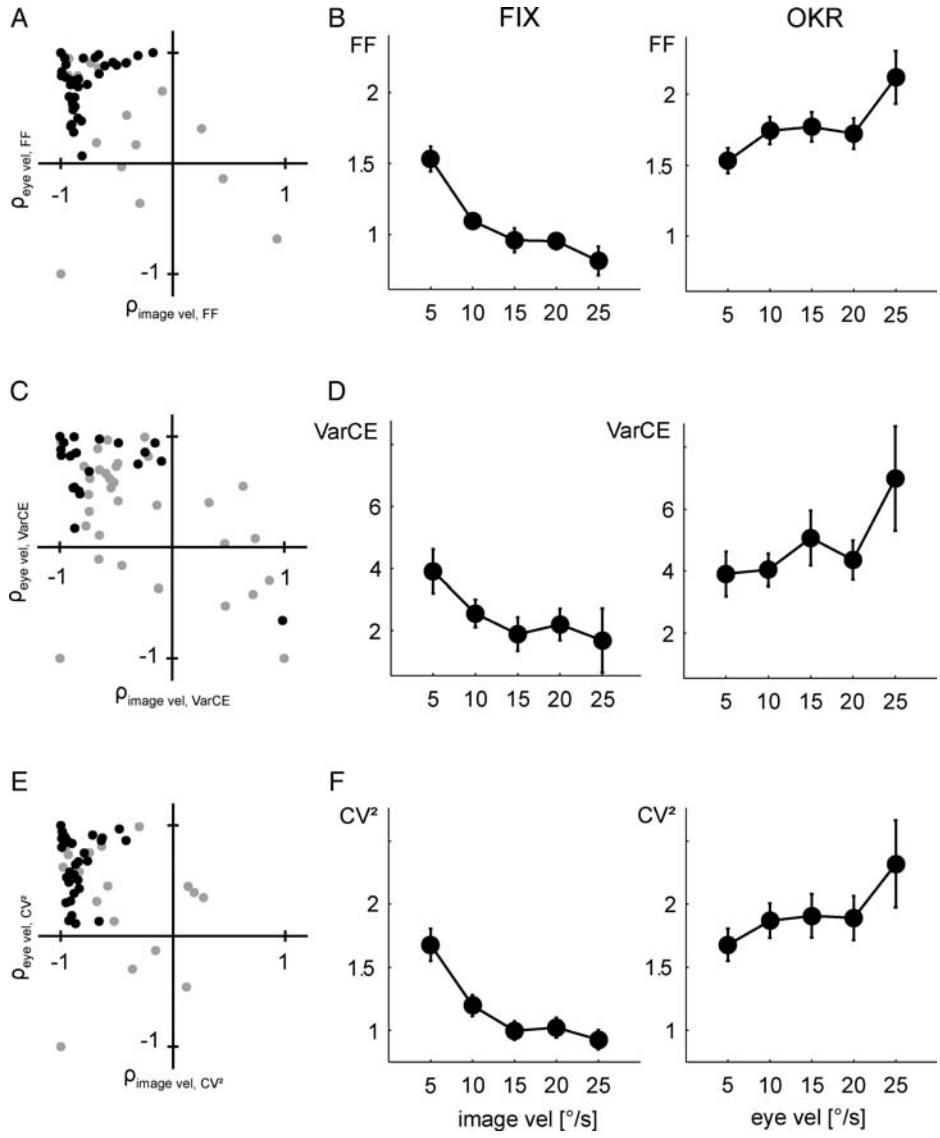

Figure 3. Spiking irregularity decreases with image velocity and increases with eye velocity. (*A*) Fano factor (FF) correlates negatively with image velocity and positively with eye velocity. For each neuron $\rho_{\text{image vel, FF}}$ and $\rho_{\text{eye vel, FF}}$ were determined as in the example shown in Figure 2*C*. Gray dots mark neurons in which neither of the correlation coefficients was significant ($P > 0.05$). (*B*) FF dependence on retinal image and eye velocity. The datasets were grouped according to their corresponding eye or image velocity. *X*-axis values denote upper limits, meaning that the value of 10°/s, for instance, comprises all datasets with velocities between 5 and 10°/s. The bin for 25°/s comprises all datasets with velocities greater than 20°/s. During FIX, mean eye velocity was <5°/s in each dataset. For OKR datasets image velocity was <5°/s. (*C*) The variance of the conditional expectation (VarCE) correlates negatively with image velocity and positively with eye velocity. (*D*) VarCE for both paradigms grouped into ranges of corresponding eye or retinal image velocities. (*E–F*) Results for the CV^2. FF and VarCE were averaged over the testing interval. CV^2, image and eye velocity were averaged across the testing interval and all trials. Vertical lines mark standard errors across corresponding datasets.

Influence of Eye Movements

Could the observed dependency of spiking irregularity on image and eye velocity be explained by differences in the variability of image and eye velocity? To allow a comparison with the measures used to evaluate neuronal variability, we analyzed the "normalized variance" of image and eye velocity, which is the variance across or within trials divided by the mean signal. As shown in Figure 6*A*, the normalized variance decreased with image velocity during FIX (across/within: $\beta = -0.02$, $P < 0.001$), but did not change with eye velocity during OKR (across: $\beta = -0.003$, $P = 0.56$; within: $\beta = 0.005$, $P = 0.17$). Accordingly, the normalized variance was positively correlated with FF during FIX (Fig. 6*B*; across: $\rho = 0.32$, $P < 0.001$; within: $\rho = 0.39$, $P < 0.01$). For OKR both measures were unrelated (across: $\rho = 0.16$, $P = 0.12$; within: $\rho = 0.09$, $P = 0.24$). Also with CV^2 there was positive correlation for FIX (across: $\rho = 0.24$, $P < 0.001$; within: $\rho = 0.30$, $P < 0.01$), and no correlation for OKR (across: $\rho = -0.06$, $P = 0.25$; within: $\rho = 0.02$, $P = 0.45$).

Until now, all measures were averaged across trials and time. In the following, we analyzed whether there also exists correlation *within* the datasets. In Figure 6*C*, the normalized variance and CV^2 were determined for each trial separately and then compared within every dataset. For the FIX condition, 25% of the datasets showed significant correlation of both measures within the datasets (mean $\rho_{\text{var/mean, CV}^2} = 0.18 \pm 0.39$), corroborating the previous results. For OKR, only few datasets showed correlation, with an average $\rho_{\text{var/mean,}}$

$_{CV^2} = 0.04 \pm 0.35$. The difference between both conditions was statistically significant (2-sample T-test: $P < 0.01$).

Another eye movement related influence could be saccades, since it has been reported that spiking activity is suppressed in many medial temporal (MT) and MST neurons during these rapid eye movements (Thiele et al. 2002). Such induced periods of silence might increase the regularity of spiking, similar to the refractory period. To analyze whether our findings might be affected by saccadic suppression of neuronal firing, we determined the number of saccades per trial for both paradigms (Fig. 6*D*). With an average of 1.6 saccades per trial, it seems unlikely that these rapid eye movements influenced neuronal variability. Furthermore, the difference between both paradigms was rather small. For FIX, there was an increase observable with image velocity. In the OKR paradigm there was only a slight change with eye velocity. Both changes were statistically not significant ($P = 0.69$ and 0.53, 1-way ANOVA). Linear correlation analysis between the number of saccades per trial and FF yielded no correlation for FIX ($\rho = 0.01$, $P = 0.22$) and OKR ($\rho = -0.18$, $P = 0.60$). The removal of saccade period data from the neuronal recordings increased neuronal variability slightly but had no influence on the observed relation to image and eye velocity (Supplementary Fig. S2).

In summary, the observed decline of spiking irregularity during the FIX condition may be related to the decline of image velocity variance. The increase of neuronal variability during the OKR condition seemed to be unrelated to the eye movements themselves.

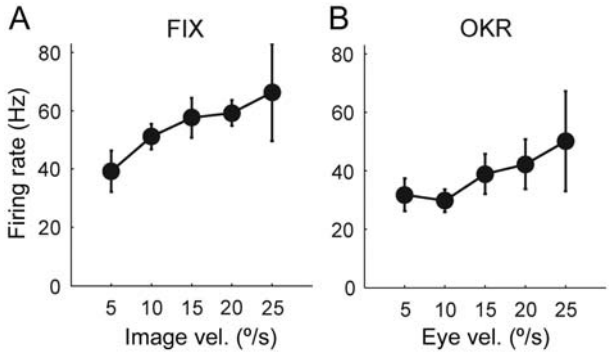

Figure 4. The firing rate (FR) increases with image and eye velocity. For each condition, FR was averaged over all trials and the testing interval. The datasets were grouped as in Figure 3. FR, image and eye velocity were averaged across the testing interval and all trials. Vertical lines mark standard errors.

Metric-Space Analysis

The mean FR of MSTd neurons increases with both, retinal image and eye velocity (see Fig. 4). Hence, the information contained in the FR alone does not allow distinguishing between a neuron being driven by image or eye velocity. On the other hand, we could show that the neuronal variability decreases with image velocity and increases with eye velocity. Might this differential behavior in spike timing allow the separation of the 2 signals?

To further examine this question, we performed a classification analysis of our data using the metric-space approach by Victor and Purpura (1996, 1997). This analysis determines to what extent pairs of responses to the same stimulus tend to be closer to each other than pairs of responses to different stimuli. Spike trains are considered similar if they have approximately the same number of spikes, and these spikes occur at approximately the same times, that is within some *a priori* defined temporal precision. The extent to which experimentally measured neuronal responses cluster in a systematic fashion is determined using an information-theoretic measure. Perfect clustering into, for example, 2 categories corresponds to a maximal value of 1 bit. For control, transmitted information was also determined for surrogate datasets, in which the spike trains were randomly shuffled from both conditions. This shows whether there is sufficient data to carry out a valid analysis. If the amount of data is sufficient, then the "shuffled" curve is well separated from the original data curve, and the amount of information in the shuffled curve should be near zero.

Figure 7 shows the results for 2 example neurons, where the mean FR was similar in both conditions. The neuron shown in the left column exhibited highly distinctive differences in spiking irregularity during FIX and OKR. Maximal transmitted information of 1 bit reflects a perfect distinction between the responses for both conditions. Perfect classification was achieved for values of temporal precision in the order of 4 ms. In the case of the neuron shown on the right column, the distinction between FIX and OKR was not as pronounced as for the other example, reaching maximal transmitted information of 0.5 bit. Good clustering was achieved for a broad range of temporal precision values between 8 and 60 ms. In both examples, the original data curves were well separated from the shuffled curves. It is important to note that the estimation of transmitted information from limited samples introduces several difficulties. The metric-space method tends to underestimate the total information that is present, since only a few stereotyped hypotheses for neural

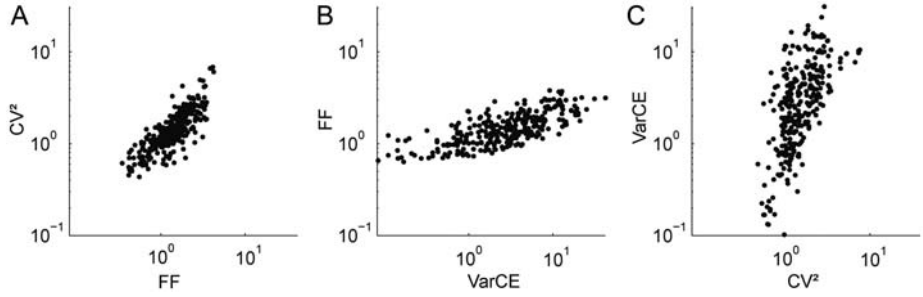

Figure 5. Correlations between FF, VarCE, and CV^2, plotted in log–log coordinates. Each dot marks one dataset. All measures were averaged as before. (*A*) There is a strong positive correlation between FF and CV^2 ($\rho_{FF,\ CV^2} = 0.79$, $P < 0.01$). (*B* and *C*) Also VarCE and FF, and CV^2 and VarCE, are positively correlated ($\rho_{VarCE,\ FF} = 0.70$, $P < 0.01$; $\rho_{CV^2,\ VarCE} = 0.53$, $P < 0.01$).

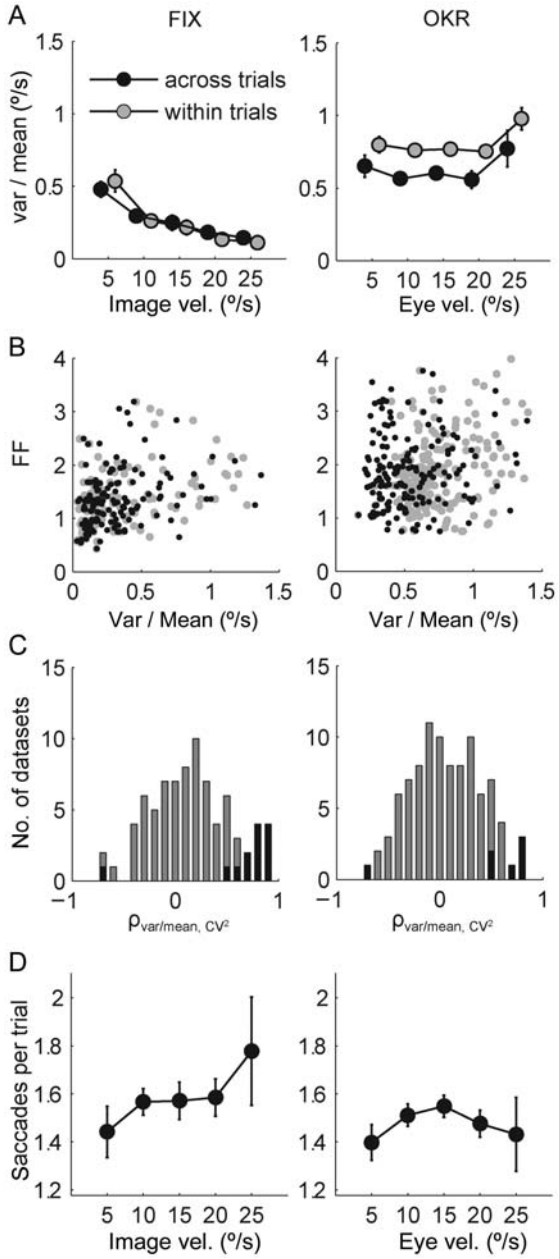

Figure 6. Relation between neuronal variability and variance in eye movements. (*A*) The normalized variance of image velocity decreases with image velocity, the normalized variance of eye velocity is independent of eye velocity. For each dataset, the variance was determined across all trials (black curve) or within each trial (gray curve), then divided by the mean, and finally averaged over the testing interval. Both curves were slightly moved for better visual separation. The datasets were grouped according to the paradigm and the corresponding image or eye velocity. (*B*) Correlation between the normalized variance across trials (black dots) or within trials (gray dots) and FF. Each dot marks one dataset. Some outliers fall outside the shown range. For FIX, there is a weak correlation, which is not present during OKR. (*C*) Distribution of datasets, in which normalized variance of image and eye velocity correlated with CV^2 *within* the datasets. Normalized variance and CV^2 were determined in every trial; then the correlation coefficient $\rho_{var/mean,\ CV^2}$ was calculated for each dataset. Black bars show datasets with significant ($P < 0.05$) correlation. (*D*) Number of saccades per trial. For each dataset the number of saccades during the testing interval was determined and averaged over all trials. Vertical lines mark standard errors.

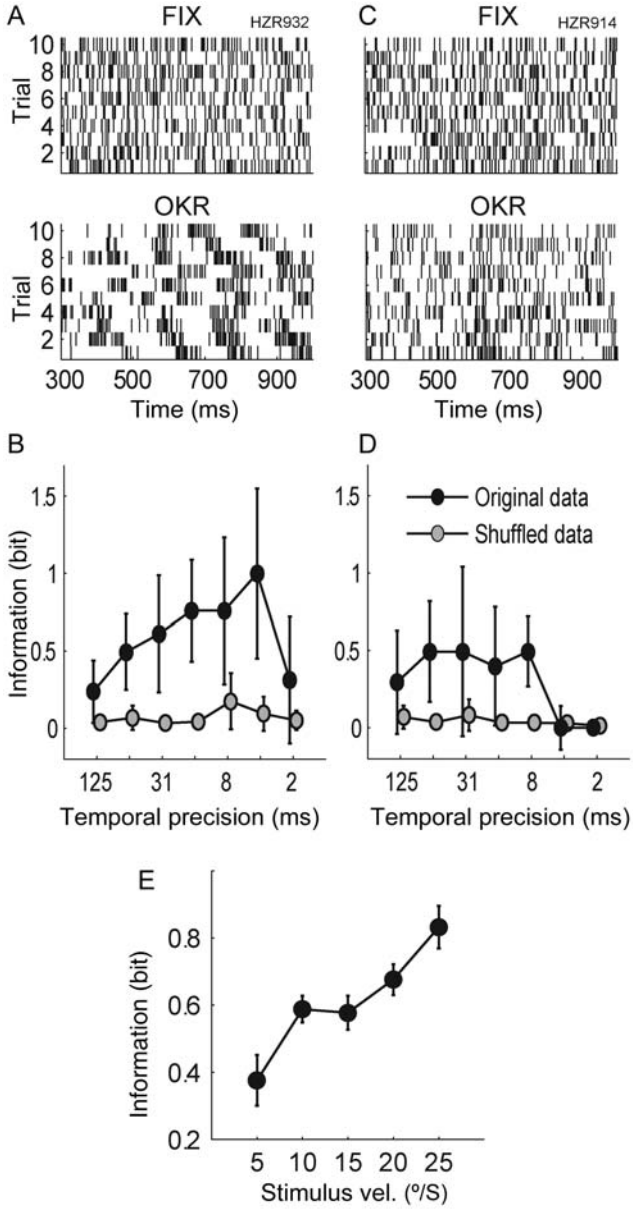

Figure 7. Metric-space analysis. (*A*) Spike raster plots showing regular activity for FIX (FR = 89 Hz, FF = 0.69, $CV^2 = 0.67$) and irregular activity for OKR (FR = 79 Hz, FF = 2.58, $CV^2 = 2.87$) during the testing interval for one example neuron. Stimulus velocity was 20°/s in both conditions. (*B*) Transmitted information of the original clustered data (black) and for shuffled data (gray) for different values of temporal precision. Vertical lines mark standard error for original data and double standard deviation for shuffled data. (*C* and *D*) Spike raster plots and transmitted information of a second example neuron showing regular activity for FIX (FR = 92 Hz, FF = 0.59, $CV^2 = 0.67$) and irregular activity for OKR (FR = 106 Hz, FF = 1.70, $CV^2 = 1.14$) during the testing interval. Here, stimulus velocity was 10°/s for both conditions. (*E*) Transmitted information increases with stimulus velocity. For each dataset pair maximal transmitted information was determined as in the examples above. Vertical lines mark standard errors.

codes are considered. On the other hand, the estimated information will be spuriously high because of chance proximities between the few examples of observed responses, if the number of presentations of each stimulus class is small. The large error bars in Figure 7*B* and *D* reflect these estimation problems.

For the 56 neurons analyzed here, there were 122 pairs of FIX and OKR datasets recorded using the same stimulus velocity. In 120 (98%) dataset pairs it was possible to discriminate between FIX and OKR spike trains using the

metric-space criterion. The average transmitted information for all dataset pairs was 0.61 ± 0.27 bit. Figure 7*E* shows that transmitted information increased with stimulus velocity. This result reflects the increasing differences in neuronal variability between both conditions with increasing stimulus velocity. For a stimulus velocity of 5°/s there was almost no difference in spiking irregularity between both conditions. Hence, classifying the spike trains into both categories was difficult. For 30°/s, on the other hand, the divergence in spiking irregularity was maximal and spike trains could be assigned almost perfectly to each category by their temporal spiking patterns.

Discussion

Our analysis of spiking irregularity in MSTd neurons revealed 5 major features. First, responses to LF visual stimulation do not only reflect external visual stimulation but are also modulated by eye movement signals. Second, also in MSTd the trial-to-trial variability of neuronal activity is quenched by stimulus onset. However, the change in variability of MSTd neuronal activity was not just related to stimulation, as proposed by Churchland et al. (2010). There was a sustained low level of variability during FIX, but for the OKR paradigm only a transient decline in FF was observable. Third, the relation between spiking irregularity and the 2 stimulation variables, image and eye velocity, was opposite. Both variables, which were uncoupled by using 2 orthogonal paradigms, affected the intra- and inter-trial variability of neuronal activity. At small stimulus velocities neuronal variability was similar for both paradigms, meaning that the change in variability was not task-dependent. All 3 measures analyzed here, FF, VarCE, and CV^2 were negatively correlated with retinal image velocity and positively correlated with eye velocity. Fourth, the decline of neuronal variability during FIX is accompanied by a decline of the normalized variance of image velocity. The increase during OKR, however, seems to be independent of the normalized eye velocity variance. Finally, we could show that the differential behavior in neuronal variability allows discriminating which of the 2 variables, image or eye velocity, has driven neuronal activity.

Previous Measurements of Spiking Irregularity

Prior studies examined spiking irregularity in MST and neighboring MT cortex. It is, nevertheless, difficult to compare their results, as stimuli and paradigms were very different. Also, previous studies did not differentiate between changing stimulus conditions. A number of studies agree in mean FF values between 1.0 and 1.4 for paradigms as different as pursuit of a moving dot (MST, Maimon and Assad 2009), FIX of a target during whole body rotation (MSTd, Takahashi et al. 2007), FIX during visual stimulation (MT, Buracas et al. 1998), or a depth discrimination task (MT, Uka and DeAngelis 2003). The mean FF of 1.47 in our data is in good agreement with these previous findings.

Churchland et al. (2010) analyzed FF time traces in MT neurons during FIX with visual stimulation and found levels around 1.8 before stimulus onset and a sustained decline to about 1.4 during visual motion. This complies qualitatively with the results of our FIX paradigm, although we measured an even larger decline in FF (2–3 to 0.7) in our MSTd data. Some previous works found a general tendency for cells in motor cortex to fire more regularly than in visual areas (Maimon and Assad 2009; Shinomoto et al. 2009). Our results seem to contradict this principle, as in our data FF decreased with visual input and increased with the oculomotor variable. Further investigation of this aspect, however, will require data from far more areas.

Werner and Mountcastle (1963) observed in thalamic neurons a decline in CV^2 from 0.9 during spontaneous activity to 0.3 during peripheral stimulation, confirming the stimulus dependence of spiking irregularity. In MT neurons CV^2 values of about 1 were found (Softky and Koch 1993; Shadlen and Newsome 1998). In these studies, the paradigms consisted of a visual motion coherence discrimination task, during which the monkeys had to fixate a target spot. The mean CV^2 of 1.12 during FIX for our MSTd data is in good agreement with these previous findings.

Relation Between Spiking Irregularity and FR

Due to refractory periods of up to 5 ms between each spike, neuronal activity tends to become more regular with higher FR (Berry and Meister 1998). Our observation of a weak, but significant, positive correlation between FF and FR in the OKR paradigm may exemplify an exception to the usually observed decrease in neuronal variability with increasing FR. A similar case was reported by Churchland et al. (2011), who observed parallel increase of variability and FR in LIP neurons. Also in pyramidal tract neurons spiking irregularity has been reported to increase during periods of high FR (Davies et al. 2006). In various other cortical areas, including MT, neurons were found where the FF changed notably during stimulation while the mean FR stayed constant (Churchland et al. 2010). Mochol et al. (2010) analyzed neurons in the cat's superior colliculus during visual stimulation. Interestingly, they found that for cells preferring low velocity, FR and FF were positively correlated, whereas for cells preferring high velocity the correlation was negative.

Possible Causes for Changing Neuronal Variability

A decline of neuronal variability after stimulus onset, which has been observed in a number of cortical regions, can be explained by certain topological structures of the underlying neuronal network. The stimulus-driven suppression of chaotic, spontaneous activity is a general feature of recurrent networks, a kind of structure presumed to be found in various cortical areas. The decline in variability depends on stimulus frequency and amplitude (Rajan et al. 2010). Our finding of decreasing spiking irregularity with increasing image velocity might be explained by the presence of recurrent circuitry in area MSTd.

Nevertheless, our observation may also be explained by another, probably more obvious, hypothesis. We could show that the normalized variance of image velocity decreases with increasing stimulus strength. The increase in regularity of spiking activity might simply reflect this reduction of the stimulus signal variability. This, however, requires that neuronal activity is able to capture high-frequency fluctuations in the stimulus signal. Most MSTd neurons fulfill this requirement during visual LF stimulation (Ono et al. 2010). The observed relation between the variability of sensory input and neuronal activity might also be important for the interpretation of earlier findings, which often were explained by an underlying

recurrent network structure. Nevertheless, both hypotheses are not contradicting each other and might also coexist.

Our second finding of an increase in neuronal variability during the OKR condition remains unexplained by both hypotheses. The normalized variance of eye velocity was neither related to stimulus strength, nor neuronal variability. Also a stimulus-dependent combination of suppression and enhancement of spontaneous activity cannot be implemented by a simple recurrent network structure. A network topology that might explain this finding would need to be asymmetrical and process both stimuli differently.

Alternatively, the opposite behavior for image and eye velocity could also result from fundamental differences in the properties of the 2 signals that form visual and oculomotor input to MSTd. It is assumed that the retinal image velocity signal is projected through connections from visual area MT into MSTd (Tusa and Ungerleider 1988). In MT neurons spiking irregularity declines with visual motion stimulation (Churchland et al. 2010), similar to our observations in MSTd. However, the source of the oculomotor signal is still disputed. Analysis of neuronal latency has shown that MSTd neurons usually start firing before the onset of OKR eye movements (Kawano et al. 1994; Brostek et al. 2011). This argues for an internally generated efference copy, rather than sensory origin of the eye velocity signal. One possibility is that thalamic projections (Tanaka 2005) directly convey extra-retinal information to MSTd and that these signals already carry the irregularity. Whereas for a long time it was assumed that MT does not receive extra-retinal input (Newsome et al. 1988), a recent work found that neurons in this area use eye movement signals to code depth-sign from motion parallax (Nadler et al. 2009). Wherever the oculomotor input to MSTd originates from, the regularity properties of this signal remain to be investigated.

Evidence for Temporal Coding?

In many neuronal systems, it could be shown that aside from mean FR the temporal pattern of spiking activity may also carry important information (MacKay and McCulloch 1952; Richmond et al. 1987; Softky 1995; Buracas and Albright 1999; Rieke et al. 1999; Singer 1999). For instance, in auditory neurons the mean FR represents some combination of amplitude and frequency of a tone. At the same time, there is the tendency for ISIs to cluster around integer multiples of the stimulus period, allowing the separation of frequency and amplitude information (Evans 1982). Also in cortical areas spiking irregularity has been used as an evidence to support the temporal coding hypotheses (Softky and Koch 1993; Stein et al. 2005).

In MSTd neurons the mean FR, which is the reciprocal of the mean ISI, codes some non-linear combination of visual and eye movement related signals (Ben Hamed et al. 2003; Brostek et al. 2011). At the same time, the variance of the ISI decreases with visual and increases with oculomotor stimulation. As we could show, this independent temporal code may allow the separation of the 2 signals, similar to phase locking in auditory neurons.

In a renewal process ISIs are assumed to be independent and identically distributed (Cox 1962). The approximate one-to-one relation between FF and CV^2 observed in our data argues for the renewal assumption. Both across-trial and within-trial variability are determined by the distribution of

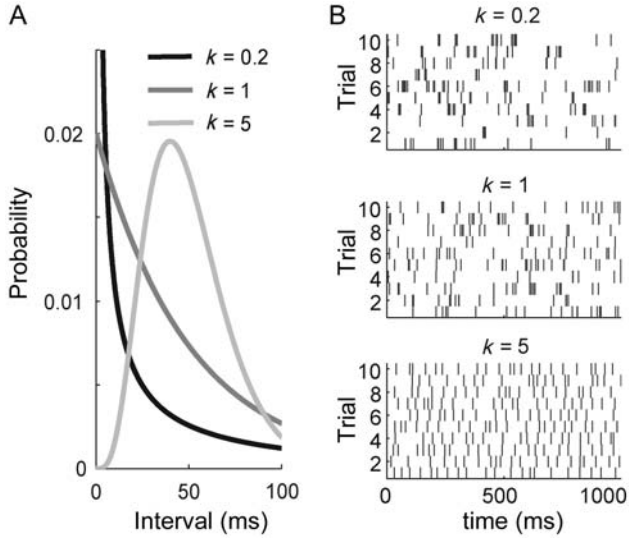

Figure 8. Spiking irregularity changes with inter-spike interval (ISI) distribution. (*A*) Gamma distributions for 3 different shape parameters *k*. (*B*) Simulated spike trains. ISIs were sampled from the 3 different gamma distributions according to a renewal process. The firing rate is 20 Hz in all 3 cases. For $k = 0.2$, spiking activity is bursty and highly variable from trial to trial ($FF = CV^2 = 2.3$). For $k = 1$, we get a Poisson process ($FF = CV^2 = 1$). For $k = 5$ spiking activity is very regular ($FF = CV^2 = 0.2$).

ISIs of the corresponding renewal process, as schematically illustrated in Figure 8. The gamma distribution is an appropriate approximation for the distribution of ISIs in most neuronal systems (Stein 1965). A change in spiking irregularity is associated with a modification of the ISI distribution. This again may result from changing membrane properties in single neurons, circuit properties of networks of neurons, or a combination of both. Miura et al. (2007), for instance, proposed a network architecture, where the FR could be decoupled from the ISI distribution by proper balance of excitatory and inhibitory inputs. However, the questions whether the change of the ISI distribution in dependence of visual and oculomotor input has a functional meaning, and whether the additional information, embodied in changing spiking irregularity, is actually used by MSTd and subsequent areas, or reflects just an epiphenomenon, remain to be solved by future investigations.

Supplementary Material

Supplementary material can be found at: http://www.cercor.oxfordjournals.org/.

Funding

This work was supported by the German Federal Ministry of Education and Research Grants 01GQ0440 (BCCN), 01EO0901 (IFB), and National Institutes of Health Grants EY06069, RR000166.

Notes

We are grateful to Seiji Ono for help in collecting the initial neurophysiological data. Furthermore, we thank Thomas Eggert and Paul MacNeilage for helpful discussions.

Conflict of interest: none declared.

References

Ben Hamed S, Page W, Duffy C, Pouget A. 2003. MSTd neuronal basis functions for the population encoding of heading direction. J Neurophysiol. 90:549–558.

Berry MJ, Meister M. 1998. Refractoriness and neural precision. J Neurosci. 18:2200–2211.

Bradley DC, Maxwell M, Andersen RA, Banks MS, Shenoy KV. 1996. Mechanisms of heading perception in primate visual cortex. Science. 273:1544–1547.

Bremmer F, Kubischik M, Pekel M, Hoffmann KP, Lappe M. 2010. Visual selectivity for heading in monkey area MST. Exp Brain Res. 200:51–60.

Brostek L, Eggert T, Ono S, Mustari MJ, Büttner U, Glasauer S. 2011. An information-theoretic approach for evaluating probabilistic tuning functions of single neurons. Front Comput Neurosci. 5:15.

Buracas GT, Albright TD. 1999. Gauging sensory representations in the brain. Trends Neurosci. 22:303–309.

Buracas GT, Zador AM, DeWeese MR, Albright TD. 1998. Efficient discrimination of temporal patterns by motion-sensitive neurons in primate visual cortex. Neuron. 20:959–969.

Churchland MM, Byron MY, Cunningham JP, Sugrue LP, Cohen MR, Corrado GS, Newsome WT, Clark AM, Hosseini P, Scott BB *et al.* 2010. Stimulus onset quenches neural variability: a widespread cortical phenomenon. Nat Neurosci. 13:369–378.

Churchland AK, Kiani R, Chaudhuri R, Wang X-J, Pouget A, Shadlen MN. 2011. Variance as a signature of neural computations during decision making. Neuron. 69:818–831.

Cox DR. 1962. Renewal theory. London: Methuen.

Cox D, Lewis P. 1966. The statistical analysis of series of events. New York (NY): Wiley.

Davies RM, Gerstein GL, Baker SN. 2006. Measurement of time-dependent changes in the irregularity of neural spiking. J Neurophysiol. 96:906–918.

Duffy CJ, Wurtz RH. 1991. Sensitivity of MST neurons to optic flow stimuli. I. A continuum of response selectivity to large-field stimuli. J Neurophysiol. 65:1329–1345.

Evans EF. 1982. Functional anatomy of the auditory system. The senses. Cambridge: Cambridge University Press, p. 251–306.

Fano U. 1947. Ionization yield of radiations. II. The fluctuations of the number of ions. Phys Rev. 72:26.

Kawano K, Shidara M, Watanabe Y, Yamane S. 1994. Neural activity in cortical area MST of alert monkey during ocular following responses. J Neurophysiol. 71:2305–2324.

Komatsu H, Wurtz RH. 1988. Relation of cortical areas MT and MST to pursuit eye movements. I. Localization and visual properties of neurons. J Neurophysiol. 60:580–603.

Ladda J, Eggert T, Glasauer S, Straube A. 2007. Velocity scaling of cue-induced smooth pursuit acceleration obeys constraints of natural motion. Exp Brain Res. 182:343–356.

MacKay DM, McCulloch WS. 1952. The limiting information capacity of a neuronal link. B Math Biophys. 14:127–135.

Maimon G, Assad JA. 2009. Beyond Poisson: increased spike-time regularity across primate parietal cortex. Neuron. 62:426–440.

Mitchell JF, Sundberg KA, Reynolds JH. 2007. Differential attention-dependent response modulation across cell classes in macaque visual area V4. Neuron. 55:131–141.

Miura K, Tsubo Y, Okada M, Fukai T. 2007. Balanced excitatory and inhibitory inputs to cortical neurons decouple firing irregularity from rate modulations. J Neurosci. 27:13802–13812.

Mochol G, Wójcik DK, Wypych M, Wróbel A, Waleszczyk WJ. 2010. Variability of visual responses of superior colliculus neurons depends on stimulus velocity. J Neurosci. 30:3199–3209.

Nadler JW, Nawrot M, Angelaki DE, DeAngelis GC. 2009. MT neurons combine visual motion with a smooth eye movement signal to code depth-sign from motion parallax. Neuron. 63: 523–532.

Newsome WT, Wurtz RH, Komatsu H. 1988. Relation of cortical areas MT and MST to pursuit eye movements. II. Differentiation of retinal from extraretinal inputs. J Neurophysiol. 60:604–620.

Ono S, Brostek L, Nuding U, Glasauer S, Büttner U, Mustari MJ. 2010. The response of MSTd neurons to perturbations in target motion during ongoing smooth-pursuit eye movements. J Neurophysiol. 103:519–530.

Ono S, Mustari MJ. 2006. Extraretinal signals in MSTd neurons related to volitional smooth pursuit. J Neurophysiol. 96:2819–2825.

Page WK, Duffy CJ. 1999. MST neuronal responses to heading direction during pursuit eye movements. J Neurophysiol. 81:596–610.

Rajan K, Abbott LF, Sompolinsky H. 2010. Stimulus-dependent suppression of chaos in recurrent neural networks. Phys Rev E. 82:011903.

Richmond BJ, Optican LM, Podell M, Spitzer H. 1987. Temporal encoding of two-dimensional patterns by single units in primate inferior temporal cortex. I. Response characteristics. J Neurophysiol. 57:132–146.

Rieke F, Warland D, de Ruyter van Steveninck R, Bialek W. 1999. Spikes: exploring the neural code (computational neuroscience). Cambridge, MA: MIT Press.

Shadlen MN, Newsome WT. 1998. The variable discharge of cortical neurons: implications for connectivity, computation, and information coding. J Neurosci. 18:3870–3896.

Shinomoto S, Kim H, Shimokawa T, Matsuno N, Funahashi S, Shima K, Fujita I, Tamura H, Doi T, Kawano K *et al.* 2009. Relating neuronal firing patterns to functional differentiation of cerebral cortex. PLoS Comput Biol. 5:e1000433.

Singer W. 1999. Time as coding space?. Curr Opin Neurobiol. 9:189–194.

Softky WR. 1995. Simple codes versus efficient codes. Curr Opin Neurobiol. 5:239–247.

Softky W, Koch C. 1993. The highly irregular firing of cortical cells is inconsistent with temporal integration of random EPSPs. J Neurosci. 13:334–350.

Stein RB. 1965. A theoretical analysis of neuronal variability. Biophys J. 5:173–194.

Stein RB, Gossen ER, Jones KE. 2005. Neuronal variability: noise or part of the signal? Nat Rev Neurosci. 6:389–397.

Steinmetz NA, Moore T. 2010. Changes in the response rate and response variability of area V4 neurons during the preparation of saccadic eye movements. J Neurophysiol. 103:1171–1178.

Takahashi K, Gu Y, May PJ, Newlands SD, DeAngelis GC, Angelaki DE. 2007. Multimodal coding of three-dimensional rotation and translation in area MSTd: comparison of visual and vestibular selectivity. J Neurosci. 27:9742–9756.

Tanaka M. 2005. Involvement of the central thalamus in the control of smooth pursuit eye movements. J Neurosci. 25:5866–5876.

Thiele A, Henning P, Kubischik M, Hoffmann K-P. 2002. Neural mechanisms of saccadic suppression. Science. 295:2460–2462.

Tusa RJ, Ungerleider LG. 1988. Fiber pathways of cortical areas mediating smooth pursuit eye movements in monkeys. Ann Neurol. 23:174–183.

Uka T, DeAngelis GC. 2003. Contribution of middle temporal area to coarse depth discrimination: comparison of neuronal and psychophysical sensitivity. J Neurosci. 23:3515–3530.

Victor JD, Purpura KP. 1996. Nature and precision of temporal coding in visual cortex: a metric-space analysis. J Neurophysiol. 76:1310–1326.

Victor JD, Purpura KP. 1997. Metric-space analysis of spike trains: theory, algorithms and application. Comput Neural Syst. 8:127–164.

Werner G, Mountcastle VB. 1963. The variability of central neural activity in a sensory system, and its implications for the central reflection of sensory events. J Neurophysiol. 26:958–977.

Title:

Eye Velocity Gain Fields in MSTd for Visuomotor Coordinate Transformations

Running title:

Eye Velocity Gain Fields in MSTd

Authors:

Lukas Brostek[1,2], Ulrich Büttner[1,3], Michael J. Mustari[4], Stefan Glasauer[1,2,3]

(1) Clinical Neurosciences, Ludwig-Maximilians-Universität, Munich 81377, Germany

(2) Bernstein Center for Computational Neuroscience, Munich 81377, Germany

(3) German Vertigo Center IFB, LMU Munich 81377, Germany

(4) Department of Ophthalmology and Washington National Primate Research Center, University of Washington, Seattle, WA 98195, USA

Corresponding author:

Lukas Brostek, BCCN Munich, Marchioninistr. 23, 81377 Munich, Germany

Phone: +49 89 7095 4833

Fax: +49 89 7095 4801

Email: Lukas.Brostek@lrz.uni-muenchen.de

Acknowledgements

We are grateful to Seiji Ono for help in collecting the initial neurophysiological data. This work was supported by the German Federal Ministry of Education and Research Grants 01GQ0440 (BCCN), 01EO0901 (IFB), National Institutes of Health Grants EY06069, RR000166, and 'Research to Prevent Blindness'. The authors declare no competing financial interests.

Abstract

Lesion studies argue for an involvement of cortical area MSTd in the control of optokinetic response (OKR) eye movements. Neurons in this area respond to visual motion and eye movement related signals. However, MSTd's function in visuomotor transformation is still unclear. Using a novel approach for characterizing neural tuning with high resolution, we show that during optokinetic stimulation the majority of MSTd neurons exhibit gain-field-like tuning functions. Rather than directly encoding one variable, neural responses showed a large diversity of tuning to combinations of retinal and extra-retinal input. Eye velocity related activity was observed prior to the actual eye movements, reflecting an efference copy. The observed tuning functions resembled those emerging in a network model trained to perform summation of two population-coded signals. Together, our findings support the hypothesis that MSTd implements the transformation from retinal to head-centered stimulus velocity signals for the control of OKR.

Introduction

The dorsal medial superior temporal area (MSTd) is located in the posterior parietal cortex (PPC) and is part of the visual motion processing system (Andersen, 1989). Besides pure retinal signals, neurons in this area are also driven by vestibular and eye movement related signals (Newsome et al., 1988; Gu et al., 2006; Ono and Mustari, 2006). This multi-modal behavior led to the suggestion that MSTd might compensate for distortions caused by self-generated eye and head movements in the perception of heading direction (Bradley et al., 1996; Page and Duffy, 1999; Gu et al., 2007; Bremmer et al., 2010).

Apart from its perceptual function, however, there is also strong evidence for an involvement of MSTd in oculomotor control. Lesions in this area lead to severe impairment of the optokinetic response (OKR), which is the involuntary eye movement that compensates for planar motion of the visual scene (Dürsteler and Wurtz, 1988; Takemura et al., 2007). Analysis of neural latencies (Kawano et al., 1994) and post-saccadic response behavior (Takemura and Kawano, 2006) gave further evidence for the participation of MSTd in OKR. Yet, it is still unknown which exact function this cortical region might serve during visuomotor transformation.

The term ‘visuomotor’ refers to the neural mechanisms by which visual stimuli are converted into motor commands. One essential processing step is the transformation of retinal or eye-centered signals to the body-centered coordinates of muscles for movement (Andersen et al., 1993; Crawford et al., 2011). A number of regions in the PPC are assumed to be involved in these coordinate transformations for various kinds of movements. For instance, the parietal reach region (PRR) is supposed to be a visuomotor interface for reaching arm movements,

whereas the lateral intraparietal area (LIP) might serve such function for saccadic eye movements (Buneo and Andersen, 2006).

'Gain fields' have been proposed to comprise the neural substrate for visuomotor coordinate transformations (Snyder, 2000). Gain-field-like tuning behavior is characterized by a modulation of the neuronal response depending on a certain variable, without changing the actual receptive field characteristics in relation to another variable (Salinas and Thier, 2000). Andersen and Mountcastle (1983) were the first to observe this kind of tuning in area 7a of the PPC, where visually responsive neurons are modulated by the eye's position. Neural network models have demonstrated that a gain field mechanism can be used to perform coordinate transformations (Zipser and Andersen, 1988; Pouget and Sejnowski, 1997).

In this work we analyzed the function of MSTd during OKR. As we will show, this kind of eye movement requires a transformation of the retinal image velocity signal to a head-centered stimulus velocity signal. The finding of neurons with gain-field-like tuning behavior in MSTd would argue for an involvement in coordinate transformation. Alternatively, the transformation might occur in an earlier processing stage. In this case, MSTd neurons could directly encode the sum of retinal image and eye velocity, i.e. visual motion in head-centered coordinates, as suggested for adjacent region MSTl for smooth pursuit eye movements (Ilg et al., 2004).

Methods:

Electrophysiology

We recorded extracellular potentials from 81 MSTd neurons in two awake monkeys (Macaca mulatta; monkey A: 70 neurons, monkey B: 11 neurons). All procedures were performed at the Washington National Primate Research Center at the University of Washington (Seattle, WA, USA) in compliance with National Institutes of Health Guide for the Care and Use of Laboratory Animals. The protocols were reviewed and approved by the Institutional Animal Care and Use Committee at the University of Washington. Surgical procedures were performed in a dedicated facility using aseptic techniques under isoflurane anesthesia (1.25-2.5%). Vital signs including blood pressure, heart rate, blood oxygenation, body temperature and CO_2 in expired air were monitored with a Surgivet Instrument (Waukesha, WI) and maintained in normal physiological limits. To permit single unit recording, we used stereotaxic methods to implant a titanium head stabilization post and a titanium recording chamber (Crist Instruments, MD) over MST cortex (posterior = 5 mm; lateral = 15 mm). In the same surgery, a scleral search coil for measuring eye movements was implanted underneath the conjunctiva of one eye. Post-surgical analgesia (Buprenorphine. 0.01 mg/kg, I.M.) and anti-inflammatory (Banamine 1.0 mg/kg, I.M.) treatment were delivered every 6 hours for several days, as indicated. For verifying MSTd location we used functional, histological, and magnetic resonance imaging criteria (described in detail in Ono et al., 2010). During the experiments monkeys were seated in a primate chair in a dark room with their head restrained in the horizontal stereotaxic plane. About 10 % of the isolated neurons in MSTd did not respond selectively to large moving visual stimuli and were discarded from our analysis. The average recording time per neuron was about 600 s.

Stimuli

The optokinetic response (OKR) is a tracking eye movement to moving large-field scenes. The term 'ocular following response' (OFR) generally refers to the immediate OKR response after the motion onset of a large visual stimulus (Miles 1998). The combination of OKR and fast resetting saccades during prolonged unidirectional stimulation is called optokinetic nystagmus (OKN). Tracking eye movements to small moving objects are called smooth pursuit. In our experiment a visual large-field stimulus (35° × 35° fixed random dot pattern with mean luminance of 100 cd/m²) was rear projected on a tangent screen. During the 'white noise motion' paradigm the stimulus was moving randomly in one direction in a translational, planar way (Duffy and Wurtz, 1991) , meaning that the position of the pattern on the screen changed continuously, but not the pattern itself. Each neuron was tested in the axis of its preferred direction, i.e. the direction which elicits maximal spiking activity. For determination of the preferred direction, the large-field pattern moved in a circular (not spiral) trajectory as a search stimulus. This ensures that every contrast element in the pattern moves at the same speed, through all directions. The preferred direction was estimated from the on-line response of each neuron. Further testing was conducted along a cardinal direction (vertical, horizontal or oblique, separated by 45°) that most closely matched the estimated preferred direction. Different speeds (typically between 10-60°/s) were used to test each neuron in the preferred direction. The maximal eccentricity of the center of the pattern was ±40°. The frequency spectrum of the white noise stimulus was flat with stimulus velocities reaching up to 200 °/s, which is about threefold maximal eye velocity. The monkey's task was to perform OKR eye movements, following stimulus motion as well as possible (Fig. 1A). Reward was given for keeping eye position in the range of ± 5-7° around the center of the stimulus pattern. Rapid changes in stimulus direction and velocity, however, impeded perfect OKR and decoupled the image velocity and eye velocity signals. Figure 1B shows a sample trace and the corresponding recording of an example neuron. Over a range of several days, the monkeys

improved in following the stimulus. In order to minimize the dependency between the image and eye velocity signals, we increased the stimulus range according to the monkey's behavior. Further, we used an algorithm for de-correlation of image and eye velocity which is described in the Data Analysis section.

Data Processing

Action potentials were detected using a hardware window discriminator (Bak Electronics, MD). Eye position signals were processed with anti-aliasing filters at 200 Hz using 6-pole Bessel filters (latency 5 ms) before digitization at 1 kHz with 16-bit precision. Subsequently, they were filtered with a Gaussian low-pass (cutoff frequency 30 Hz) and 3-point differentiated to obtain velocity traces. Saccade periods were detected and removed from the data using a previously described algorithm (Ladda et al., 2007). Briefly, an estimate of the slow-phase component (SPC) was initialized to zero and iteratively improved in each step. The difference between the actual eye velocity trace and the current SPC served as an estimate of the fast-phase component (FPC). When the FPC exceeded a threshold (100 °/s in the first step, 50 °/s in the second step), a saccade was detected. The new SPC was then computed by linear interpolation of the eye velocity across saccades and subsequent filtering with a Gaussian low-pass (cutoff frequency: 5 Hz in the first step, 10 Hz in the second step).

Information-theoretic Data Analysis

Our mutual information based approach for neural data analysis has been described in detail previously (Brostek et al., 2011). Briefly: Let S denote a binary random variable for the observation of a spike or non-spike, with $p(s)$ denoting the probability mass function of spike occurrence. The discrete random variable V denotes the observation of a specific combination of explanatory variables with associated probability mass function $p(v)$. Herewith, it is possible to define a probabilistic neural tuning function by the conditional probability $p(s|v)$

of observing a spike given any combination of explanatory variable. By multiplication with the sampling rate, this probability translates directly into an expectation value of the spiking rate. Using Bayes' theorem, $p(s|v)$ can be expressed as the quotient of the joint probability mass function $p(s,v)$ divided by $p(v)$:

$$p(s \mid v) = \frac{p(s,v)}{p(v)}.$$

Estimates of $p(v)$ and $p(s,v)$ can be attained by histogramming the experimental data (Fig. 1C). To smoothen the histograms we used a symmetrical Gaussian low-pass filter with a standard deviation of two bin widths. This approach of tuning function determination poses three major challenges: first, the variable space needs to be fully covered, while ensuring statistical independence of all explanatory variables. Second, neural latencies have to be considered, as the tuning function $p(s|v)$ critically depends on it. Third, the dependence of neural activity on each explanatory variable needs to be estimated. Concerning the former issue, we used a 'white noise motion' paradigm as described above. Additionally, we used an algorithm to remove samples with high linear correlation from the datasets. This algorithm randomly selects parts of the original dataset for the analyzed set as long as a maximal level of linear correlation between image velocity and eye velocity is not exceeded. We set this limit to a Pearson's correlation coefficient of 0.2. The average percentage of discarded samples was 39.7 ±23.3 %. To estimate the neural latency, we analyzed the mutual information I between explanatory variables V and spiking activity S:

$$I(V;S) = H(S) - H(S \mid V),$$

with $H(S)$ being the entropy of S and $H(S|V)$ the conditional entropy of S given V. These are given by

$$H(S) = -\sum_{S} p(s) \log p(s)$$

$$H(S \mid V) = -\sum_{V} p(v) \sum_{S} p(s \mid v) \log p(s \mid v).$$

By maximizing the mutual information $I(V;S)$, our approach estimates neural latency in such a way that the dependence of the neural activity on the independent variables is maximized. Furthermore, the evaluation of mutual information allows us to compare maximized $I(V;S)$ values using different combinations of explanatory variables to determine those variables which are most related to spiking activity.

Transformation Index

The transformation index (TI) quantifies the 'slope' of the two-dimensional tuning function and was determined as follows: Let x and y denote the two axes of the tuning function, and z the activity axis. In this three-dimensional coordinate system a plane

$$z = ax + by + c$$

is least-squares fitted to the left flank of the activity hill. The TI-value is then the logarithm of the slope of the line of intersection of the fitted plane in the x-y-plane:

$$TI = \log \frac{a}{b}.$$

Negative TI-values indicate predominant vertical tuning, corresponding to higher selectivity for image velocity, whereas positive values indicate horizontal, eye velocity related tuning. We used the function 'regress' from the Matlab Statistics Toolbox (The MathWorks Inc., Natick, MA) for estimating the TI-values and the 95 % confidence intervals of the estimated parameters. Based on these, a 95 % confidence interval was determined for each TI-value.

Modeling

We used two different models: a system-level model of the OKR control system (Fig. 5A) and a neural network model of the coordinate transformation (Fig. 5C). The system-level model simulates the interaction and signal-flow between different anatomical regions during OKR and was implemented in Simulink 7.1 (The MathWorks Inc., Natick, MA) using standard

differential equation solver settings. The transfer functions for the eye plant, which models the inertia of the eye-muscle system, and the internal plant model, which estimates eye velocity from an efference copy of the motoneuron signal, are given in Fig. 5A.

The neural network model was adapted from (Pouget and Sejnowski, 1997). The 31 image velocity input units were Gaussian-tuned with $\sigma = 32$ °/s and equally distributed peaks p_i between -60 and 60 °/s:

$$h_i = e^{-\frac{(iv-p_i)^2}{2\sigma^2}}$$

where h_i is the activity of unit i and iv is image velocity. The 21 eye velocity input units were sigmoid-tuned with slope factors $\tau = 16$ °/s and equally distributed inflection points ip_i between -40 and 40 °/s:

$$h_i = \frac{1}{1+e^{-\frac{ev-ip_i}{\tau}}}$$

with ev being eye velocity. The 41 stimulus velocity output units were also sigmoid-tuned with slope factors $\tau = 16$ °/s and equally distributed inflection points ip_i between -100 and 100 °/s. Each of the 651 intermediate layer units received input from each input layer unit, weighted with factors u_i and v_i for image and eye velocity, respectively. Each output layer unit received input from each intermediate layer unit, weighted with factors w_i. To avoid negative unit output, linear-threshold activation functions were used. During the learning process the weights u_i, v_i, and w_i were adjusted using the back-propagation algorithm in online mode (Rumelhart et al., 1986). The training set comprised arbitrary, equally distributed input and output value combinations. The learning procedure was continued until the error between desired and actual output, averaged over the last 10 iterations, showed no more significant decrease.

Results

In the first part we present our electrophysiological findings. Thereafter, we compare these data with theoretical predictions from a computational model.

MSTd neural tuning during OKR

The visual stimulus consisted of a large-field random dot pattern moving randomly in the axis of preferred direction, which was separately determined for each neuron. The monkey's task was to follow this planar 'white noise motion' stimulus as well as possible, performing optokinetic response eye movements (OKR). Maximal stimulus velocities of up to 200 °/s allowed us to cover wide ranges of both eye velocity and retinal image velocity values at the same time.

For analyzing the data we used a novel approach (Brostek et al., 2011), which estimates the latency and dependence of neural activity on different visual and eye movement related variables based on maximization of mutual information. Neural activity correlated mainly with two variables: image velocity and eye velocity, which accounted on average for 35 % and 30 % of mutual information with spiking activity, respectively. The remaining mutual information was shared by eye acceleration (13 %), image acceleration (12 %), and eye position (10 %), showing that the latter three variables correlated marginally with neural activity.

Figure 2 shows the latency of spiking activity relative to the image and eye velocity signals. All neurons fired *after* the image velocity signal, with a mean neural latency of +63 ±27 (s.d.) ms. This value for the visual response latency agrees well with previous findings (Kawano et al., 1994; Schmolesky et al., 1998). For eye velocity the distribution was bimodal. Most

neurons (77 %) fired *before* the eye velocity signal with a mean latency of -34 ±26 ms. This signal therefore cannot be of sensory origin, but indicates a premotor variable, which probably reflects an internally generated efference copy of the eye velocity signal. Neurons with positive neural latency relative to eye velocity were excluded from further analysis. We will refer to these units in the next section. Interestingly, we observed that neurons which were recorded in neighboring tracks seemed to share similar latency estimates. The subpopulation with positive latency relative to eye velocity also seemed to cluster in one specific region. However, anatomical sampling in this study was too sparse for reporting significant effects.

Figure 3 provides an overview of two-dimensional tuning functions determined from our recordings. Neural latencies were estimated for each neuron and compensated in the subsequent analysis. The stimulus range was adapted continuously to the monkey's behavior and therefore varied across datasets. Preferred image velocity differed across the population in accordance with previous findings (Churchland and Lisberger, 2005). The flame-like type of tuning functions reflects a gain field with an approximately Gaussian-shaped selectivity for image velocity, modulated by eye velocity (Fig. 3A+B). In all gain field neurons the visual response increased with increasing eye velocity in the neuron's preferred direction, and decreased with eye movement in the opposite direction. The shape of the tuning functions, however, differed notably across neurons. Some tuning functions were comparatively 'broad', with neurons showing less selectivity for image velocity with increasing eye velocity (e.g. A97.4 and A100.2). In other units tuning functions exhibited rather 'sharp' forms, preserving their visual selectivity for high eye velocities (e.g. B28.1). In some cases preferred velocity seemed to shift towards lower values with increasing gain (e.g. A94.5).

In 29 neurons (36 %) tuning functions expressed clear gain-field-like behavior. Another 33 units (41 %) showed a modulation of visual response with increasing eye velocity, but had open, sigmoid tuning for image velocity resembling part of a gain field (Fig. 3C+D). We therefore refer to these units as 'partial gain fields'. Prior studies in the neighboring middle temporal cortex (MT) that tested for wider velocity ranges usually found closed image velocity tuning functions (Mikami et al., 1986). As the image velocity signal is assumed to be projected via MT to MST (Tusa and Ungerleider, 1988), the open image velocity tuning in part of our neurons could have resulted from a limited testing range. In 7 cases (9 %) neurons exhibited virtually pure selectivity for image velocity, whereas in 2 neurons (2 %) neural activity increased mainly with eye velocity, showing marginal modulation by image velocity.

To quantify the 'slope' of the two-dimensional tuning functions we determined the transformation index (TI, see Methods) for all neurons (Fig. 3E). A negative TI-value indicates stronger dependency of neural activity for image velocity, whereas a positive value indicates more eye velocity related tuning. A TI-value of 0 indicates uniform increase of neural activity with image and eye velocity. This relation would be expected in neurons that directly encode the stimulus velocity, which is the sum of image and eye velocity. However, only 3 units (4 %) had TI-values that were not different from zero on a 5 % significance level. The distribution of estimated TI-values was Gaussian-shaped (Lilliefors test: $P = 0.07$; mean $= 0.05$, $\sigma = 0.82$). Hence, no specific form of gain field dominated the population. We found a variety of different shapes between the two extremes of pure vertical, image velocity related and pure horizontal, eye velocity related tuning. Finally, Figure 3F shows the population's mean firing rates for image and eye velocity values of 20 °/s extracted from the tuning functions. This Gamma-shaped distribution (Kolmogorov-Smirnov test for Gamma distribution with $\alpha = 1.65$, $\beta = 27.63$: $P = 0.43$) covers a wide range from 10 to 200 Hz.

Neurons with late eye movement related responses

In a subpopulation of 19 neurons (23 %) spiking activity had a mean latency of +105 ±39 ms relative to the eye velocity signal (see Fig. 2). Similar latencies after eye movement onset are typically observed in 'smooth pursuit neurons' (Newsome et al., 1988; Ono et al., 2010), a type of MSTd neuron exhibiting increased activity during tracking of small moving targets. Most neurons of this subpopulation not only differed in neural latency but also exhibited significant differences in tuning behavior. In 6 out of these 19 units (32 %) the tuning functions exhibited peak values for positive image velocity and negative eye velocity (Fig. 4). Such opposite preferred directions for visual and eye movement related activity were also previously reported in MSTd smooth pursuit neurons (Komatsu and Wurtz, 1988; Shenoy et al., 2002). In another 5 out of the 19 neurons (26 %) the mutual information between spiking activity and eye position or acceleration exceeded the mutual information values between spiking activity and image velocity. This means that neuronal activity in these neurons was best correlated with eye movement rather than with image related variables. The subpopulation of MSTd neurons with positive neural latency relative to eye velocity is probably not participating in OKR. Rather, it might be involved in smooth pursuit control (Ono and Mustari, 2006; Ono et al., 2010) or pursuit compensation for the perception of heading direction (Bradley et al., 1996).

Modeling results

Figure 5A shows a system-level model of the OKR control circuit, analogous to well-established models of the smooth pursuit system (Robinson et al., 1986; Glasauer, 2007). The 'eye plant' is usually modeled by a low pass filter with a time constant of 200 ms and simulates the inertia of the eye-muscle system. It receives as input the motoneuron signal and yields as output the eye velocity signal. The signal processing time in retina, thalamus, and visual cortical areas is modeled by a 60 ms delay, resembling the measurements from our

MSTd data. Due to this delay, a pure negative feedback circuit, with image velocity driving the eye plant directly, would not be stable. A straightforward way to prevent instability is the introduction of an internal positive feedback to the control signal (Young, 1971). An internal model of the eye plant, presumably located in the cerebellum (Wolpert et al., 1998; Glasauer, 2003; Porrill et al., 2004) or PPC (Mulliken et al., 2008), might receive an efference copy of the motor command and use it to estimate eye velocity. The summation of image velocity and estimated eye velocity yields the estimated stimulus velocity signal. This processing step can also be conceived as transforming a retinal signal to head-centered coordinates. The resulting signal can be used to drive the eye plant. To account for the observed neural latency regarding the eye movement, we introduced a delay of 20 ms to the eye plant. The resulting model of the OKR system is stable and yields realistic step function responses with an eye movement onset latency of 80 ms (Fig. 5B). It should be mentioned that leading of the internally estimated eye velocity signal relative to the actual eye velocity signal (i.e. negative latency) is not critical for stability. The system is also stable for a positive delay of the internal eye velocity signal, as would be expected for proprioceptive feedback. In this case, however, the model's step response exhibits slower rising and does not fit the data as well.

To analyze the sensorimotor coordinate transformation at a deeper, more biological level, we designed a firing-rate neural network to model the summation of retinal image velocity with eye velocity (Fig. 5C). As in the electrophysiological study, we restricted this analysis to one (preferred) direction. The velocities of image, eye, and stimulus were coded by three different neural populations. Using the back-propagation learning algorithm (Rumelhart et al., 1986), the network was trained to estimate the proper stimulus velocity value for any given combination of image and eye velocity input values. The shapes of the resulting tuning functions of the network's intermediate layer units had remarkable similarity to our MSTd tuning functions. All tuning functions obtained from the simulation exhibited gain-field-like

shape. Some neurons had sharp, vertical tuning functions, whereas other units showed rather horizontal, image velocity related tuning. The similarity to our electrophysiological results was corroborated by the neural network's distribution of TI-values (Fig. 5D). Before learning all weights were randomly sampled from a uniform distribution. The resulting tuning functions were quite similar in shape, reflected by a narrow distribution of TI-values. During the training process, however, this distribution broadened, demonstrating the network's demand for a certain diversity of broad and sharp gain fields for accomplishing the transformation task. After completion of the learning process, the distribution of TI-values showed no significant differences to our MSTd data (Two-sample T-test: $P = 0.48$). In 10 units (2 %) the TI-value was not significantly different from zero. Figure 5E shows the average activity of the trained intermediate units for image and eye velocity values of 20 °/s after learning. As in our data, the activity was also not Gaussian distributed (Lilliefors test: $P = 0.013$). However, the neural network's units exhibited much less variability in their activity than MSTd neurons. The distribution of input and output weight values is shown in Figure 5F. Input weights for image and eye velocity were distributed almost equally between -0.02 and 0.07 after learning. Also the distribution of output weights was flat and nearly symmetrical between -0.05 and 0.055.

Discussion

Our finding of eye velocity gain fields is in line with the hypothesis of MSTd's participation in the OKR control system by implementing the transformation from retinal image velocity to an estimate of stimulus velocity. In this sense, eye velocity gain fields constitute an intermediate step in transforming the eye-centered to a head-centered visual motion signal. In contrast to the neighboring MSTl (Ilg et al., 2004), neurons in MSTd do not to directly encode one specific variable. Our analysis rather revealed a large diversity of gain field shapes including asymmetric and non-separable tuning functions. The distribution of gain fields was almost identical to the predictions from a neural network model trained to perform the summation of image and eye velocity. Negative latency of the modulatory activity component indicates its premotor character and argues for an estimate of the eye velocity signal, generated by an internal model of the eye plant system.

Gain fields have been found before in various other areas of the PPC. For instance, visual responses of neurons in LIP and cortical area 7A are gain-modulated by eye and head position signals (Snyder et al., 1998). The activity of neurons in PRR is modulated by eye and limb position (Chang et al., 2009). Yet, all studies so far have suffered from the problem that characterization of the neural responses was incomplete in the sense that only very few and specific combinations of visual input and motor output could be tested. Our 'white noise motion' paradigm overcomes these difficulties and allows us to characterize neural tuning in high resolution, thereby enabling us to analyze the distribution of gain field types. The finding of a well-defined subpopulation with differing tuning and latency behavior is in agreement with previous MSTd studies and further demonstrates the strengths of our approach.

Previous electrophysiological studies in area MSTd predominantly focused on its role in perception of self-motion and heading direction. In general, radial visual stimulation was used in combination with small target pursuit eye movements. Our OKR results are not directly comparable to these studies, as most MSTd neurons show different behavior during smooth pursuit and OKR (Kawano et al., 1994), as well as for radial and planar visual stimulation (Duffy and Wurtz, 1991), respectively. Nevertheless, studies using smooth pursuit and radial stimulation found that visual responses of MSTd neurons are modulated during eye movements (Bradley et al., 1996; Page and Duffy, 1999; Ben Hamed et al., 2003; Bremmer et al., 2010), which is in compliance with our results.

Other studies that investigated neural tuning in MSTd during small target pursuit and planar visual stimulation yielded diverging conclusions. Kawano and colleagues suggested that MSTd neurons might directly encode the velocity of a large-field visual stimulus in head-centered coordinates (Inaba et al., 2007, 2011; Inaba and Kawano, 2010). A similar study by Chukoskie and Movshon (2009), also using small target pursuit, could confirm this hypothesis only in parts. They found some neurons in MSTd that encoded stimulus velocity. Most of the neurons, however, exhibited a variety of different other tuning behaviors ranging from pure retinal to head-centered stimulus velocity coding. Considering the difference of paradigms used, this finding has remarkable similarity to our results. We found only few neurons with a TI-value close to zero, which could also be interpreted as coding stimulus velocity in a restricted range of stimulus space. However, instead of smooth pursuit, we were using an OKR paradigm and could therefore assume an involvement of the analyzed neurons in control of these eye movements (Dürsteler and Wurtz, 1988). This allowed us to shift the focus from the question ‘which signals are coded?’ to ‘what functions are implemented?’. Our coordinate transformation hypothesis offers a straightforward explanation for the diversity in tuning behaviors found in MSTd.

Traditionally, most researchers attempted to correlate neuronal activity with certain variables, assuming direct encoding of sensory or motor signals by different neural populations. This approach may be appropriate for early input or output stages of neuronal processing. However, it poses difficulties when intermediate processing steps of sensorimotor transformation are analyzed. Theoretical work has shown that a neural coding scheme where each object in each reference frame is represented by a different set of neurons quickly will reach limitations due to the combinatorial explosion in the number of required cells (Poggio, 1990). It was therefore suggested that a much more efficient scheme for neuronal representation might be used: instead of representing each variable by a certain pool of neurons, one set of basis functions can represent a number of different variables simultaneously. Arbitrary variables are then represented by simple linear combination of these basis functions (Girosi et al., 1995; Pouget and Sejnowski, 1997).

Gain fields, as demonstrated by Pouget and Sejnowksi (1997), exhibit all characteristics necessary to form a set of basis functions. The diversity of tuning functions we observed in our data is consistent with this theory. Hence, eye velocity gain fields in MSTd could be used to generate a number of other visual motion related variables, as for instance an estimate of heading direction (Ben Hamed et al., 2003) or perceived self-motion velocity. In our case of planar visual stimulation, perceived self-motion velocity is the stimulus velocity signal directed towards the opposite side. Such inversion can be easily obtained by changing the weights of the connections to the output layer in our neural network model. The self-motion signal might be generalized for head- and body-motion by the inclusion of vestibular information (Gu et al., 2006, 2007). Our results are therefore compatible with the idea of area MSTd serving various functions in self-motion perception, as well as in oculomotor control.

References

Andersen RA (1989) Visual and eye movement functions of the posterior parietal cortex. Annu Rev Neurosci 12:377–403.

Andersen RA, Mountcastle VB (1983) The Influence of the Angle of Gaze Upon the Excitability of the Light- Sensitive Neurons of the Posterior Parietal Cortex. J Neurosci 3:532–548.

Andersen RA, Snyder LH, Li C-S, Stricanne B (1993) Coordinate transformations in the representation of spatial information. Curr Opin Neurobiol 3:171–176.

Ben Hamed S, Page W, Duffy C, Pouget A (2003) MSTd Neuronal Basis Functions for the Population Encoding of Heading Direction. J Neurophysiol 90:549 –558.

Bradley DC, Maxwell M, Andersen RA, Banks MS, Shenoy KV (1996) Mechanisms of Heading Perception in Primate Visual Cortex. Science 273:1544 –1547.

Bremmer F, Kubischik M, Pekel M, Hoffmann KP, Lappe M (2010) Visual selectivity for heading in monkey area MST. Exp Brain Res 200:51–60.

Brostek L, Eggert T, Ono S, Mustari MJ, Büttner U, Glasauer S (2011) An Information-Theoretic Approach for Evaluating Probabilistic Tuning Functions of Single Neurons. Front Neurosci 5.

Buneo CA, Andersen RA (2006) The posterior parietal cortex: Sensorimotor interface for the planning and online control of visually guided movements. Neuropsychologia 44:2594–2606.

Chang SWC, Papadimitriou C, Snyder LH (2009) Using a Compound Gain Field to Compute a Reach Plan. Neuron 64:744–755.

Chukoskie L, Movshon JA (2009) Modulation of Visual Signals in Macaque MT and MST Neurons During Pursuit Eye Movement. J Neurophysiol 102:3225–3233.

Churchland AK, Lisberger SG (2005) Relationship Between Extraretinal Component of Firing Rate and Eye Speed in Area MST of Macaque Monkeys. J Neurophysiol 94:2416–2426.

Crawford JD, Henriques DYP, Medendorp WP (2011) Three-Dimensional Transformations for Goal-Directed Action. Annu Rev Neurosci 34:309–331.

Dürsteler MR, Wurtz RH (1988) Pursuit and optokinetic deficits following chemical lesions of cortical areas MT and MST. J Neurophysiol 60:940–965.

Duffy CJ, Wurtz RH (1991) Sensitivity of MST neurons to optic flow stimuli. I. A continuum of response selectivity to large-field stimuli. J Neurophysiol 65:1329 –1345.

Girosi F, Jones M, Poggio T (1995) Regularization Theory and Neural Networks Architectures. Neural Comput 7:219–269.

Glasauer S (2003) Cerebellar Contribution to Saccades and Gaze Holding. Ann NY Acad Sci 1004:206–219.

Glasauer S (2007) Current models of the ocular motor system. Developments in ophthalmology 40:158.

Gu Y, DeAngelis GC, Angelaki DE (2007) A functional link between area MSTd and heading perception based on vestibular signals. Nat Neurosci 10:1038–1047.

Gu Y, Watkins PV, Angelaki DE, DeAngelis GC (2006) Visual and Nonvisual Contributions to Three-Dimensional Heading Selectivity in the Medial Superior Temporal Area. J Neurosci 26:73–85.

Ilg UJ, Schumann S, Thier P (2004) Posterior Parietal Cortex Neurons Encode Target Motion in World-Centered Coordinates. Neuron 43:145–151.

Inaba N, Kawano K (2010) Responses of MSTd and MT Neurons During Smooth Pursuit Exhibit Similar Temporal Frequency Dependence on Retinal Image Motion. Cereb Cortex 20:1708–1718.

Inaba N, Miura K, Kawano K (2011) Direction and speed tuning to visual motion in cortical areas MT and MSTd during smooth pursuit eye movements. J Neurophysiol 105:1531–1545.

Inaba N, Shinomoto S, Yamane S, Takemura A, Kawano K (2007) MST Neurons Code for Visual Motion in Space Independent of Pursuit Eye Movements. J Neurophysiol 97:3473–3483.

Kawano K, Shidara M, Watanabe Y, Yamane S (1994) Neural activity in cortical area MST of alert monkey during ocular following responses. J Neurophysiol 71:2305–2324.

Komatsu H, Wurtz RH (1988) Relation of cortical areas MT and MST to pursuit eye movements. I. Localization and visual properties of neurons. J Neurophysiol 60:580 – 603.

Ladda J, Eggert T, Glasauer S, Straube A (2007) Velocity scaling of cue-induced smooth pursuit acceleration obeys constraints of natural motion. Exp Brain Res 182:343–356.

Mikami A, Newsome WT, Wurtz RH (1986) Motion Selectivity in Macaque Visual Cortex. I. Mechanisms of Direction and Speed Selectivity in Extrastriate Area MT. J Neurophysiol 55:1308–1327.

Mulliken GH, Musallam S, Andersen RA (2008) Forward estimation of movement state in posterior parietal cortex. PNAS 105:8170–8177.

Newsome WT, Wurtz RH, Komatsu H (1988) Relation of cortical areas MT and MST to pursuit eye movements. II. Differentiation of retinal from extraretinal inputs. J Neurophysiol 60:604 –620.

Ono S, Brostek L, Nuding U, Glasauer S, Büttner U, Mustari MJ (2010) The Response of MSTd Neurons to Perturbations in Target Motion During Ongoing Smooth-Pursuit Eye Movements. J Neurophysiol 103:519 –530.

Ono S, Mustari MJ (2006) Extraretinal Signals in MSTd Neurons Related to Volitional Smooth Pursuit. J Neurophysiol 96:2819 –2825.

Page WK, Duffy CJ (1999) MST Neuronal Responses to Heading Direction During Pursuit Eye Movements. J Neurophysiol 81:596 –610.

Poggio T (1990) A theory of how the brain might work. Cold Spring Harb Symp Quant Biol 55:899–910.

Porrill J, Dean P, Stone JV (2004) Recurrent Cerebellar Architecture Solves the Motor-Error Problem. Proc R Soc Lond B 271:789–796.

Pouget A, Sejnowski TJ (1997) Spatial Transformations in the Parietal Cortex Using Basis Functions. J Cognitive Neurosci 9:222–237.

Robinson DA, Gordon JL, Gordon SE (1986) A model of the smooth pursuit eye movement system. Biol Cybern 55:43–57.

Rumelhart DE, Hinton GE, Williams RJ (1986) Learning representations by back-propagating errors. Nature 323:533–536.

Salinas E, Thier P (2000) Gain Modulation: A Major Meeting Report Computational Principle of the Central Nervous System. Neuron 27:15–21.

Schmolesky MT, Wang Y, Hanes DP, Thompson KG, Leutgeb S, Schall JD, Leventhal AG (1998) Signal Timing Across the Macaque Visual System. J Neurophysiol 79:3272–3278.

Shenoy KV, Crowell JA, Andersen RA (2002) Pursuit Speed Compensation in Cortical Area MSTd. J Neurophysiol 88:2630 –2647.

Snyder LH (2000) Coordinate transformations for eye and arm movements in the brain. Curr Opin Neurobiol 10:747–754.

Snyder LH, Grieve KL, Brotchie P, Andersen RA (1998) Separate body- and world-referenced representations of visual space in parietal cortex. Nature 394:887–891.

Takemura A, Kawano K (2006) Neuronal responses in MST reflect the post-saccadic enhancement of short-latency ocular following responses. Exp Brain Res 173:174–179.

Takemura A, Murata Y, Kawano K, Miles FA (2007) Deficits in Short-Latency Tracking Eye Movements after Chemical Lesions in Monkey Cortical Areas MT and MST. J Neurosci 27:529–541.

Tusa RJ, Ungerleider LG (1988) Fiber pathways of cortical areas mediating smooth pursuit eye movements in monkeys. Ann Neurol 23:174–183.

Wolpert DM, Miall RC, Kawato M (1998) Internal models in the cerebellum. Trends Cogn Sci 2:338–347.

Young LR (1971) Pursuit eye tracking movements. The control of eye movements:429–443.

Zipser D, Andersen RA (1988) A back-propagation programmed network that simulates response properties of a subset of posterior parietal neurons. Nature 331:679–684.

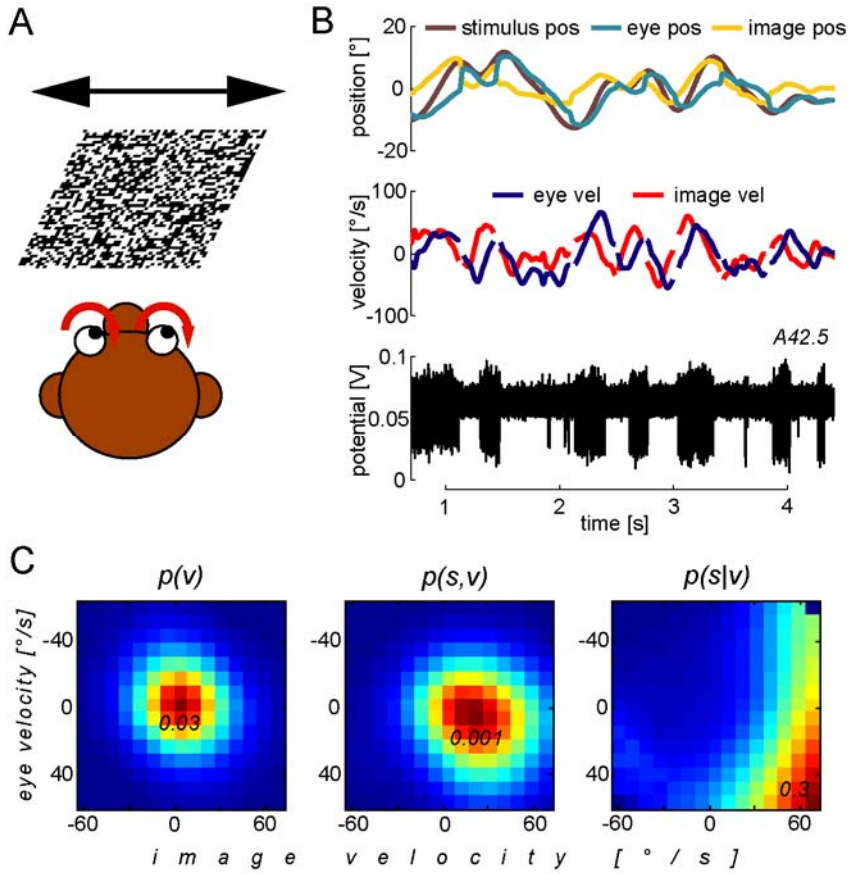

Figure 1: White noise motion paradigm.
(A) The visual large-field stimulus moved rapidly and randomly along the axis of each neuron's preferred direction. The monkey's task was to follow this stimulus as well as possible, performing optokinetic eye movements (OKR).
(B) The top plot shows example traces of stimulus (brown) and eye (cyan) position. Retinal image position (yellow) is the difference between stimulus and eye position. The velocity traces of eye (blue) and retinal image (red) are shown in the middle plot. Saccades were removed from both traces. The bottom plot shows a corresponding extra-cellular recording from an example MSTd neuron.
(C) Determination of the probabilistic tuning function demonstrated for the example neuron shown in (B): $p(v)$ denotes the probability mass function of the occurrence of a specific combination of image velocity and eye velocity for the whole dataset. $p(s,v)$ denotes the joint probability mass function of coincident spike and variable occurrence. Dividing $p(s,v)$ by $p(v)$ yields the conditional probability $p(s|v)$ of observing a spike given any combination of image velocity and eye velocity. Colors from blue to red indicate probability values dependent on image velocity (horizontal axis) and eye velocity (vertical axis). Peak values are denoted in each colormap. By multiplication with the sampling rate of 1 kHz, $p(s|v)$ translates directly into an expectation value of the spiking rate.

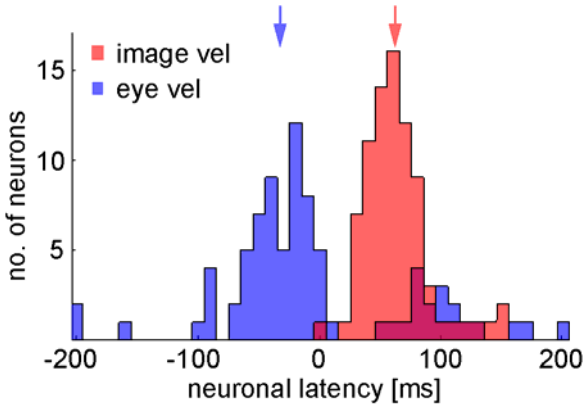

Figure 2: Neural latency relative to image and eye velocity.
For each neuron two latency values were estimated: (1) relative to image velocity (red), and (2) relative to eye velocity (blue). Our estimation procedure maximized the mutual information between neural activity and both signals (see Experimental Procedures). Neural activity lagged about 60 ms behind the image velocity signal. In contrast, most neurons fired before the eye velocity signal, as indicated by negative latency values. Vertical arrows indicate the mean values for both distributions.

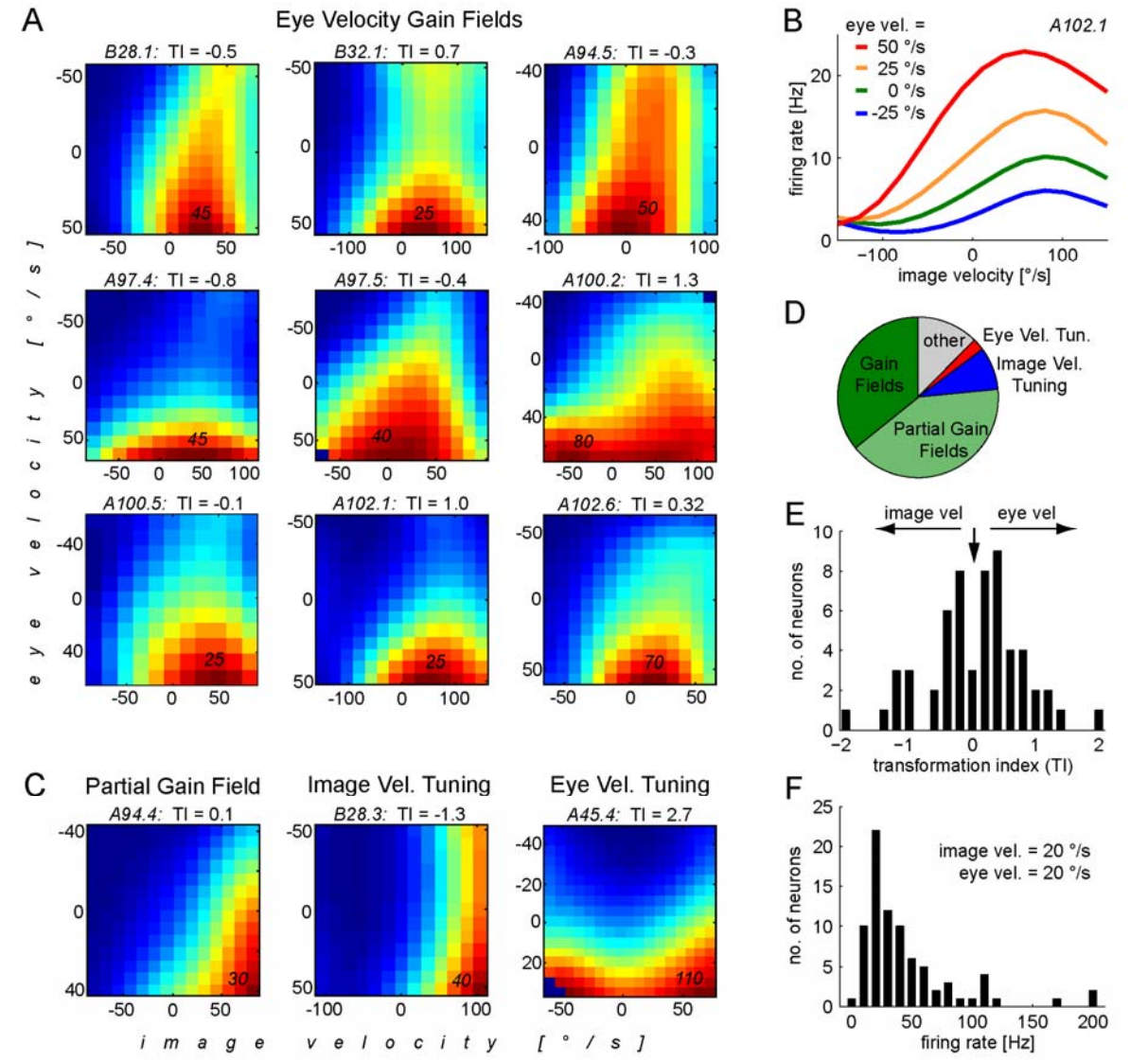

Figure 3: MSTd tuning functions for image and eye velocity.
(A) Two-dimensional tuning curves of 9 example neurons exhibiting gain field-like behavior. Colors from blue to red indicate the mean firing rate [Hz] dependent on image velocity (horizontal axis) and eye velocity (vertical axis). Peak values and corresponding transformation indices (TI) are denoted in each colormap.
(B) Image velocity tuning curves of neuron *A102.1* for different eye velocity values. Each curve represents a slice through the two-dimensional tuning function in (A). Values between centers of the bins were linearly interpolated.
(C) Other typical tuning functions: 1) Partial gain-field structure, probably resulting from a limited stimulus range; 2) 'Vertical' tuning, showing almost pure selectivity for image velocity; 3) 'Horizontal' tuning, exhibiting primarily modulation by eye velocity.
(D) Distribution of observed types of tuning functions. 'Other' includes neurons with positive neural latency relative to eye velocity.
(E) Transformation indices of the analyzed population. The TI value indicates the slope of the tuning function. Negative values indicate predominant vertical tuning, corresponding to higher selectivity for image velocity. Positive values indicate horizontal, eye velocity related tuning. The vertical arrow indicates the mean of the distribution.
(F) Distribution of mean firing rates for image and eye velocity values of 20 °/s.

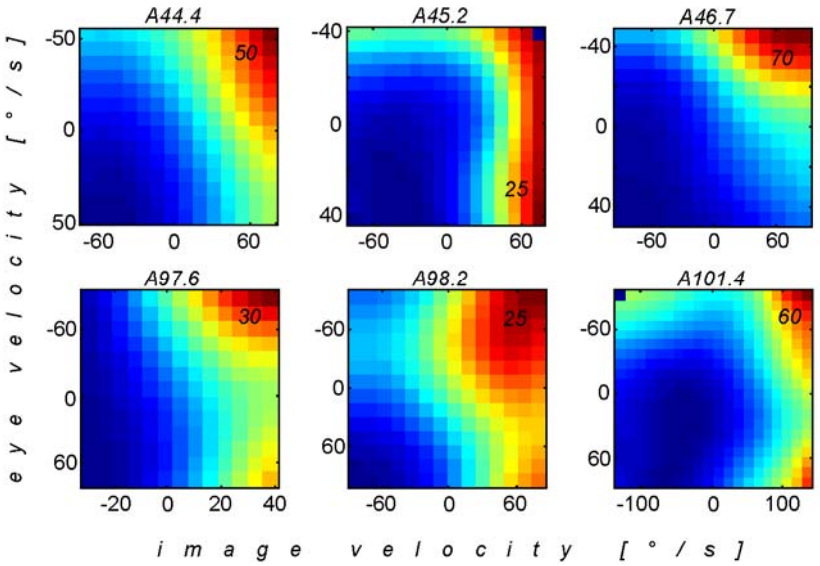

Figure 4: Neurons with opposite visual and eye movement related selectivity.
Tuning functions of 6 units in which spiking activity increased with image velocity in preferred and eye velocity in anti-preferred direction. In all these neurons neural latency relative to eye velocity had positive values.

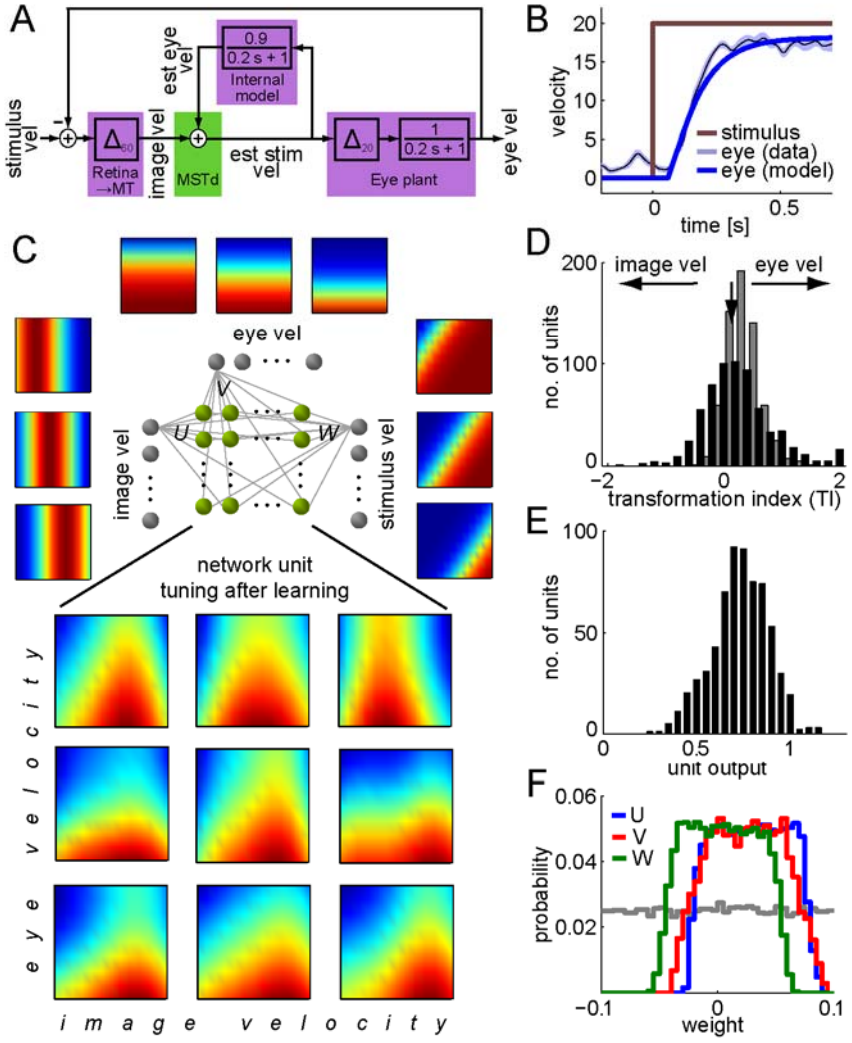
A
stimulus vel
Retina →MT
image vel
MSTd
est eye vel
0.9
0.2 s + 1
Internal model
est stim vel
Eye plant
1
0.2 s + 1
eye vel
B
velocity
stimulus
eye (data)
eye (model)
time [s]
C
eye vel
image vel
stimulus vel
V
U
W
network unit
tuning after learning
eye velocity
image velocity
D
image vel
eye vel
no. of units
transformation index (TI)
E
no. of units
unit output
F
probability
U
V
W
weight

Figure 5: Modeling the visuo-motor coordinate transformation.
(A) Basic system-level model of the OKR. Image velocity is the difference between stimulus and eye velocity. A delay of 60 ms accounts for the latency of the image velocity signal due to retinal and neural processing along the visual system. The eye plant is modeled by a low-pass filter with a time constant of 200 ms and an additional delay of 20 ms. Image velocity is transformed to an estimated stimulus velocity signal by adding the estimated eye velocity signal, provided by an internal model of the eye plant. We assume that this coordinate transformation involves area MSTd.
(B) The step function response of the model (blue) for a sudden increase in stimulus velocity to 20 °/s (brown). The light blue trace shows example eye velocity data from (Ono et al. 2010).
(C) Neural network model of the coordinate transformation. The network consists of two input layers, one intermediate network unit layer, and an output layer. The image velocity input layer has 31 units. Each unit is Gaussian tuned with differing preferred image velocity. The eye velocity input layer has 21 units. Each unit has a sigmoid tuning with differing inflection velocity. The stimulus velocity output layer consists of 41 sigmoidally tuned units. Each of the 651 intermediate units is connected with each input and output unit. During the back-propagation learning process the weights of these connections are modified. Below the model, the tuning functions for image and eye velocity of 9 example network units after learning are shown.
(D) Distribution of transformation indices of all intermediate unit tuning functions before (grey) and after (black) learning. The vertical arrow indicates the mean of the distribution after learning.
(E) Output values of the trained network units for image and eye velocity values of 20 °/s.
(F) Distribution of weight values before (grey) and after learning for image velocity input (U, blue), eye velocity input (V, red), and output weights (W, green).

Eidesstattliche Versicherung/Affidavit

Hiermit versichere ich an Eides statt, dass ich die vorliegende Dissertation

„Eye Velocity Gain Fields for Visuo-Motor Coordinate Transformations: A Multi-Level Analysis of Neuronal Activity in Cortical Area MSTd“

selbstständig angefertigt habe, mich außer der angegebenen keiner weiteren Hilfsmittel bedient und alle Erkenntnisse, die aus dem Schrifttum ganz oder annähernd übernommen sind, als solche kenntlich gemacht und nach ihrer Herkunft unter Bezeichnung der Fundstelle einzeln nachgewiesen habe.

I hereby confirm that this dissertation is the result of my own work and that I have only used sources or materials listed and specified in the dissertation.

Authors contributions to each publication:

„The Response of MSTd Neurons to Perturbations in Target Motion During Ongoing Smooth-Pursuit Eye Movements.“:
The author of this doctoral thesis contributed to this work by performing the data analysis, writing parts of the manuscript and designing the figures.

„An Information-theoretic Approach for Evaluating Probabilistic Tuning Functions of Single Neurons“:
The author of this doctoral thesis contributed to this work by developing the novel data analysis approach, performing the data analysis, writing the manuscript and designing the figures.

„A Method for Evaluating Tuning Functions of Single Neurons based on Mutual Information Maximization“:
The author of this doctoral thesis contributed to this work by developing the data analysis approach, performing the data analysis, writing the manuscript and designing the figures.

„Neuronal Variability of MSTd Neurons Changes Differentially With Eye Movement and Visually Related Variables“:
The author of this doctoral thesis contributed to this work by designing the experiment, performing the data analysis, writing the manuscript and creating the figures.

„Eye Velocity Gain Fields in MSTd for Visuomotor Coordinate Transformations“:
The author of this doctoral thesis contributed to this work by designing the experiment, performing the data analysis, developing the computational models, writing the manuscript and creating the figures.

München, den 15.10.2012